A STUDY OF THE EFFECT OF MINING INDUCED STRESSES ON A FAULT AHEAD OF AN ADVANCING LONGWALL FACE IN A DEEP LEVEL GOLD MINE

Matthew Francis Handley

A dissertation submitted to the Faculty of Engineering, University of the Witwatersrand, Johannesburg, in fulfilment of the requirements for the degree of Master of Science in Engineering.

Johannesburg, 1987.

DECLARATION

I declare that this dissertation is my own unaided work with the exception of a small part of the underground work which was carried out by my colleagues at the Rockburst Project, Western Deep Levels Limited. All the work represented by this dissertation was carried out at Western Deep Levels Limited, while I was an employee of the company. It is being submitted for the Degree of Master of Science in Engineering in the University of the Witwatersrand, Johannesburg. The dissertation has not been submitted before for any degree or examination in any other University.

M F Handley
31 July 1987

ABSTRACT

The effect of mining induced stress changes on a faulted rock mass in a deep South African gold mine was investigated to clarify the relationship between stress, geological structure and mining induced seismicity. The study commenced with absolute in situ stress measurements at a site straddling a reverse fault 2863 m below surface. A period of stress change monitoring followed at the same position while an extensive tabular mining excavation approached and intersected the fault. These measurements were supported by numerical stress analyses, underground displacement levelling and seismic activity monitoring. The study revealed a stress discontinuity across the fault surface. It persisted from the beginning to the end of the study, and appears to have suppressed seismic activity associated with the fault. This explains the variance of the fault behaviour with the numerical predictions, highlighting the complexity of stress fields in natural rock masses, and their influence on mining induced seismicity.

ACKNOWLEDGEMENTS

I wish to thank the Technical Development Services of Anglo American Corporation Limited for granting permission to submit the results of the work carried out for an MSc Eng.(Mining) in the University of the Witwatersrand, Johannesburg. Special thanks to Messrs T. O. Hagan, D. M. Grobbelaar, R. L. de Kock and P. J. Holtzhausen of the Rockburst Project who provided guidance, underground cabling, computer programmes and results from an underground survey respectively; to Messrs A. v. Z. Brink, P. I. Mountfort, P. Grobler, C. G. F. Olivier, H. F. Möller, K. C. Collins and A. Mareé who all helped to install and calibrate an accelerometer at the underground site, and who provided general assistance and guidance in the maintenance and repair of electronic equipment. Many thanks to Messrs B. Davies and R. Dixon as well as Mrs M. van Aswegen, who provided assistance with the numerical analyses carried out at the Anglo American Corporation Rock Mechanics Department, Welkom. Thankyou to Dr N. C. Gay for the guidance given for the manipulation and interpretation of the strain relief results. Finally, I wish to extend gratefully my thanks to Professor S. Budavari who, as my supervisor, kindly guided and encouraged me throughout the study, to my mother Mrs C. Handley, who patiently typed the manuscript, and to my wife Ireine, who provided much encouragement and assistance with proof-reading of the manuscript.

To my wife Ireine

CONTENTS

LIST OF FIGURES

LIST OF TABLES

LIST OF SYMBOLS

Quantity	Symbol
angle in a plane	α, θ
bulk modulus	K
change in a quantity	Δ
coefficient of friction	μ
cohesive strength	C_o
co-ordinate axes (rectangular)	x,y,z
correlation coefficient	r
error: inherent	ζ
: stress change	ξ
force	F,R
joint normal stiffness	k_n
joint shear stiffness	k_s
joint spacing	s
period	T
Poisson's ratio	ν
shear modulus	G
strain: normal	ε
shear	γ
strain invariant	e
stress: normal	σ
shear	τ
stress concentration factors	a,b,c
stress invariant	Θ
Young's modulus	E

CHAPTER 1

INTRODUCTION

Rock bursts in the deep level hard rock gold mines of South Africa have spurred intensive and sustained research into their origin for the past three decades. Successful determination of the conditions necessary and processes responsible for rock bursts has been achieved, while the violent and transient nature of the phenomenon has inhibited progress towards complete quantification of the mechanism. Amongst the parameters that still remain unmeasured is the stress state in the rock before, during and after a rock burst, both in the rock surrounding an affected mining excavation, and at the seismic source, which may be hundreds of metres away.

The relationship between rock stress, mining induced seismicity and rock bursts still requires much study, especially when the numerous variables that come into play are considered. The current understanding of the seismic and rock burst mechanisms is first described in order to illustrate their relationship with stress in general as well as some of the other important factors. Rock mechanics research in the South African gold mining industry during the twentieth century is then briefly reviewed, with particular emphasis on these aspects. Finally the argument justifying this study is developed, and the objectives of the research are outlined.

1.1 Mining Induced Seismicity and Rock Bursts

Underground mining results in the creation of voids originally occupied by unmined ore in the case of producing excavations and country rock in the case of other excavations. The stress field that exists before mining is altered by the creation of a void and this process can be viewed as the superposition of a mining induced stress field on the original stress field.

Exploitation of the narrow and laterally persistent gold bearing orebodies of the Witwatersrand Supergroup result in tabular excavations whose height is negligible in relation to their length

CHAPTER 1

INTRODUCTION

Rock bursts in the deep level hard rock gold mines of South Africa have spurred intensive and sustained research into their origin for the past three decades. Successful determination of the conditions necessary and processes responsible for rock bursts has been achieved, while the violent and transient nature of the phenomenon has inhibited progress towards complete quantification of the mechanism. Amongst the parameters that still remain unmeasured is the stress state in the rock before, during and after a rock burst, both in the rock surrounding an affected mining excavation, and at the seismic source, which may be hundreds of metres away.

The relationship between rock stress, mining induced seismicity and rock bursts still requires much study, especially when the numerous variables that come into play are considered. The current understanding of the seismic and rock burst mechanisms is first described in order to illustrate their relationship with stress in general as well as some of the other important factors. Rock mechanics research in the South African gold mining industry during the twentieth century is then briefly reviewed, with particular emphasis on these aspects. Finally the argument justifying this study is developed, and the objectives of the research are outlined.

1.1 Mining Induced Seismicity and Rock Bursts

Underground mining results in the creation of voids originally occupied by unmined ore in the case of producing excavations and country rock in the case of other excavations. The stress field that exists before mining is altered by the creation of a void and this process can be viewed as the superposition of a mining induced stress field on the original stress field.

Exploitation of the narrow and laterally persistent gold bearing orebodies of the Witwatersrand Supergroup result in tabular excavations whose height is negligible in relation to their length and breadth. These excavations superimpose large mining induced stresses on the rocks that host the orebodies and on the unmined portions of the orebodies themselves. The rocks of the Witwatersrand Supergroup are generally strong and brittle and are capable of withstanding high stresses before failure occurs.

Failure is usually stable, that is, it takes place in the form of the stable development of brittle fractures which are ubiquitous in excavations deeper than 2000 m below surface. Occasionally failure takes place suddenly and violently, which results in a transient earth motion called a seismic event. The violent failure is accompanied by the release of large amounts of strain energy stored in the rock at the seismic source and this energy is converted to kinetic energy in the surrounding rock.

The kinetic energy is radiated outwards from the se[illegible]ource in the form of strain waves which may interact wit[illegible]round excavation by accelerating the rock surrounding it [illegible]void causing damage to the excavation itself, its supports and objects within. This phenomenon is called a rock burst. Observations reveal that not all seismic events cause rock bursts and that the probability of rock burst damage increases in sympathy with the proximity of an excavation to the seismic source and with the amount of energy released.

1.1.1 Causes of mining induced seismicity

Two conditions must exist for a seismic event to occur. The first is that the stresses in the rock must cause it to reach a state of unstable equilibrium, and the second is that some further disturbance must take place to upset that equilibrium. The first condition is met in the gold mines by the imposition of large mining induced stresses on the rock immediately surrounding extensive tabular excavations. The second condition is satisfied by a number of factors either singly or in combination with one another. These include the energy radiated to the surrounding rock during the course of the daily blast; the imposition of further stress changes induced in the surrounding rock when excavations are enlarged by mining; the rock mass response to the imposition of induced stress changes such as creep, stable development of brittle fractures and disturbances caused by the transmission of seismic waves through unstable volumes of rock.

The first two factors exert a very strong influence on the temporal distribution of mine seismicity. Cook et al (1966) show that approximately 50% of all seismic events detected at a deep gold mine on the East Rand occurred during the hour preceding, and four hours succeeding the daily blast. In contrast rock mass responses to mining induced stress are more continuous and account for a more even distribution of seismic events through time.

Several other variables, broadly classified as mining and natural, influence the frequency of seismicity and rock bursts. They include mining and support methods, mining geometry and layout, extent and scale of mining operations, rock properties, rock mass structure, geological structure, depth and the initial stress state prior to mining. The mining variables can be altered to effect reductions in the seismic and rock burst frequency while the natural variables are beyond the control of the engineer.

1.1.2 Seismic mechanism

Deductions made from fundamental principles, seismological theory and observations show the seismic source mechanism to be slip on a rupture surface within the rock. The rupture can take place on an existing discontinuity of any description or can develop within previously intact rock (Ortlepp, 1983).

In simple mechanistic terms, the process is driven by shear stress acting parallel to the rupture surface. Slip movement along the rupture surface is inhibited by a resisting stress which is the product of the normal stress acting perpendicularly to the surface and the dynamic coefficient of friction of the surface. Further resistance to slip on the rupture surface is provided by surrounding stable volumes of rock not involved in the seismic event. Ortlepp (1983) presents a simple block and spring model to illustrate the mechanism, as shown and described in Figure 1.1.

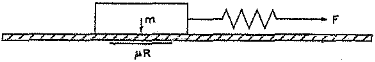

1: A force F acts through an elastic spring attached to a block with mass m resting on a horizontal surface

2: Stable equilibrium persists as long as the inequality $F - \mu R < 0$ is satisfied, where μ is the static coefficient of friction, and R is the reaction force

3: Unstable equilibrium is created by slowly increasing F until it is equal to the resisting force μR

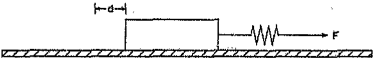

4: Once F is increased or μR decreased infinitesimally, the block starts to move, and the dynamic coefficient of friction becomes operative

5: As a result an initial net force of magnitude $(\mu_s - \mu_d)R$ accelerates the block, where μ_s and μ_d are the static and dynamic coefficients of friction respectively

6: The block again comes to rest after moving distance d when the force F in the spring becomes too small to continue moving the block

Figure 1.1

Block and spring analogy for a seismic event generated on a geological discontinuity

Movement on the rupture surface results in the reduction in shear stress until it is too small to continue to drive the slip. In seismology the shear stress reduction is referred to as the stress drop. The effect of slip on the normal stress acting across the rupture surface is not well known.

The seismic mechanism is confirmed by surface evidence in some Californian earthquakes (Richter, 1958) and by underground evidence in a South African gold mine (Ortlepp, 1983). The wide variety of conditions found at rock burst sites suggests that more than one mechanism may be responsible for the damage, although slip on a surface has been noted in a number of cases (Ortlepp, 1984).

1.1.3 Seismic source parameters

Seismic source parameters are determined from observations based mainly on seismic traces or seismograms. The traces represent records of either the velocity or acceleration imparted to the rock by the passing strain waves. Geophones and accelerometers respectively are used to measure these quantities. An array of at least four geophones or accelerometers are necessary to gather sufficient data to locate the source of the seismic energy (Eccles and Ryder, 1984). The position of the seismic source is of prime importance to mining research.

The most convenient and widely used seismic source parameter is the magnitude which is expressed in terms of an open-ended logarithmic scale developed by Richter (1958). Although it is a crude measure of the size of a seismic event it is of value because of its strong empirical relations with other quantities such as seismic moment, seismic energy and frequency of occurrence (McGarr, 1984).

The seismic moment expressed in energy units, is a more reliable measure of the event size, and can be estimated from a seismogram by the relation given in McGarr (1984). Alternatively, it is the product of the rock modulus of rigidity, the area of the rupture surface over which slip took place and the average displacement on the surface, if these quantities are known or can be estimated from observations. In gold mining the moment can be related to the magnitude by an empirical relation given by McGarr (1984). Accordingly a seismic event with magnitude 2,5 on the Richter Scale would have a corresponding seismic moment of approximately 5×10^{13} joules.

The seismic energy radiated in the form of strain waves from such an event can be related to its magnitude by a similar relation and approximates 4×10^{8} joules (McGarr, 1984). This represents about 0,0008 per cent of the energy involved in the seismic moment. The fraction radiated is so small because much of the energy involved is expended doing work against the resisting stress, creating the rupture, as well as fracturing and heating the rock.

A study of seismic traces generated in gold mines reveals that the energy is radiated for about 0,1 seconds. For the above event this represents a power of 4×10^{9} watts which is equivalent to the maximum power output of the largest coal-fired power stations currently under construction in the Eastern Transvaal. Clearly, any mining excavations exposed to such large power outputs are likely to suffer rock burst damage.

1.2 Review of Rock Mechanics Research in South Africa

The descriptions of mining induced seismicity and rock bursts given are based on the outcome of research begun on the Witwatersrand just after the turn of the century. The amount of work done since then is vast and cannot be adequately covered in a brief review. Research of particular importance to mining induced seismicity, rock bursts and stress only, is outlined briefly in order to highlight important findings and identify areas that need further investigation.

1.2.1 Qualitative research

Salamon (1983) identifies two major periods of mining rock mechanics research in South Africa. The first commenced early in the century, ended around 1950, and consisted mainly of qualitative research.

Work began in 1908 with the appointment of the Ophirton Earth Tremors Committee to investigate the origin of the earth tremors then causing concern amongst the residents of Ophirton (High-Level Committee on Rockbursts and Rockfalls, 1977). The committee found the cause of the tremors to be the shattering or punching of pillars of unmined reef left to support the excavations. Similar committees, appointed in 1915 and 1924 to re-investigate rock bursts endorsed the findings of the 1908 committee and extended them to remnants and shaft pillars.

In the succeeding years much data was gathered by individuals, institutions and the mines themselves. Much of the work was based on observations such as those by Hill (1944), who contrasted the high incidence of rock bursts in excavations adjacent to isolated remnants with the low incidence then observed in newly established longwalls. Although these and other investigations were extremely limited in their potential to reveal the rock burst mechanism, they did show that rock bursts are more prone in highly stressed rock, a fact that was appreciated at the time.

This type of investigation culminated in that of Cook et al (1966) who reviewed the findings of work carried out on rock burst incidence during the previous decade. They contrasted and compared the effect of several mining variables on the rock burst incidence graphically, and were able to demonstrate the effect of stope span, different abutment types and depth below surface on rock burst frequency. The findings can be roughly summarized to state that in regions where the total stresses are greatest, rock bursts are most frequent. When considering the influence of geological features the authors showed that a readily discernible increase in rock burst activity occurred when stope faces advanced to within 30 m of both faults and dykes.

These and the previous findings discussed consider only rock bursts which form a fraction of total mining induced seismicity. This limits the value of the results to providing broad indications of rock burst activity only. Mining induced seismicity was not researched in any detail during these years aside from the work of Gane et al (1946) and others before them who monitored seismic events on the Central Rand using surface geophones.

The technology for in situ stress measurement and numerical stress estimation did not exist at the time, hence very little research was carried out. Most discussions of the role of stress were based on visual observations underground and therefore tended to be qualitative in nature. The end of the first period came with the realization that rock mechanics research based on qualitative studies alone would not result in any further progress.

1.2.2 Quantitative research

The second period of research began around 1950 with the intensification of effort and a more fundamental approach (Salamon, 1983). The new direction resulted in a vast expansion in the knowledge of rock mechanics. Great advances were made in the understanding of mining induced seismicity, in situ stress measurements became possible and numerical stress analysis was introduced. The study of rock bursts has not advanced at a similar pace, but has nevertheless benefited from the advances made in other areas.

Mining induced seismicity
Appreciation of the fact that close similarities exist between mining induced seismicity and natural earthquakes gave the search for a solution to rock bursts new impetus. Following on from studies by Gane et al (1946), Cook (1964) pioneered a three-dimensional seismic location system in a deep gold mine on the Witwatersrand.

His work showed that not all seismic events cause rock bursts; that the traces from seismic events which cause rock bursts are similar to those that do not; that most of the seismic sources cluster around the mine workings; and that shear is a mechanism of failure. These findings have been substantiated by the vast amount of seismic data since gathered by seismic location systems functioning on several gold mines today.

Spottiswoode (1984) used a seismic location network on a mine situated near Carletonville to study seismic source mechanisms and estimate seismic source parameters. Potgieter and Roering (1984) carried out source mechanism studies on seismic events recorded in the Klerksdorp Goldfield. They suggest that all the seismic events studied occurred either on faults, dykes or possibly on pre-existing mining induced fractures. Gay et al (1984) correlate mining induced seismicity with geological structure in the Klerksdorp Goldfield. They conclude that the results do not readily advance the understanding of large seismic events because the data are insufficient to explain why some faults are seismically active while others are not.

Practical application of elastic theory to mining problems

Rock mechanics received a tremendous boost when Salamon (1965) introduced the face element principle of stress estimation. For the first time the stress state in rocks surrounding the tabular excavations of the gold mines could be estimated. Elastic theory demands that the medium in which the stresses are calculated is linearly elastic, homogeneous, isotropic, continuous, and mining induced strains are small. The technique is therefore unable to include for analysis the envelope of fractured rock about 20 m deep that surrounds all extensive tabular excavations at depth. It is also incapable of taking into account stress and strain discontinuities often associated with geological structures.

Independent studies undertaken by Ortlepp and Nicoll (1965) and Ryder and Officer (1965) showed that the behavior of Witwatersrand sediments in general conformed with the assumptions made in elastic theory. Shortly thereafter, the first analysis of stresses and displacements in the rock surrounding typical gold mine excavations began with the use of the electrolytic tank (Salamon et al, 1965). The analogue method of stress estimation was later replaced by digital computer methods, of which the MINSIM-D suite of computer programs are the latest development (Chamber of Mines Research Organisation, 1985).

In addition to stress, displacement, and energy changes that take place in mining, the programs can be used to estimate the normal and shear stresses at any number of points on a plane having an arbitrary orientation in space. This provides the analyst with the means to assess the seismic hazard from the fault slip point of view posed by a discontinuity when subjected to mining induced stresses. This technique is limited by the fact that stresses in the vicinity of faults and dykes often vary from theorectical preditions, and that the coefficient of friction of any discontinuity surface must be assumed to be constant. Nevertheless, it promises to be of great value to the mining industry in reducing the rock burst hazard.

In situ stress measurement

Natural stress distributions in rock masses do not conform exactly to simple gravity loading by the superincumbent strata. They are complicated by the spatial variation of elastic properties of the rock, discontinuities, the superposition of tectonic stress fields, and stresses induced by temperature, chemical alteration, groundwater, topography, natural voids and man-made excavations. The effects of voids, gravity loading and groundwater can be accounted for by existing analytical techniques, whereas the other variables can only be accounted for by in situ stress measurements.

Stress measurements on the South African gold fields commenced in the early sixties with the use of a strain gauge-based system developed by the CSIR and described by Leeman (1965b). Gay (1975) summarized the results of stress measurements undertaken in Southern Africa up to that time. The results indicate that the major principle stress at depth lies within 20° of the vertical, and that the resultant vertical stresses calculated from the measured tensors are in reasonable agreement with the expected stresses due to the respective overburden weights. The horizontal stress results from all the measurement locations in the gold mines were found to agree remarkably well with that predicted by the denudation theory of Voight (1966). In gold mines exceeding 2000 m in depth the vertical stress can be assumed to approximate the overburden weight, and a horizontal to vertical stress ratio of 0,5 can be used.

Local deviations from these patterns occur, especially in the vicinity of excavations and geological discontinuities. These have been reported by Leeman (1965c), and investigated by Deacon and Swan (1965), Pallister (1969), Gay (1972) and Gay (1979). In general, the data indicate that stresses are reduced in fractured ground and increased near and within shear zones, and within dykes. These anomalies may be sufficient in some cases to render the rock mass unstable and therefore prone to seismic activity.

In situ stress monitoring or the measurement of stress changes with time, have not been undertaken in the gold mines aside from the attempt by Leeman (1965c), who measured stress changes ahead of an advancing longwall with Maihak strain cells and the CSIR biaxial strain cell. The study was complicated by the failure of the free surface of the boreholes in which the strain cells were installed. The results indicated a two-fold increase in stress about 30 m from the longwall face.

The recent introduction of the vibrating wire stressmeter designed by Hawkes and Hooker (1974) has solved many of the problems previously associated with stress monitoring. Sellers (1977) has listed a number of cases in which the stressmeter was used in mines in the United States of America. The instrument was not tried in the South African gold mines until 1984 when it was selected to measure in situ stress changes for this study.

1.3 The Present Problem

In spite of the substantial advances made in rock mechanics as applied to mining, numerical modelling methods, laboratory testing and underground experiments and observations there is still no clear solution to the rock burst problem. Presently, there are a number of countermeasures designed to minimize where possible the frequency and effects of rock bursts. In the main, they are improved excavation support methods and safer mining methods which include partial extraction and planned sequences of ore exploitation. Large scale filling of mined voids with mill tailings or waste rock is the subject of extensive research at present. The effects of this support method on rock bursts when applied over a wide area, still remains to be seen.

The increasing scale of mining operations together with the greater average depth and extent of mining excavations tend to militate against the countermeasures employed. This is evident in the more or less constant mine employee accident rate attributable to rock bursts for the years 1975 to 1981 (Morris and Vorster, 1984). When compared with all other accidents on the gold mines during the six decades ending in 1985, rock bursts and rock falls have claimed a consistently larger proportion of all fatalities each succeeding decade, with the exception of a small drop in the years spanning 1976 to 1985 (Hagan, 1987). The current rate of approximately 0,7 fatalities per thousand employees per annum due to rock falls and rock bursts has remained more or less constant since 1936, and now accounts for more than half the fatalities on the gold mines.

These figures do not suggest that inadequate efforts are being made to counter rock bursts. On the contrary they reflect considerable achievements by the gold mining industry in containing a worsening problem whilst extracting ore at ever increasing depths. Despite this fact, the frequency of rock bursts has reached distressingly high levels in South Africa's gold mines. In 1985, gold mining generated approximately 600 seismic events with a magnitude of 2,5 or greater on the Richter scale (Fernandez et al, 1986). Seismic events of this magnitude almost invariably result in rock bursts underground. The potential rewards in reducing the hazards posed by rock bursts are therefore large, even if the benefits are confined to a reduction in the fatality rate alone.

Further successes in countering rock bursts would undoubtedly be possible if a more detailed knowledge of stress distributions within rock masses were acquired. This would render mining induced seismicity and the resulting rock bursts more predictable and would provide guidelines toward developing more effective stress analysis techniques, especially when geological structure is involved. The most promising approach to the problem is to concentrate attention on the seismic source itself, with special emphasis on the stress fields responsible for the phenomenon.

Although recent research has made great advances towards a solution, the following questions still remain partially unanswered:-

i) what exactly is the seismic source mechanism?

ii) which factors are most important in bringing about a seismic event?

iii) how large are the stresses that drive it?

iv) what happens to the stress state at initiation, during and after a seismic event?

v) why do some seismic events cause rock bursts while others do not?

vi) why are some faults and some dykes seismically active when exposed to mining induced stresses while others are not?

Improvements in instrument design during the past fifteen years have made it possible to measure with reasonable accuracy stresses and stress changes at any point within a rock mass. Stress analysis by numerical methods is now widely accepted and practised. It can be applied to provide guidelines and background information to in situ stress and stress change measurements. Armed with these tools it is possible to investigate rock mass stress distributions and the effects of mining induced stress changes on rock in situations which cannot be modelled by analytical techniques alone.

1.4 Objects of the Study

The objects of this study are to address some of the questions listed above by monitoring the in situ the stress state of a faulted rock mass while it is exposed to changing mining induced stresses. This was done by measuring the initial stress state in the vicinity of a fault 2863 m below surface at Western Deep Levels Limited, and then monitoring the stress changes as the fault was exposed to mining induced stresses by an approaching longwall face. The location of Western Deep Levels and the stress monitoring site are illustrated in Figure 1.2.

A well defined fault situated ahead of an advancing longwall was

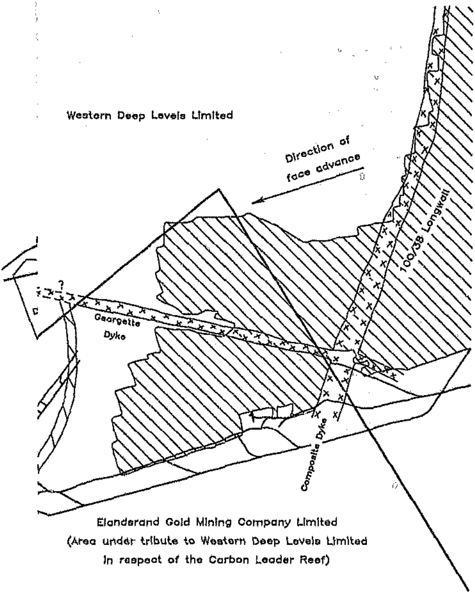

selected for underground stress monitoring
Scale: 1:5000

ıg site

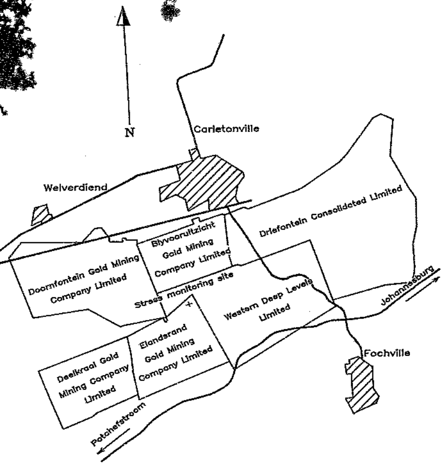

a: Location of Western Deep Levels Limited
and the Carletonville Goldfield
Scale: 1:200000

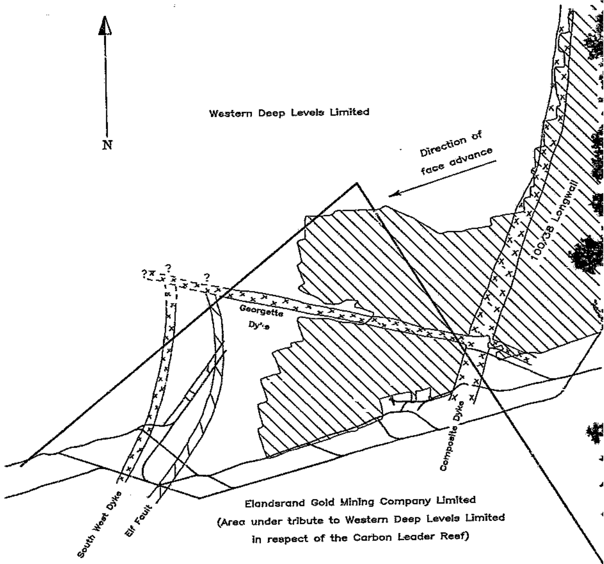

b: Site selected for underground stress monitoring
Scale: 1:5000

Figure 1.2
Location of underground stress monitoring site

chosen as the focus of the study because this type of situation has so often been identified as being responsible for enhanced levels of seismicity in deep gold mines. The case studied was particularly convenient in that the fault was exposed in several mine excavations, allowing study at different points, as well as some flexibility in the design of the experiment.

In the given situation the detailed objects were to:-

i) measure the initial in situ stress state both to the east and west of the fault using the CSIR biaxial or "Doorstopper" strain gauge system;

ii) monitor the stress changes at the same points as the long-wall approaches the fault;

iii) monitor movements, if any, on the fault by means of visual observations and an underground levelling survey;

iv) monitor mining induced seismicity in the area with the intention of correlating particular seismic events located on the fault with movements on the fault surface and stress changes in the surrounding rock;

v) calculate stresses, stress changes and displacements by computer in order to provide a comparator for the in situ measurements.

The remainder of the dissertation deals with a description of the study in which aspects of the layout and design of the experiment are discussed and the instrumentation used is described. The results of the underground measurements are then presented together with an assessment of the errors involved. The numerical analyses are described next and the results presented. A discussion of all the results follows in which it is shown that good agreement between the measured and numerical results was obtained.

The measurements reveal a stress discontinuity at the Elf Fault that persisted throughout the duration of the study. This complex stress state had such a strong influence on the seismic behaviour of the fault that the distribution of seismic activity bore no relationship with that suggested by stress analyses. These observations emphasize the complexity of rock masses, their stress fields, and some of the shortcomings of the assumptions underlying stress analysis techniques currently in use. At the monitoring site the fault proved to be aseismic, a condition that is supported by the analyses, measurements and underground observations. This has helped to confirm the conditions necessary for fault stability, which can be adequately expressed by the recently introduced criterion called Excess Shear Stress in situations where a discontinuity has no influence on the stress field in its vicinity.

CHAPTER 2

STRESS MEASUREMENT STUDY

Excavations employed for mining purposes are designed for mining only, leaving little room for experimentation. The researcher faces difficult challenges in this situation as he is required to make the best of it without interfering with mining activity in any way. Moreover, the underground conditions place severe demands on the equipment used there.

The design of the stress measurement study is a compromise between the demands of in situ stress measurement and monitoring as well as the limitations imposed by underground conditions. This chapter is broken down into five parts which deal with the underground site, the measurements, the equipment, the layout and numerical modelling. Each is described in full, together with limitations where they are relevant.

2.1 Monitoring Site

Measuring in situ stress and stress change in the vicinity of an accessible geological feature requires a site which is to be subjected to readily measurable stress changes in a reasonably short period of time. When the study was formulated, a suitable site had not yet been found. General considerations for an appropriate monitoring site are discussed after which the site selected for the underground measurements is described.

2.1.1 Geological and mining considerations

In order to study the effect of mining induced stress on a geological feature, two requirements must be met. The first is a conveniently situated and accessible feature which has considerable extent and a known orientation. The second requirement is that at the beginning of the study the stress state should be as close as possible to virgin conditions, and that during the course of the project considerable additional stress should come to bear on the feature.

A fault or a dyke is most suitable for this study because both are usually extensive, with known orientations, and many are associated with enhanced levels of mining induced seismicity (Cook et al, 1966). A longwall mining situation is best suited to the second requirement because of its relatively simple geometry and the fact that large mining induced stresses are imposed on the surrounding rock mass.

The major disadvantage of a longwall mining system is that the rock mass ahead of the advancing faces is usually inaccessible. Nevertheless, this disadvantage is outweighed by the compatibility of a longwall with the requirements of the project, consequently the search for a suitable site began on Western Deep Levels Limited.

2.1.2 Selection and description of monitoring site

Few sites were available on the mine because very few mine excavations had been developed ahead of the advancing longwall faces. A total of seven possibilities were investigated, and the 100/25 Replacement Crosscut North area was chosen because it conformed best to the requirements of the study.

The site is situated on the Carbon Leader Reef horizon at a depth of 2863 m below surface and some 3 km to the west of No.2 Shaft (Figure 2.5). A steeply dipping reverse fault with a strike of 30 degrees east of north and a dip of 75 degrees to the south-east had been exposed at two points in the area in 1978. The fault was found to have a downthrow of 36 to 40 m to the west and was evidently still undisturbed by the 100/38 Longwall which was temporarily halted and situated about 150 m to the east (Figure 2.1).

About 60 m to the west of the fault, a dyke 10 to 15 m wide was exposed at three places. The dip of the dyke is vertical, with a strike more or less parallel to that of the fault. Both features

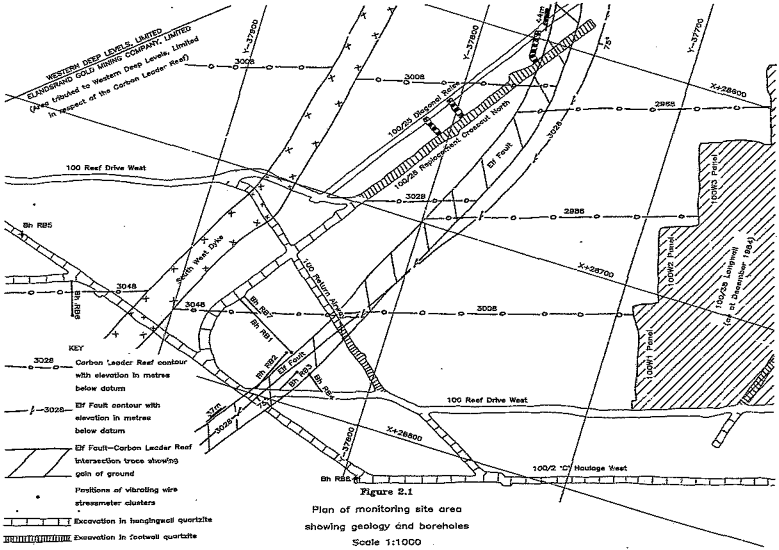

Figure 2.1

Plan of monitoring site area showing geology and boreholes

Scale 1:1000

had an unknown seismic history and neither had been exposed in any other workings on the mine. Although they were exposed at points less than 100 metres apart, it was clear that they were fairly extensive and therefore suitable for the study. The features were named the Elf Fault and the South West Dyke respectively by the Western Deep Levels Geological Department, which had mapped the area in 1978 when 100/2 'C' Haulage and 100 Reef Drive West penetrated the features. This information was sufficient at the conceptual stage of the study but was inadequate for the detailed engineering characteriziation of the rock mass.

Underground Mapping

Unfortunately, the age of the tunnels, together with the fact that they had been supported with grouted rockbolts, wire mesh and lacing and then painted, rendered more detailed mapping impossible. More significantly, scanline surveys of rock structure could not be carried out because of the above conditions. Detailed structural mapping of the rock mass was therefore only carried out on the cores recovered from the stress measurement boreholes. (See Section 3.1).

The major features such as the Elf Fault and the South West Dyke were still visible and these were re-mapped as accurately as possible where they were exposed. The work was done by off-setting the fault and dyke traces in relation to mine survey pegs with the use of a measuring tape. The attitude of the structures was determined by means of a clino-rule. The geology of the monitoring site is plotted in plan in Figure 2.1 while Figure 2.2 is a perspective of the inferred geological structure above and below the monitoring site.

Geological description of exposed rocks

The rocks exposed at the monitoring site belong to the Randfontein Formation in the Central Rand Group, Witwatersrand Supergroup. The Carbon Leader Reef is present in this formation and is the main economic horizon exploited by the mine. The reef is exposed ahead of the 100/38 Longwall in 100 Reef Drive West as well as in 100/25 Replacement Crosscut North (Figure 2.1). It has a more

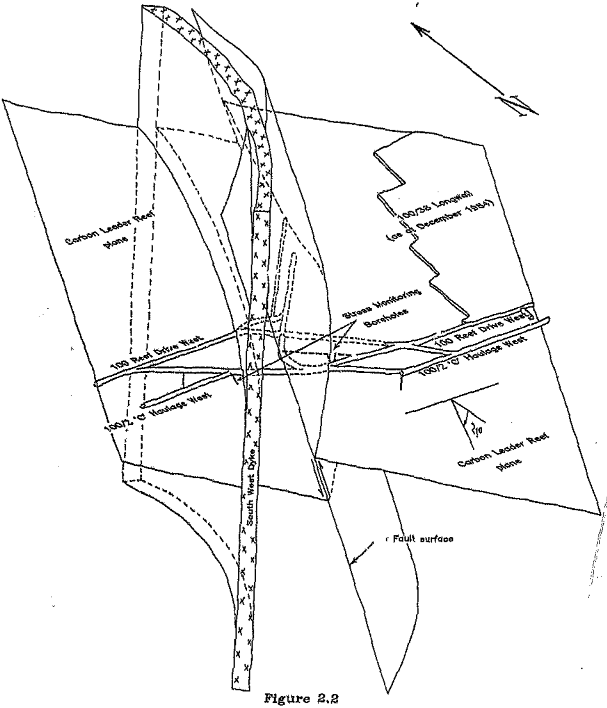

Figure 2.2

Perspective of *monitoring* site showing inferred geological structure

Scale 1:2500

or less conformable relationship with the surrounding rocks and dips at an angle of 21 degrees to the south-south-east.

The rocks underlying the Carbon Leader Reef are known locally as footwall quartzites. They are yellowish green to grey medium to coarse grained quartzites with occasional sericite partings and scattered grit bands. This quartzite grades slowly with depth into shaly quartzites and shales of the Jeppestown Formation, West Rand Group, which is defined to begin at the base of the North Leader, some 15 m below the Carbon Leader Reef.

The reef itself varies from 0 to 30 cm in thickness in the monitoring site area. It consists of closely packed, well rounded small to meduim quartz pebbles set in a dark grey matrix of quartzitic composition. Pyrite mineralization and occasional carbon are present in the matrix.

Immediately overlying the reef is 2 m of light grey fine to medium-grained highly siliceous quartzite. Overlying this quartzite is the 2 m thick layer of dark greenish grey chloritoid shale called the Green Bar. This layer is notorious for its rôle in creating bad hangingwall conditions in the mines of the Carletonville Goldfield. Above the Green Bar lies a thick succession of greenish grey medium to coarse grained quartzites with occasional pebble bands and sericite partings. These are referred to as hangingwall quartzites. The Ventersdorp Contact Reef lies some 900 m above the Carbon Leader Reef, and provides the second most important source of ore to the mine.

The strata are displaced by the Elf Fault and intruded by the South West Dyke described above. The fault plane contains about 10 cm of mylonitized quartzite and further north is intruded by stringers of igneous material. The South West Dyke is a fine grained , massive rock of andesitic composition, probably of Ventersdorp age. Both features are parallel to the major north-north-east south-south-west structural trend present in the Carletonville Goldfield. The Georgette Dyke, which is orientated along a direction approximately 15 degrees south of east intersects both features about 330 m to the north-east of stress monitoring positions (Figure 1.2). This dyke has a downthrow of 24 m to the north and has been left as a pillar because of mining difficulties associated with it. It is of similar composition to the South West Dyke and is probably also of Ventersdorp age. No other significant geological features are present in the site area.

Mining in the monitoring site area

The long-term mine plan showed that the 100/38 Longwall, if advanced at the mine average of 10 m per month, would reach the Elf Fault some 18 months after June 1984, when mining was expected to recommence. The overall longwall line was more or less parallel to the fault and dyke, which resulted in their being subjected to more or less uniform mining induced stresses for some 250 m along strike. This provided some flexibility in the placement of measuring instruments.

It was clear from the geometry that the fault would at all times be exposed to larger mining induced stress than the dyke as a result of the approach of the 100/38 Longwall (Figure 2.1). This consideration singled the fault out as the feature to be monitored during the period that the longwall advanced towards it.

The geometrical simplicity of the situation had the additional advantage that a less elaborate arrangement of instruments would be sufficient to carry out the measurements. The main disadvantage of the site was its remoteness, which introduced problems such as access and the reliability of compressed air and water supplies.

2.2 Measurements Planned for the Study

Most of the structural features developed in a rock mass are the result of the presence of stress. Consequently, the response of a rock mass at depth to any activity whether human or natural is almost purely driven by the ambient or changing stress field. S[illegible]asurements are therefore of central importance to the stu[illegible] Other important measurements include the deformational response of the rock mass to the changing stress field.

These embrace seismic monitoring and underground levelling together with visual checks of other evidence of rock mass deformation. Measurements of elastic constants of intact rock material were planned so that stresses could be estimated from the measured strains. This information, in conjunction with rock mass characterization was used to estimate the elastic constants for the rock mass. More detailed descriptions of stress measurements, seismic monitoring and rock mass deformation measurements follow below.

2.2.1 Stress measurement program

The planned program for stress measurements consists of three phases:

i) initial stress measurements for absolute stress data;

ii) stress monitoring to obtain change of stress data;

iii) final stress measurements, to provide absolute stress data in the situation where the longwall had reached the fault.

The three phases follow on from one another, beginning with the first and ending with the third phase.

The initial stress measurements define the stress state at the beginning of the project, to which are added by the principal of superposition the stress change data from the second phase. The third phase measurements provide a check on the stress change measurements as well as a comparison with data derived from the numerical analyses.

2.2.2 Seismic monitoring

The fault has no history of seismic activity whether natural, or induced by mining. The geometry of the situation, together with the steep dip of the fault suggests that mining induced seismicity may occur. Any seismicity that occurs in the area is recorded by the mine wide seismic system. This information provides a tool with which deductions about the stability of the fault can be made.

2.2.3 Rock mass deformation measurement

An underground levelling survey was planned to supply information on fault and rock mass movements in response to the mining induced stresses. Visual checks on fault movement such as the dislocation of paint strips across the fault plane traces in the underground excavations were planned to supplement the levelling data. Any other large scale movements visible in the excavations were to be recorded if and when they occured. The deformation data would assist in assessing the stability of the fault when subjected to mining induced stresses.

2.3 Description of Equipment

Equipment and instrumentation for the measurement of absolute stress, the monitoring of mining induced seismicity and underground levelling was available at the outset. This equipment and its operation is described briefly together with the limitations of both the equipment and the data derived from it. Instrumentation to measure long term stress changes was not available. The equipment selected and purchased is described in detail in Section 2.4.

2.3.1 Absolute stress measuring equipment

The absolute stresses at the beginning and end of the project were measured using the CSIR biaxial strain gauge-based system described by Leeman (1965b). This system was designed specifically for rock mechanics applications and results derived from it since its introduction in the early 1960's have enjoyed wide acceptance.

The CSIR biaxial stress measurement system
The equipment consists of three main components, namely, the *digital strain meter*, the *strain cell* installing equipment and the biaxial or "Doorstopper" strain cell. It is shown schematically in Figure 2.3.

The digital strain meter and manual point selector is manufactured by Hottinger Baldwin Messtechnik of West Germany. Connected w.th

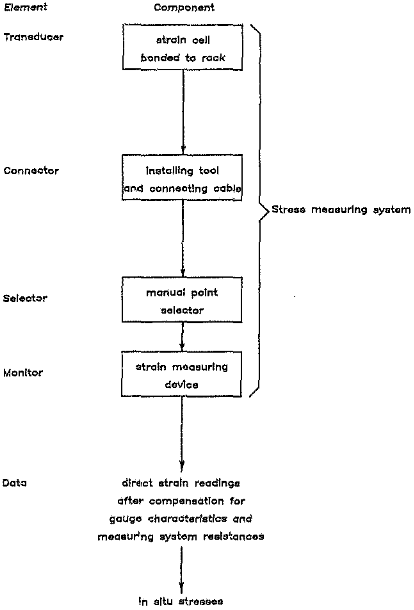

Figure 2.3

Schematic layout of CSIR stress measuring system the manual point selector a total of ten individual strain gauges can be measured by switching from one to the next. The strain gauge to be measured is connected in series in the installing tool to a "dummy" gauge glued to a piece of rock similar to the rock in which the measurements are being carried out. In this way temperature effects are eliminated. The two gauges form two limbs of a Wheatstone Bridge which is completed in the manual point selector by the addition of another two limbs with known resistances. This system enables the strainmeter to measure strains to the nearest microstrain with precision.

The digital strainmeter comprises a strain meter circuit which measures the voltage across the formed Wheatstone Bridge, a measuring amplifier and integral digital indicator, all of which are powered by built-in rechargeable batteries. The manual point selector consists of resistance circuitry to make up the remaining limbs of the Wheatstone Bridge circuit and a series of switches with highly reproducible transfer resistances. This reduces the error of measurement to a minimum when switching to different gauges. The output of the equipment is in the form of microstrain, which can be used directly when calibration to compensate for connecting cable and installing tool resistances has been carried out.

The installing equipment consists of the installing tool, aluminium rods and connecting cable. These are all detailed by the CSIR (1966).

The strain cells and their construction are described by Pallister (1969). Since that time the original three gauge rosette has been replaced by a TML PQ10 four-gauge rosette manufactured by Tokyo Sokki Kenkyujo Limited of Ja... This has allowed the individual measurements to be assessed for error (Section 3.2). Individual strain cells can be used only once, however their low cost enables many measurements to be taken without seriously affecting the total cost of a strain relief measurement program.

Measurement procedure

The measurement of absolute stresses in situ, using the CSIR *biaxial strain cell*, is carried out by the overcoring method which is illustrated in Figure 2.4. The rationale behind the technique is simple. When a borehole is drilled by diamond rotary coring methods into a stressed rock mass the core that is removed is no longer subject to the ambient stress field. As a result, it will expand or contract slightly, depending on the nature of the stress field it has been removed from. If the strain in the core is known both prior to and after its removal from the rock mass, the difference between the two strains can be used to estimate the stress. The strain difference is called a strain relief because it is the result of the relieving of stress in the core by extending the borehole beyond the measurement point. This process is called overcoring and gives the technique its name. Details of the practicalities of obtaining strain relief data are reported by the CSIR (1966) and Pallister (1969).

The strain reliefs are then used to estimate the stresses present at the end of the borehole using relations available in solid mechanics theory. These stresses are not equal to the stresses acting within the rock mass but are related to them by the following equations:-

$$\sigma_1' = a\sigma_1 + b\sigma_2 + c\sigma_3 \qquad \ldots\ldots\ldots 2.1$$

$$\sigma_2' = b\sigma_1 + a\sigma_2 + c\sigma_3$$

Where a, b, and c are stress concentration factors, σ_1, σ_2, and σ_3 are the principal stresses in situ and σ_1' and σ_2' are the principal stresses measured at the borehole end.

The above relations are given assuming that the borehole is aligned parallel to the minor principal stress. The stress concentration factors are still the subject of research because they are sensitive to a number of variables, the effects of which have as yet not been completely explored. The individual is therefore left to ascertain empirically the values of stress concentration factors best suited to the conditions under which the measurements were made. This aspect is dealt with in Section 3.4.2.

The stress state in two dimensions only is determinable from measurements taken in one borehole. The three dimensional stress tensor is obtainable from two non-parallel boreholes if these

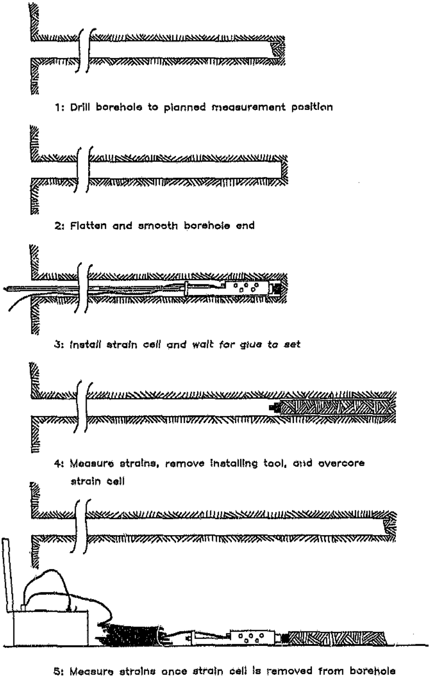

Figure 2.4

Example of overcoring technique

have been drilled along principal stress directions. Generally, measurements must be carried out in at least three non-parallel boreholes in order to determine the three dimensional rock stress tensor (Gray and Toews, 1968).

Limitations of equipment and technique

The strain measurement equipment is complex and operates on low voltages and currents. It is therefore sensitive to temperature, humidity and the ingress of moisture, which can introduce unnecessary error into the results. The equipment should be stored on surface when not in use underground to avoid these complications.

At least two, and generally three boreholes must be drilled to determine the three-dimensional stress tensor. This often limits the number of prospective sites from which the measurements can be done. It also introduces variability into the results because stress is usually not uniformly distributed throughout a rock mass, especially in areas where fracturing and differing rock types are present. Typically, the rock stress tensor is determined with an error of 20% when using this technique (Pallister, 1969). The errors that arose during the measurements and their sources are detailed in Section 3.2.

2.3.2 The seismic monitoring system

Western Deep Levels Limited has operated a seismic monitoring system since 1974. It is capable of locating any seismic event with a Richter Magnitude of 0,0 or greater that occurs on the mine property, with an average accuracy of 50 metres. The purpose of the system is to provide mine management with a tool to direct rescue efforts in cases of damaging seismic events as well as to help identify areas and geological features that are hazardous to mining from a seismic point of view. The data are also used for statistical and research purposes.

The energy emanating from a seismic source is registered by a total of sixteen geophones and accelerometers located at the positions shown in Figure 2.5. These are linked to a Hewlett-Packard HP1000 computer system on surface by a cable network

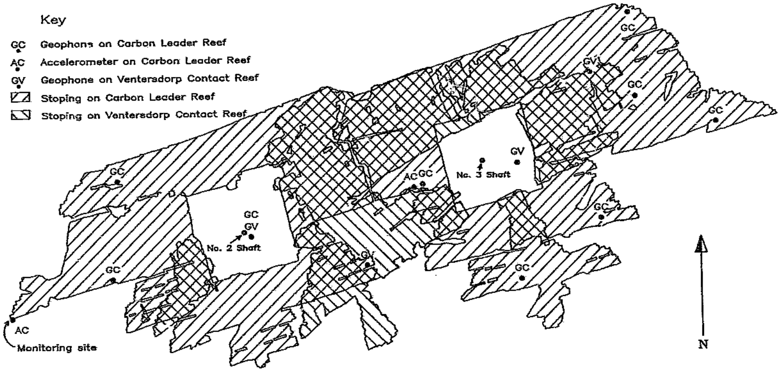

Figure 2.5

Geophone and accelerometer positions at Western Deep Levels Limited

Scale 1:30000

as shown in the schematic layout in Figure 2.6. A seventeenth geophone, positioned on surface is used to determine the energy released by each event and hence its magnitude.

Location procedure

Once the seismic traces have been transmitted to surface they are translated to digital information and stored temporarily. Members of staff at the Rockburst Project then call the seismic traces for a particular event to a screen in order to determine the p- and s- wave onsets for each geophone or accelerometer. This information is then read by a location program which determines the position of the source of the seismic energy in terms of the mine co-ordinate system. The located event is then transferred to the computer-run data base.

Limitations of the system

The computer digitizes all the incoming seismic traces from a single event for two seconds. If more than one seismic event occurs within this period, their traces become mixed in the temporary storage and a location is usually impossible from the information received. About 0,1% of the seismicity is lost this way.

The Carbon Leader and Ventersdorp Contact Reef horizons are both exploited by the longwall system which offers few opportunities of locating sensors ahead of advancing longwall faces. Seismicity that occurs on the eastern and western extremities on the mine cannot be located with an accuracy of less than 50 m because most of the events lie beyond the sensor network. The error of the locations in the monitoring site area was affected by this phenomenon until an accelerometer was placed there. Location accuracies then improved to about 30 metres.

Most of the sensors are coplanar, and this can sometimes lead to large location errors in the vertical. The location accuracy of the system makes it difficult to implicate a particular structure from the event location alone. Visual inspection underground is always necessary to confirm a location if a particular geological feature is suspected of being the source.

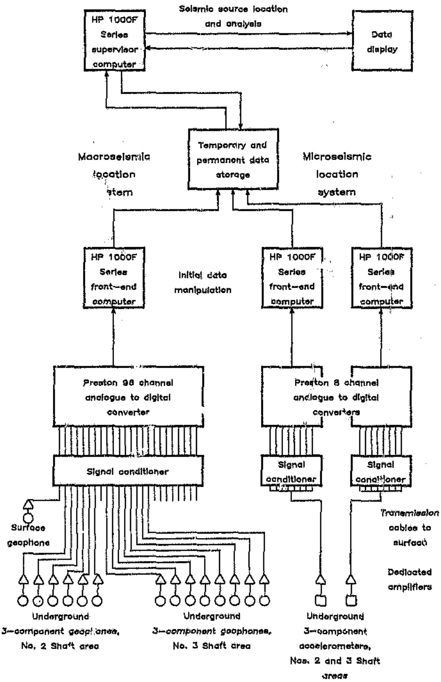

Figure 2.6

Schematic layout of seismic location system

2.3.3 Levelling equipment

A Kony Ni 007 automatic precision level fitted with a micrometer and automatic compensator was used. The level is capable of levelling to an accuracy of +/- 0,5 mm over 1 km when using graduated invar levelling staves.

The invar staves were suspended by a spherical ball and seat arrangement attached to a series of rockbolts that were installed in vertical drillholes above 100/2 'C' Haulage West (Figure 2.7). The *length of the profile* levelled was 2[illegible]0 m. The anchor points of the rockbolts were on average 2,5 m above the haulage roof, where effects such as bedding separation were expected to be very small.

Measurement procedure

The rise and *fall method of inverted levelling* is employed in which the relative elevations of two rock anchors are determined with the level. This procedure is repeated until all the anchors in the traverse have been covered, at which point the process is repeated in a back traverse until the starting point has been reached.

Limitations of procedure

All the measurements are relative, and in the vertical sense only. No horizontal movements can be measured using this method.

2.4 Stress Change Measurement Equipment

Stress monitoring is of central importance to the project, and this necessitated careful consideration of the available instrumentation before a choice could be made. The instrumentation for underground application is first reviewed briefly and the reasons for the choice of the IRAD vibrating wire stressmeter system are then discussed. The equipment selected is then described together with particulars of its installation and operation. Finally the limitations of the instrument are discussed.

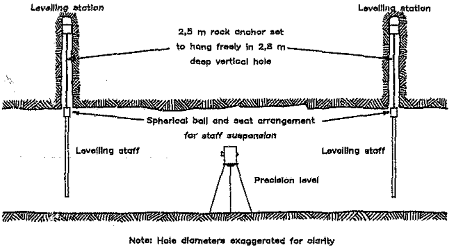

a: Method

Scale 1:100

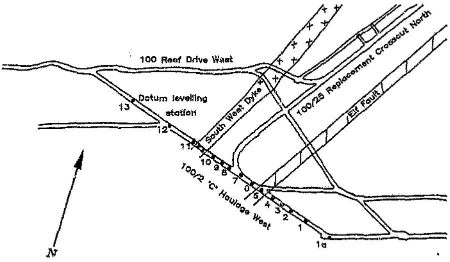

b: Levelling station positions

Scale 1:2500

Figure 2.7

Details of method and layout of levelling survey

2.4.1 *Brief review of stress change measuring instruments*

Leeman (1965b) noted that prior to that date most borehole stress measuring instruments had been developed specifically for the measurement of stress changes, and that a few had been designed for the measurement of *absolute stress.* He divided the instruments into three broad classifications according to the quantities they measured as follows:-

i) borehole deformation gauges
ii) borehole inclusion stressmeters
iii) borehole strain gauge devices.

This review is based upon the above three classifications, and locally available instruments falling into each class are discussed.

Borehole deformation gauges

Borehole deformation gauges include the CSIR triaxial strain cell described by Leeman (1968), the USBM borehole deformation cell described by Merrill (1967), and the CSIRO hollow inclusion stress cell described by Worotniki and Walton (1976). All the gauges listed were designed specifically for the determination of the absolute stress by the measurement of strain reliefs in the rock annulus surrounding the borehole in which they are installed.

Change in stress in a rock mass results in a corresponding change in strain, which could be measured by these instruments. Pariseau (1978) and Amadei (1985) have described solutions for the assessment of in-situ stress changes from measured borehole deformation changes.

The gauges discussed have the advantage that a single gauge is capable of sensing biaxial stress changes in the case of the USBM borehole deformation cell and triaxial stress changes in the case of the CSIR and CSIRO cells. However all these gauges are complex, and were not designed to withstand long term exposure to harsh conditions. Amadei (1985) hints at this by proposing a device based on the principles of the CSIR and CSIRO cells, but capable of long-term reliability and stability with respect to creep, temperature and moisture.

Borehole inclusion stressmeters

This type of instrument comprises a stiff element which is wedged into a borehole either by mechanical or hydraulic means. Changing stresses result in a deforming rock - borehole - gauge system which can be monitored by measuring deformations in the gauge. Stress changes in the surrounding rock mass can then be found by functions relating gauge deformations to rock stress changes. A number of examples of this type of gauge are described by Leeman (1965b) and Obert and Duvall (1967).

The *vibrating wire stressmeter described* by Hawkes and Hooker (1974) and Sellers (1977) is an example of a borehole inclusion stressmeter that has become commercially available because of its success in use. It has the advantage of being tough and reliable, exhibits little or no drift in the long term and can be used in a wide variety of circumstances. It is disadvantaged by being sensitive only to uniaxial stress changes.

Borehole strain gauge devices

The only instrument of this type locally available is the CSIR biaxial strain cell discussed earlier. This cell was designed to measure absolute stress and would tend to suffer the same disadvantages as the borehole deformation strain cells.

2.4.2 Selection of the vibrating wire stressmeter

Mining in the monitoring site area indicated that stress change measurements would be necessary for a period of at least eighteen months or longer. This meant that the instrument chosen would be exposed to the harsh underground environment for this period, and may furthermore be subjected to the shocks from mining induced seismicity.

The requirements for such an instrument are that it should be:-

i) tough and reliable;

ii) resistant to humidity, corrosion and temperature;

iii) stable in the long term;

iv) *capable of sensing small* stress changes while at the same time having a large range;

v) installed without undue difficulty;

vi) able to measure at least biaxial stress changes.

The borehole deformation strain cells would meet the first requirement as well as the last three. *Since the CSIR and CSIRO cells rely* on an epoxy resin for borehole deformation measurement, the performance of these glues must be called into question especially when used in a hot moist environment, where the distinct possibility exists that they may lose their strength in the long term. Furthermore, the stability of the gauges in the long term *is questionable* as is their resistance to moisture. The same arguments apply to the CSIR biaxial strain cell. The USBM borehole deformation cell is at an advantage here because it does not rely on glues for contact with the borehole sidewalls.

The vibrating wire stressmeter meets the first five requirements listed above, and the last requirement by installing three stressmeters in different directions in the same borehole. Sellers (1977) demonstrated clearly the reliability of the instruments in applications varying from longwall coal mining to cut and fill stoping and block caving mining environments.

Since all the other instruments reviewed would introduce a real chance of failure to stress change measurements in the long term, it was decided to use the vibrating wire stressmeter.

2.4.3 *Description of the vibrating wire stressmeter* system

The system was manufactured by IRAD Gage of Lebanon, New Hampshire, U.S.A. and consists of the stressmeters, installing equipment and readout instrumentation.

The vibrating wire stressmeter

The transducer consists of a thick-walled cylinder across which a high tensile steel wire is tensioned. The construction is shown in Figure 2.8. It is wedged into a borehole by the wedge and platen assembly shown, and any borehole deformation causes

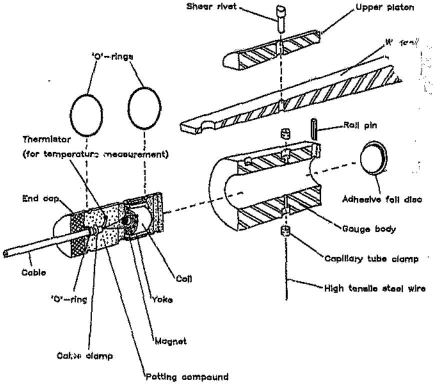

Figure 2.8

Construction of vibrating wire stressmeter

(After Hawkes and Hooker, 1974)

the stressmeter body to flex much like a proving ring, which in turn brings about changes in tension in the wire.

If excited in some way, the wire will vibrate with a frequency related to its tension, much in the same way as the strings of a violin. The period of the wire, that is the time it takes the wire to complete one cycle of vibration is related to its tension, length and density by a relation given in Hawkes and Hooker (1974). The vibration period of the tensioned wire is determined by an electronic instrument described below.

The stress changes in the rock are represented by changes in the vibrating wire period, which increases positively with an increas[illegible]essive stress. The gauge is unidirectional, that [illegible]se only uniaxial rock stress changes in a direction [illegible]t with that of the tensioned wire. The uniaxial stress change that may take place in a rock mass is related to the initial vibrating wire period T_o taken at time t_o, and the period T taken at time t by the equation (after Hawkes and Hooker, 1974):-

$$\Delta\sigma_r = \frac{1}{\alpha}\left[1-\left(\frac{To}{T}\right)^2\right]\left[\frac{3,507}{To}\right]^2 \text{ Pa} \qquad \text{.........} \; 2.2$$

where $\Delta\sigma_r$ = uniaxial rock stress change in the direction of the vibrating wire stressmeter;

α = dimensionless stress sensitivity factor given by $\alpha = 9,4 - 0,073E_r$ where E_r is the rock modulus of elasticity in GPa;

To = initial vibrating wire period reading in seconds;

T = [illegible]g wire period in seconds measured at time t.

The wire is tensioned by the manufacturer to vibrate with a period of 150 to 220 x 10^{-6} seconds when the gauge is undeformed. The maximum period that can be reliably measured in 450 x 10^{-6} seconds. The maximum usable range of the stressmeter thus lies between those two extremes, which represents a maximum measurable uniaxial stress change of 97 MPa if set in a rock mass with a modulus of elasticity of 60 GPa. If biaxial and triaxial stress changes are required, a minimum of three and six gauges respectively, each set in a different direction, are necessary.

The gauge itself is relatively insensitive to temperature changes because the tensioned wire and the gauge body have similar coefficients of expansion. When the stressmeter is set in a rock mass whose temperature is changing, a correction is required to account for the different coefficients of expansion of the rock material and gauge body. If required, the stressmeter is equipped with a thermistor that works on the Wheatstone Bridge principle in order to measure temperature changes. The correction factor in the vibrating wire period for temperature changes in most rocks is roughly $-0,2 \times 10^{-6}$ seconds for each °C rise in temperature (Sellers, 1977).

The gauges are designed for use in a standard EX diamond drilled borehole. They are simple, tough, moisture and corrosion resistant, and reliable. Further details of manufacture and performance are given by Sellers (1977).

The installing equipment

The installing equipment used is hydraulically operated. It consists of a pump, pressure gauge, hydraulic cable with reel, setting rods and a hydraulically operated setting tool. The complexity of this equipment renders it impossible to be illustrated effectively, and the reader is referred to Sellers (1977).

The setting tool holds the gauge and wedge assembly to be installed in a borehole in a split cylindrical housing at the front. A shear rivet holds the wedge assembly together which in turn is linked by a pin to the hydraulic piston assembly. The function of the tool is to permit correct orientation of the gauge and wedge assembly in the borehole, to pull the wedge back to provide diametral expansion of the gauge-wedge assembly to affix it in the hole, and to disengage the pin mechanism from the wedge so that the setting tool can be retracted from the installed gauge. The procedure is carried out by operating the hydraulic pump at the borehole collar. The process of setting a gauge in a borehole is illustrated schematically in Figure 2.9, and described below.

No provision is made for orientating the gauges accurately in

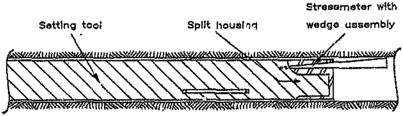

1: Advance setting tool with mounted stressmeter to required position in borehole

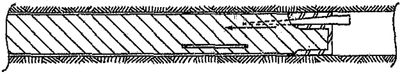

2: Retract wedge *hydraulically until stressmeter is firmly wedged* in borehole

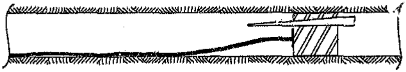

3: Release and retract setting tool, leaving stressmeter wedged in borehole

Figure 2.9

Vibrating wire stressmeter setting procedure

Scale 1:2.5

the borehole, however the installing rods are fitted with bayonet type couplings which maintain a precise rod-to-rod orientation. The coupling of the last rod protruding from the borehole when the setting tool and stressmeter are at the installation depth is thus used as a reference for gauge orientation.

Vibrating wire stressmeter readout

The readout instrumentation was originally designed for use in coal mines. This necessitated the development of an intrinsically safe electronic system for "plucking" the wire and then measuring its natural period of vibration.

The requirements resulted in a sophisticated electronic system which emits pulses of varying frequencies, and detects the resulting response of the tensioned wire. As soon as a pulse of frequency equal to the wire vibration frequency is emitted, and a response is obtained, the circuitry "locks on" to this resonant frequency and provides further pulses until the wire vibration is of sufficient amplitude to permit the measurement of its period. A hundred cycles of vibration are then timed and the period, in units of 10^{-6} second, appears on the digital display. An extremely stable and accurate crystal oscillator is built into the circuitry for timing purposes which means that the display readings are of an absolute nature, with no compensation required.

The readout unit is built into a rugged waterproof box and is powered by rechargeable batteries. A readout unit manufactured by a rival manufacturer together with a vibrating wire stressmeter and wedge assembly are shown in Figure 2.10.

2.4.4 Stressmeter installation and monitoring

Installing and monitoring stressmeters is relatively straightforward. The steps taken to install a stressmeter are briefly listed below:

i) drill a standard EX (38 mm diameter) borehole to the desired depth. A maximum of 35 m is possible with the available equipment

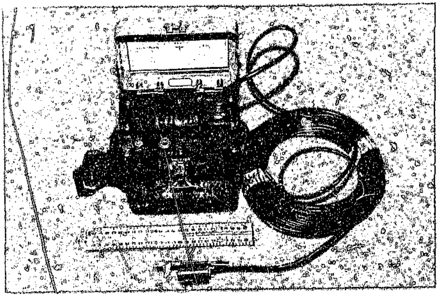

Figure 2.10
Vibrating wire readout box with stressmeter

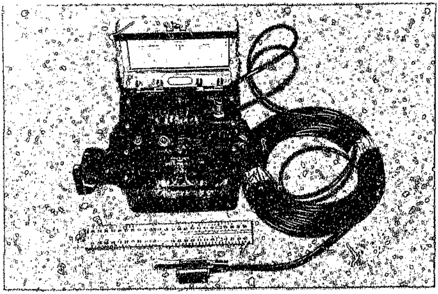

Figure 2.10

Vibrating wire readout box with stressmeter

ii) clear the borehole of any debris using water or compressed air

iii) take the vibrating wire period reading of the stressmeter to be installed

iv) thread the stressmeter cable through the setting tool in grooves provided, and when complete mount the stressmeter in the split housing at the front

v) connect wedge assembly to retracting pin assembly and retract pin by activating hydraulic pump gently until platen rests firmly against setting tool housing

vi) insert setting tool and vibrating wire stressmeter assembly in borehole and push up to desired depth

vii) connect readout unit to protruding stressmeter cable and switch readout on

viii) orientate stressmeter in desired direction

ix) activate pump, this causes hydraulic system to retract wedge further, wedging stressmeter in borehole. The vibrating wire period reading should increase while this is occuring as the stressmeter becomes compressed by the wedge. The pressure gauge reading should also increase

x) continue to slowly increase pressure with the pump until the shearing rivet is sheared off. This event can be clearly observed by the sudden drop in the hydraulic pressure reading on the gauge

xi) continue to increase pressure slowly until the vibrating wire period reading is 10 to 20 x 10^{-6} seconds greater than the reading taken before the stressmeter was inserted in the borehole

xii) release pressure in the hydraulic system by opening the valve on the pump.

The stressmeter should be firmly wedged in the borehole and the setting tool free to be removed. A maximum of three stressmeters, set in differing directions can be set in one borehole in this way. It is assumed in the method described that the stress changes to be measured are compressive. If tensile stress changes are expected, the stressmeter should be compressed to a greater extent by retracting the wedge further in order to prevent the gauge from coming loose at an early stage.

The vibrating wire period reading taken at the time the setting tool is removed from the hole is known as the "lock-off" reading and should be recorded for reference. There is usually a settling-in period ranging from a few hours to a few days in which the vibrating wire period readings are observed to drop slightly. The stressmeters should be monitored regularly during this period in order to identify the point at which settling is complete. This reading is then taken as the initial period reading, and all subsequent readings and stress change calculations are made with reference to it.

Subsequent monitoring of installed stressmeters consists of regular visits to the boreholes where the vibrating wire period readings are taken and recorded. This operation is simple and no special skills are required.

2.4.5 Limitations of the equipment

The term stressmeter implies that the gauge should be capable of measuring stress change in a solid medium without any knowledge of its elastic properties. Leeman (1965a) investigates this aspect and shows that if the stressmeter-rock modulus ratio is greater than five, only an approximate knowledge of the rock mass modulus of elasticity is necessary.

The modulus of elasticity of the quartzites at the monitoring site is of the order of 70 GPa while that of the vibrating wire stressmeter was calculated to be 130 GPa (after Hawkes and Hooker, 1974). The criterion given by Leeman (1965a) is therefore not met, and an accurate knowledge of the rock mass modulus of elasticity is necessary.

The degree of accuracy required is demonstrated by the set of curves presented in Figure 2.11. They were determined by assuming the rock mass modulus of elasticity is known with a certain percentage error, and then determining the corresponding error in the stress sensitivity factor introduced by Hawkes and Hooker (1974) and presented earlier.

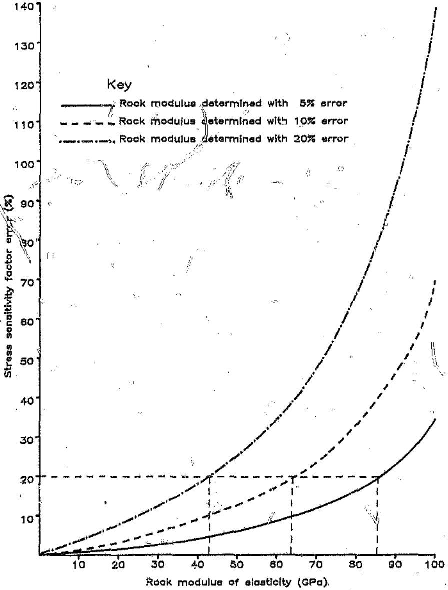

Figure 2.11

Plot of stress sensitivity factor error versus rock modulus of elasticity

The curves show that if the stressmeters are set in stiff rocks the modulus of elasticity must be known with increasing accuracy. This is often an impossible task because of the well known variability of the static elastic constants of rock.

If an error of stress change determination of 20 per cent is acceptable, and the modulus of elasticity of the rock can be determined with a 10 per cent error, then the use of the stressmeter should be confined to rocks with elastic moduli of less than 64 GPa. The possibility of measuring stress changes in the South West Dyke was therefore not considered because the intact rock material was found to have an elastic modulus of 95 GPa.

A further limitation of the stressmeter is its ability to measure uniaxial stress changes only in the plane perpendicular to the borehole axis. Biaxial stress change measurements are possible by setting a minimum of three gauges in one borehole, while triaxial stress change measurements require a minimum of nine gauges set in three non-parallel boreholes.

2.5 Design of Borehole and Instrument Layout

A triaxial rock stress tensor determination using the CSIR biaxial strain gauge based system generally requires the measurement of strain reliefs in at least three nonparallel boreholes (Gray and Toews, 1968). In the special case where the principal stress directions are known, a minimum of two boreholes drilled along principal stress directions are sufficient.

Additional requirements are that the measurements should be carried out in relatively unfractured rock remote from extensive mining excavations; adequate supplies of compressed air and water should be available; the working conditions should be safe; the borehole and drill machine positions should cause the minimum of interference with routine mining operations; and negligible mining induced stress changes should occur during the course of the measurement program.

The curves show that if the stressmeters are set in stiff rocks the modulus of elasticity must be known with increasing accuracy. This is often an impossible task because of the well known variability of the static elastic constants of rock.

If an error of stress change determination of 20 per cent is acceptable, and the modulus of elasticity of the rock can be determined with a 10 per cent error, then the use of the stressmeter should be confined to rocks with elastic moduli of less than 64 GPa. The possibility of measuring stress changes in the South West Dyke was therefore not considered because the intact rock material was found to have an elastic modulus of 95 GPa.

A further limitation of the stressmeter is its ability to measure uniaxial stress changes only in the plane perpendicular to the borehole axis. Biaxial stress change measurements are possible by setting a minimum of three gauges in one borehole, while triaxial stress change measurements require a minimum of nine gauges set in three non-parallel boreholes.

2.5 Design of Borehole and Instrument Layout

A triaxial rock stress tensor determination using the CSIR biaxial strain gauge based system generally requires the measurement of strain reliefs in at least three nonparallel boreholes (Gray and Toews, 1968). In the special case where the principal stress directions are known, a minimum of two boreholes drilled along principal stress directions are sufficient.

Additional requirements are that the measurements should be carried out in relatively unfractured rock remote from extensive mining excavations; adequate supplies of compressed air and water should be available; the working conditions should be safe; the borehole and drill machine positions should cause the minimum of interference with routine mining operations; and negligible mining induced stress changes should occur during the course of the measurement program.

In the case of the stress monitoring program the two major requirements are that readily measurable stress changes are induced by mining while at the same time safe and easy access to the measuring boreholes is maintained. The nature of the project and its conflicting requirements imposed such severe limitations on the choice of the measurement site that some of the requirements had to be compromised.

2.5.1 Borehole layout

The borehole locations were controlled by the position of the fault. The excavations in which they could be located were found to be 100 Reef Drive West and 100/25 Replacement Crosscut North (Figure 2.1). The return airway was rejected because fans and coolers were located at the fault exposure and the excavation was unsupported. Moreover, it was to be abandoned as soon as mining induced stresses made it unsafe.

The crosscut provided access to the fault for some 200 m on strike. However, near its northern extremity, measurements would be difficult because of mining activity and the fact that the limitations of the stress measurement and monitoring equipment precluded their use in boreholes beyond 35 m in depth. Boreholes therefore orientated at 90 degrees to the fault strike would be necessary, but this would make assessments of the shear stress on the fault plane impossible. Boreholes angled at say 45 degrees to the fault strike would result in stress and stress change measurements being made too far from the fault plane. This conclusion was drawn at the time because it was not known that the fault changed from a north-east to a northerly trend, as shown in Figure 2.1 .

The measuring site position was therefore located ahead of the southernmost panel of the 100/38 Longwall. This position was not considered to be ideal, but it did have the advantage of guaranteed long term access and minimum interference with mining. Furthermore, the instruments would not be far removed from the reef plane in the vertical, and therefore the maximum stress changes induced by mining, as would have been the case further to the north.

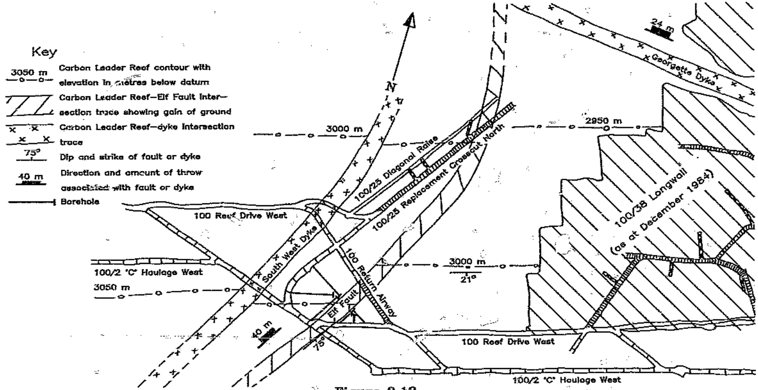

Figure 2.12

Proposed stress measurement boreholes at the monitoring site

Scale 1:2500

The fault in this area is straddled for about 5 m on either side by a zone of fairly intensely fractured rock in which measurements would produce highly variable results. Measurements were planned in less fractured rock at least 5 m away from the fault plane which meant that inference of conditions at the fault plane itself could best be made by averaging results obtained from both sides. This of course would never produce a clear picture of conditions on the fault plane, but would provide an indication of the stresses transmitted to it by the surrounding rock mass.

In order to eliminate the risk of shear dislocation of boreholes drilled through the fault plane, three on either side were planned parallel, at 45 degrees and perpendicular to the strike of the fault (Figure 2.12). The converging layout shown was chosen because it had the advantage of minimising stress and stress change measurement errors that may arise from the spatial variation of rock elastic constants and field stresses. Horizontal boreholes were specified because it was expected that vertical stresses and stress changes would be largest and therefore measured with the smallest error.

Circumstances at the time of the commencement of the project did not permit the drilling of all six boreholes as planned. Mining of the 100/38 Longwall recommenced in June 1984 while an underground drill only became available in August 1984. The absolute stress measurements were therefore in danger of being subject to increased error resulting from stress changes induced by mining.

Fortunately Leeman (1968) and Gay (1972) had both carried out absolute stress measurements about 3 km east and 3 km west of the monitoring site respectively. Their results, presented in Table 2.1 and represented graphically in Figure 2.13, show in both cases that the minor principal stress were both fairly close to the horizontal and lay in directions parallel and perpendicular to the strike of the Elf Fault. The vertical stress at each site agreed fairly well with the theoretical overburden stress in both cases. These results enabled the autho[illegible] me that conditions were similar at the monitoring [illegible] consequence that the two boreholes angled at 45 d[illegible] the fault

TABLE 2.1: VIRGIN ROCK STRESSES IN THE CARLETONVILLE AREA

MEASURED by	LOCALITY	DEPTH BELOW SURFACE (m)	σ_{ob} (MPa)	σ_v (MPa)	σ_h / σ_v	STRESS	MAGNITUDE (MPa)	PLUNGE (degrees)	PLUNGE Direction (degrees)
Leeman (1968)	Western Deep Levels Limited	1770	48,5	55,1	0,59	σ_1 σ_2 σ_3	55,2 30,6 13,0	70 26 11	280 126 28
Gay (1972)	Doornfontein Gold Mining Company Limited	2320	63,5	56,8	0,54	σ_1 σ_2 σ_3	62,5 40,5 19,5	70 5 15	285 30 120

NOTES

i) σ_{ob} = theoretical vertical stress due to overburden weight.

ii) σ_v = vertical component of normal stress calculated from measurements.

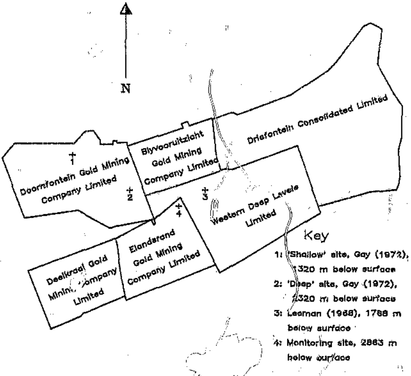

a: Locations of stress measurement sites

Scale 1:200000

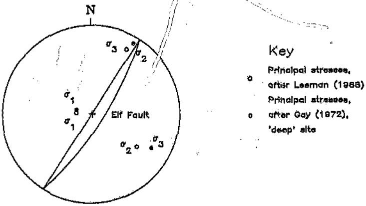

b: Lower hemisphere stereoplot of principal stress directions and Elf Fault

Figure 2.13

Absolute stresses measured in the Carletonville Goldfield strike could be eliminated in order to speed up the absolute stress measurements. This compromise meant that the stress change measurements would only be meaningful in the planes perpendicular to the remaining borehole axes, if the assumptions about the stress state in the vicinity of the Elf Fault were invalid. The borehole used to measure the final absolute stresses is situated next to and parallel to Borehole RB1

A horizontal control borehole was located to the west of the South West Dyke where mining induced stress changes were expected to remain small for the duration of the project. A single vibrating wire stressmeter orientated vertically was planned to measure mining induced stress changes in the far field where rock mass behaviour was expected to be elastic.

The accelerometer was originally planned to be located in RB5. The location had to be changed to RB8 because the new fan chamber was to be relocated next to RB5, where mechanical vibrations would interfere with the accelerometer output. The locations of all the boreholes appear in Figure 2.1.

2.5.2 Borehole sizes

The four boreholes drilled at the Elf Fault are NXCU boreholes which produced core 72 mm in diameter from a hole 92 mm in diameter. This size of borehole was chosen so that intact test specimens could be extracted from the core parallel to the measurement directions for laboratory determination of the elastic constants.

The vibrating wire stressmeters require an EX borehole 38 mm in diameter. These holes were drilled as extensions to the NXCU boreholes once the absolute stress measurements were completed. The control borehole is a standard AX borehole from which an EX borehole was drilled to accommodate the stressmeter at the required depth. The accelerometer requires an NX borehole of diameter 76 mm.

2.5.3 Instrument layout

A cluster of three stressmeters set in the horizontal-45 degrees-vertical pattern was planned for the EX extension of each stress measurement borehole. The distances between the stressmeters was set at a minimum of 0,2 m so that all were exposed to true borehole deformations. The layout for each borehole is shown in Figure 2.14. A thirteenth stressmeter was installed in a control borehole while a fourteenth was kept on surface as a reference.

2.5.4 Limitations of borehole layout

The chief limitation of the borehole layout is that both stress and stress change measurements would be representative of conditions on the fault plane at the monitoring site only. Since it is close to the southern abutment of the longwall, the stress change patterns would not be representative of the fairly uniform loading of the fault by the advancing longwall further to the north. As mentioned earlier, the geometry of the situation together with mining activity considerations prohibited the possibility of any further meaningful measurements from 100/25 Replacement Crosscut to the north of the monitoring site.

The layout as shown is capable only of secondary principal stress change determinations in planes normal to the borehole axes. Thus, incomplete stress change information was obtained, which could conceivably be misleading when assessing the fault stability as the longwall approached it.

2.6 Numerical Modelling

The monitoring site layout and the nature of the measurement results obtained necessitate the use of numerical modelling techniques not only to provide background information to the measurements but also to supplement them and provide a comparator for them.

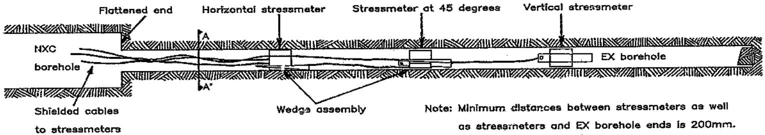

a: Plan

Scale 1:5

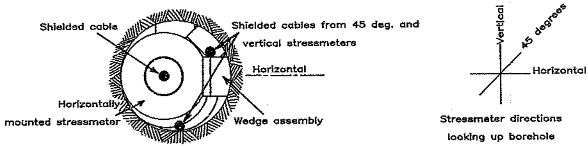

b: Section A–A'

Scale 1:1

Figure 2.14

Layout of stressmeters in Boreholes RB1 to RB4

The MINSIM - D suite of computer programs developed for the South African Mining Industry by the Chamber of Mines Research Organization is most suitable for the analysis at hand. It is designed to analyse stress and displacements around the tabular excavations typical of most coal and gold mines in South Africa.

2.6.1 Description of the MINSIM-D stress analysis program

The suite of programs comprises two main processing programs named SOLUTION and BENCHMARK which are supplemented with data input and graphic output programs. The SOLUTION program generates closure and ride solutions for a particular mining geometry and the BENCHMARK program calculates stress and displacements at requested points on and around the mining excavations.

The programs are based on the theory of boundary elements which is applied to the mining layout and the assumption that the rock enclosing the orebodies behaves elastically. They are capable of application to single and multiple reef problems at any orientation and at any depth. Dislocated reefs may also be modelled.

The main output is derived from the BENCHMARK program, and a wide variety of parameters are available to assess the state of stress at a benchmark point. These may be selected by the user to suit the needs of the problem being analysed.

MINSIM-D is described comprehensively by the Chamber of Mines Research Organisation (1985) as well as Ryder and Napier (1985), while the analytical model used to generate the required data is described in Section 5.1.

2.6.2 Limitations of the program

The programs are based on the assumption that the rock in which the mining is taking place is homogeneous, isotropic, linearly elastic and intact. The rock mass is further assumed to have infinite strength. Rockmass features such as changing elastic constants both in space and time, discontinuities, layering, intrusives, anistropy, non-linear elastic behaviour and even inelastic behaviour after failure cannot be accounted for. Nevertheless, the information is still useful because comparisons with measurements provide some idea of the combined effects the features typical of all rock masses may have on their behaviour.

2.7 Concluding Remarks

The instrumentation used for the underground measurements was not compromised because of the severe demands placed on it by the conditions in use. Any inadequacies could result at best in spurious results and at worst in the total failure of the study.

The general inaccessibility of the rock mass ahead of advancing longwalls, the demands of mining and the conflicting requirements of stress measurement and stress change monitoring, forced a number of compromises in the underground layout of the instrumentation. As such, the *stress measurements* are *not* as complete as originally envisaged, and therefore greater reliance on numerical modelling was necessary than had been originally planned.

CHAPTER 3

INITIAL AND FINAL STRESS RESULTS

The prime object of this chapter is to report unbiased initial and final stress estimates for the monitoring site. The estimates are based on strain relief readings, rock elastic constants and rockmass structure as well as observations of the prevailing underground conditions. First the borehole logs and the resulting rockmass characterization are discussed, after which the strain relief readings are presented and analysed. The laboratory determination of rock elastic constants is covered and then the initial and final stress estimates are given. These are in good agreement with stresses resulting from the overburden weight, in keeping with several other in situ stress measurements carried out in deep gold mines.

3.1 Borehole Logs

Detailed logs of Boreholes RB1 to RB5 were kept in order information of the nature of the rock mass in the monit site area. Descriptions of the rock mass features observed the core conform to the standards laid down by the Core Logging Committee of the South Africa Section of the Association of Engineering Geologists (1976). The logsheet designed for the purpose is similar to that described by Page et al (1976), with modifications to suit the data most relevant to the project.

Particular attention was paid to the description of discontinuities because they have a strong influence on the elastic properties of the rock mass. An attempt was made to classify each discontinuity according to its origin. The classes chosen were mining induced fractures, fractures that developed during the drilling process and natural discontinuities that were present in the rock prior to mining. The latter class was further subdivided according to the nature of the discontinuity, for example faults, joints, bedding planes and geological contacts between different rock types. The frequency in each discontinuity class present together with the general inclination range were noted for each metre of core. Other features such as filling in discontinuity planes, discontinuity surface roughness, spacing and the number of discontinuity sets were noted.

Assessments of material recovery, core recovery and RQD (Deere, 1964) were made for each drilling run. A geological description of the core and notes of rock mass classification were allotted space on the right hand side of the log sheet. The completed borehole logs appear in Appendix A, while the major features of the rock mass deduced from the borehole logs appear in Table 3.1.

3.2 Strain relief data

Four strain relief measurements spaced directionally at 45° to each other are obtainable from the "Doorstopper" strain cell. This facility provides the researcher with a tool to assess the error inherent in the strain reliefs, and a means of averaging the normal and shear strains derived from each overcored strain cell. Typically, errors are fairly large and are therefore the subject of detailed discussion. The analysis that follows first deals with a means of rejecting certain measurements and finally considers the accepted measurements.

3.2.1 Definition of quantities measured

Before commencing with the analysis, it is necessary to define a standard applicable to all the stress and strain analyses throughout. As far as the notation of stress and strain components are concerned, the standard rock mechanics convention is applied (Jaeger and Cook, 1979).

The stresses and strains in each borehole are described with reference to a set of Cartesian axes as shown in Figure 3.1 a and b which lie perpendicular to the borehole axis, and are viewed from the borehole collar. In all cases, the x axis is horizontal, the

TABLE 3.1 SUMMARY OF MAJOR ROCK MASS CHARACTERISTICS

BOREHOLE	AVERAGE RQD (%)	AVERAGE FRACTURE FREQUENCY (m^{-1})+	TUNNELING QUALITY INDEX Q*	ROCK MASS RATING RMR**	ROCK MASS QUALITY
RB1	65	1	8	73	Fair to good quality rock mass
RB2	44	3	6	63	Fair to good quality rock mass
RB3	89	0,4	5	70	Fair to good quality rock mass
RB4	52	0,5	7	75	Fair to good quality rock mass
RB5	83	2	10	74	Fair to good quality rock mass

\+ *Natural fractures only - mining induced fractures were ignored*

* NGI Tunnelling Quality Index (Barton et al 1974)

** Geomechanics Classification of Jointed Rock masses (Bieniawski, 1976).

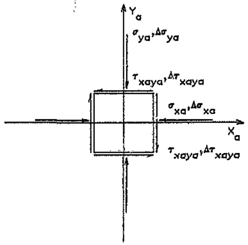

Note: Subscript α refers to borehole number

a: Borehole system of axes and stress components as viewed from collar

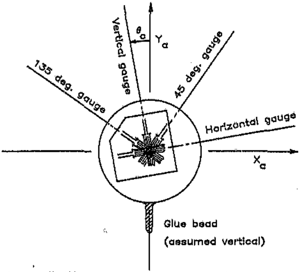

b: Definition of gauge correction angle
Scale 1:1

Figure 3.1
Sketch defining borehole systems of axes, stress components, and gauge correction angle

y axis is vertical and positive angles represent anti-clockwise rotations from the x axis. The subscripts refer to the borehole for which each coordinate system has been defined e.g. x_1 y_1 refers to the x-y axis system in the plane of borehole RB1.

The vertical gauge of a properly orientated strain cell should coincide with the y - axis as defined above. It was found that the orientation device in the installing tool permitted deviations of up to 16 degrees. An angular error of this magnitude was considered significant and some means of correcting it was sought. When Araldite slow-setting epoxy was used, a bead of excess glue formed at the bottom of the strain cell and flowed downwards before setting. It was assumed that the glue bead, shown in Figure 3.2, represented the true vertical, thus allowing the true orientation of the strain cell to be measured in relation to it. The angle of deviation from the vertical was termed the gauge correction angle θ_c and was taken positive when the vertical strain gauge had been displaced in an anticlockwise direction from the true vertical.

3.2.2 Raw strain reliefs

The raw strain relief data are presented in Table 3.2. The strain reliefs are all normal strains measured in four directions denoted the horizontal, 45°, vertical and 135° directions. In order to relate these directions to the defined systems of axes, the gauge correction angle must be introduced (Figure 3.1b). This angle was obtained from each overcored strain cell by measuring the angle between the vertical gauge and the glue bead.

Inherent error

Two planar strain invariants e_a and e_b can be calculated from each set of measured strain reliefs. The first invariant e_a is the sum of strain reliefs obtained from the horizontal and vertical gauges while the second e_b represents the sum of the 45° and 135° strain gauges. In an ideally elastic solid, the two strain invariants are equal for any given stress state. The fact that they are not equal in practice is a measure of the inherent error in each measurement, or measurement quality, as well as the rock properties. In order that this error can be made directly comparative for successive

TABLE 3.2: STRAIN DATA FROM STRAIN RELIEF MEASUREMENTS

BOREHOLE	DEPTH (m)	DATE	STRAIN RELIEFS ($\times10^{-6}$)				GAUGE CORRECTION ANGLE θ_c (Degrees)	PLANAR STRAIN INVARIANTS ($\times10^{-6}$)		INHERENT ERROR %	REMARKS
			HORIZONTAL	+45°	VERTICAL	+135°		e_a	e_b		
RB 1	9,90	24/9/84	-216	+ 230	+ 605	+ 99	+10	+ 390	+ 529	17,0	Poor strain cell - rock bond.* PS Adhesive**
	21,12	11/9/84	-	-	-	-	-	-	-	-	Strain cell dislodged during overcoring. PS Adhesive
	30,46	16/9/84	+262	+ 934	+1076	+263	+ 8	+1328	+1197	10,4	Araldite***
	30,86	20/9/84	+232	+ 698	+1230	+646	0	+1462	+1344	8,4	Araldite
	31,23	16/10/84	+265	+ 838	+1373	+604	+ 9	+1638	+1522	7,3	Araldite
	31,54	19/10/84	+169	+1385	+1068	+592	+ 9	+1233	+1977	46,4	Moisture in cables - spurious readings.* Araldite
	32,56	23/10/84	+306	+ 972	+1091	+457	+11	+1397	+1429	2,3	Araldite
RB 2	21,28	2/10/84	+226	+ 957	+1413	+495	+ 8	+1639	+1452	12,1	PS Adhesive
	21,38	8/10/84	-	-	-	-	-	-	-	-	Strain cell dislodged during overcoring. PS Adhesive
	21,80	12/10/84	+956	+1302	+1170	+937	+12	+2126	+2239	5,2	Araldite
	22,36	18/10/84	+426	+ 609	+ 886	+734	0	+1312	+1343	2,3	Araldite
	22,82	22/10/84	+396	+1111	+1269	+526	+10	+1665	+1637	1,1	Araldite
RB 3	10,16	5/12/84	+457	+ 676	+1110	+842	- 2	+1567	+1317	3,2	Araldite
	10,46	9/12/84	+294	+ 763	+1096	+665	+ 6	+1390	+1410	2,0	Araldite
	10,73	11/12/84	+289	+ 765	+1152	+609	+ 5	+1441	+1374	4,0	Araldite
RB 4	9,11	6/12/84	+275	+ 849	+1141	+499	+16	+1416	+1349	4,9	Araldite
	9,29	10/12/84	+395	+ 868	+1196	+633	+13	+1691	+1601	6,8	Araldite
	9,65	12/12/84	+267	+ 826	+1167	+668	+ 9	+1434	+1496	4,2	Araldite
RB 7	8,73	11/9/86	-	-	-	-	-	-	-	-	Improper preparation of borehole end. Strain cell dislodged
	9,64	12/9/86	-552	+ 474	+1497	+174	+ 3	+ 936	+ 648	36,3	Bedding plane and quartz filled joint near strain cell.*
	10,00	16/9/86	+164	+1166	+1680	+684	+ 4	+1862	+1840	0,7	Araldite
	10,36	16/9/86	-	-	-	-	-	-	-	-	Strain cell damaged during overcoring
	10,20	17/9/86	+197	+1276	+1499	+423	+ 9	+1696	+1690	0,7	Araldite
	10,46	18/9/86	+113	+1230	+1693	+524	+10	+1806	+1762	2,5	Araldite
	10,66	19/9/86	- 82	+ 913	+1204	+209	+13	+1161	+1122	2,6	Araldite
	10,76	22/9/86	+160	+1216	+1621	+630	+ 1	+1780	+1748	1,9	Araldite

Notes: *Not included in subsequent analysis. **Manufactured by Tokyo Sokki Kenkyujo Ltd. Japan. ***Manufactured by Polycell Products, South Africa.

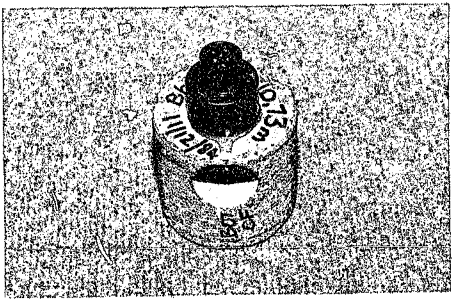

Figure 3.2

Overcored "Doorstopper" strain cell
showing glue bead

measurements, it should be standardised and expressed as a percentage as follows:-

$$\zeta = \frac{2|e_a - e_b|}{e_a + e_b} \% \quad \ldots\ldots 3.1$$

where ζ is the inherent error and e_a and e_b are the planar strain invariants

The inherent error in each measurement may arise from a combination of some or all of the following sources, listed in the order of decreasing importance:-

i) imperfect strain cell-rock bond;
ii) strain measurement equipment error;
iii) the presence of discontinuities in the rock near the overcored strain cell;
iv) directional variability of the rock elastic constants in the plane of the borehole end (ie rock anisotropy);
v) time dependent elastic relaxation of the overcored rock, also anisotropic manifestation of this phenomenon;
vi) non-linearity of the stress-strain relationship;
viii) the presence of strain gradients in the plane of the borehole end;
viii) intrinsic error in the strain gauges.

Large errors can result from the first three sources, and care must be taken to avoid these during a strain measurement program. The following four sources are likely to be insignificant in relation to the first three because the quartzites in which the measurements were undertaken are not strongly anisotropic on the scale of the strain gauges; the quartzites do not exhibit strong creep effects (Briggs 1982); the stress strain relationship is approximately linear for the greater part of the stress-strain curve; and strain gradients in the plane of the borehole end would have to be very large to produce the observed error in the strain invariants. The intrinsic error in the strain gauges is quoted by the manufacturer as 0,3%, which is considerably smaller than that possible from the other sources.

Rejection criteria

For the purpose of this analysis it has been assumed that the error arising from the first three sources will be overwhelming, rendering the errors from the remaining six sources negligible in comparison. Therefore two criteria have been established for the rejection of strain relief data:

i) visual evidence of a poor strain cell-rock bond and/or strain measurement equipment error and/or the presence of discontinuities in the core that may have affected strain readings;

ii) the inherent error having a value greater than 20%.

The first criterion is self evident while the second requires explanation. The stress estimates are based on the assumption that the rock is linearly elastic, homogeneous and isotropic. If an individual measurement displays an inherent error of greater than 20% then the assumptions about rock elasticity are significantly at variance with observations. The level of 20% was chosen as the criterion because of the work of Pallister (1969), who determined the in situ stress tensor in a deep gold mine with an overall error of 20% if the 95% confidence intervals were chosen. His estimates contained the pooled error of the strain relief measurements, rock elastic constant determination error and the error between successive strain measurements. It was therefore reasoned that if the inherent error already exceeded 20% then the result should not be included in the analysis. The values rejected on the basis of the two criteria are shown together with the reason for rejection in the remarks column of Table 3.2.

3.2.3 Strain components

The strain at a point is completely defined in two dimensions by a strain rosette if three normal strains are measured in three known, but differing directions. In the case of a rectangular rosette in which the gauges are orientated at 0°, 45° and 90° the normal and shear strains are given in the coordinate system defined by the rosette (Jaeger and Cook, 1979):-

$$\begin{aligned} \varepsilon_x &= \varepsilon_0 \\ \varepsilon_y &= \varepsilon_{90} \qquad \qquad \ldots\ldots\ldots\ 3.2 \\ \gamma_{xy} &= 2\varepsilon_{45} - (\varepsilon_0 + \varepsilon_{90}) \end{aligned}$$

The coordinates defined by the strain rosette are generally not parallel to the systems of axes defined for each borehole but differ in direction in the above case by the gauge correction angle. Since four strain relief measurements were obtained in the 0°, 45°, 90° and 135° directions from each strain cell it is possible to define four sets of strain components with equations 3.2 by using four combinations of three gauges each as shown in Table 3.3. Each combination of gauges is directionally removed by a different angle to the pre-defined borehole system of axes. This angle is denoted the combination angle ϕ and is listed with each combination of strain gauges.

Once the four sets of strain components are defined, each can be rotated through its respective combination angle to the borehole system of axes. In the limiting case where $e_a = e_b$, the respective strain components from each set are equal and no averaging is required. This condition never arose in the strain measurement program, consequently the strain components for each measurement were averaged before being presented in Table 3.4. In addition the resulting principal strains were calculated for each set of average strain components together with the resulting planar strain invariant. Finally, all the results were averaged for each borehole.

Spatial error

It is apparent in the table that the respective strain components vary considerably in each borehole. This phenomenon appears to be common to all rock masses and becomes pronounced when measurements are undertaken close to discontinuities of all descriptions and where boreholes traverse different rock types (Pallister, 1969, Cahnbley, 1970 and Gay, 1972). The most important causes of this phenomenon lie in the quality of the measurements and in the structural complexity of the rock mass. The variation that results from the latter can be termed the spatial error.

At the outset it must be emphasized that some of the variability observed in Table 3.4 can be accounted for in the quality of the measurements, and not to the rock mass characteristics alone. Nevertheless, the important factors that can introduce spatial variability into the measurement results are as follows:

i) spatial and directional variability of the elastic constants of the intact rock material;

TABLE 3.3: STRAIN GAUGE COMBINATIONS FOR A FOUR-GAUGE RECTANGULAR ROSETTE

COMBINATION	STRAIN GAUGES	COMBINATION ANGLE θ (degrees)
1	0° - 45° - 90°	θ_c
2	45° - 90° - 135°	$\theta_c + 45°$
3	90° - 135° - 0°	$\theta_c + 90°$
4	135° - 0° - 45°	$\theta_c + 135°$

TABLE 3.4: AVERAGED STRAIN COMPONENTS AND PRINCIPAL STRAINS

BOREHOLE	DEPTH (m)	AVERAGE STRAIN COMPONENTS $(x10^{-6})$ ϵ_x	ϵ_y	γ_{xy}	PRINCIPAL STRAINS $\epsilon_1(x10^{-6})$	$\epsilon_2(x10^{-6})$	θ_1(deg.)	PLANAR STRAIN INVARIANT $e(x10^{-6})$
RB1	30,46	+142	+1120	+418	+1163	+ 99	-12	+1262
	30,86	+203	+1201	+ 52	+1202	+202	- 1	+1404
	31,23	+239	+1341	+196	+1350	+230	- 5	+1580
	32,56	+246	+1167	+183	+1176	+237	- 6	+1413
AVERAGES		+208	+1207	+212	+1218	+197	- 6	+1415
RB2	21,28	+139	+1407	+117	+1410	+136	- 3	+1546
	21,80	+919	+1263	+246	+1302	+880	-18	+2182
	22,36	+434	+ 894	-125	+ 902	+426	+ 8	+1328
	22,82	+308	+1338	+248	+1353	+293	- 7	+1646
AVERAGES		+450	+1226	+122	+1231	+445	- 4	+1676
RB3	10,16	+439	+1103	-121	+1108	+434	+ 5	+1542
	10,45	+299	+1105	- 53	+1106	+298	+ 2	+1404
	10,73	+265	+1143	+ 4	+1143	+265	+ 0	+1408
AVERAGES		+334	+1117	- 57	+1118	+333	+ 2	+1451
RB 4	9,11	+231	+1151	-162	+1158	+224	+ 5	+1382
	9,29	+362	+1184	-140	+1190	+356	+ 5	+1546
	9,55	+280	+1185	-126	+1189	+276	+ 4	+1465
AVERAGES		+291	+1173	-143	+1179	+285	+ 5	+1464
RB7	10,00	+136	+1710	+255	+1720	+126	- 5	+1846
	10,29	+ 98	+1599	+408	+1626	+ 71	- 8	+1697
	10,46	+ 28	+1756	+131	+1758	+ 26	- 2	+178[illegible]
	10,65	-150	+1287	+ 82	+1288	-151	- 2	+1137
	10,75	+139	+1624	+635	+1689	+ 74	-12	+1763
AV. [illegible]AGES		+ 50	+1595	+302	+1610	+ 35	-6	+1645

ii) changes in rock types traversed by the borehole;

iii) variation in the rock mass structure traversed by the borehole;

iv) the presence of strain gradients developed in intact rock material as a result of deformation mechanisms such as slip and rotation;

v) changing mining induced stress both in time and space;

vi) variations in strain cell orientation with respect to vertical.

The investigator has very little control over the first four factors since these are intrinsic to the rock mass in which the measurements are made. The relative importance of each will change from situation to situation and it appears in the case under study that the first and fourth factors were the most important while the second and third factors were relatively unimportant. The chief reason for this is that all the accepted strain measurements were carried out over distances of two metres or less in each borehole in geologically similar rock. The second and third factors were therefore neglected. The fifth factor was not considered to be important because the mining induced stress changes were small at the time of the strain measurement program.. The last factor is accounted for in an earlier discussion.

The most important factor is the spatial variation of the rock elastic constants, which were determined in the laboratory from the recovered borehole cores (Section 3.3). The planar strain invariant can be linearly related to the planar stress invariant by the equation from first principles as follows:-

$$\varepsilon_1 = \frac{1}{E}[\sigma_1 - \nu\sigma_2]$$
$$\varepsilon_2 = \frac{1}{E}[\sigma_2 - \nu\sigma_1] \qquad \ldots\ldots\ldots 3.3$$

adding:

$$\varepsilon_1 + \varepsilon_2 = \frac{1}{E}[\sigma_1 + \sigma_2 - \nu(\sigma_1 + \sigma_2)]$$

manipulating and re-arranging

$$e\frac{E}{1-\nu} = \Theta$$

where the planar strain invariant $e = \varepsilon_1 + \varepsilon_2$

and the planar stress invariant $\Theta = \sigma_1 + \sigma_2$

If the overcored strain cells were removed from a uniform stress field then the planar stress invariant can be assumed constant in any given direction. This implies that if θ varies along a borehole, then $E/(1 - \nu)$ should vary antipathetically. The data from Boreholes RB1 and RB4 can be pooled together as can that from RB2 and RB3 because of their similar directions. Two scatter plots of the data are shown in Figure 3.3. In both there is clearly an antipathetic relation between the two variables, but with poor correlation, especially in the case of Boreholes RB2 and RB3.

Two observations can be made from the comparisons. Firstly, the variables are related albeit not very strongly. Secondly, the structure of the rock mass has introduced considerable variability which tends to reduce the degree of correlation between the two variables. The presence of the fault is seen to be the major contributor to the poor correlation because of the effects it has on the local stress field. Assuming the planar stress invariant in any given direction to be constant is therefore likely to be incorrect. It can be concluded from the correlations that the spatial variability of the elastic constants does have considerable influence on the strain relief values retrieved and that the presence of major structures will tend to increase the variability thus clouding the relationship.

3.3 Laboratory Testing

A knowledge of the elastic constants of intact rock material from the site was required for estimation of the in situ stress from the strain relief results. The data were obtained from right cylindrical rock samples tested in uniaxial compression at the Department of Mining Engineering, University of the Witwatersrand. The samples were extracted from the borehole cores as close as possible to each strain relief measurement in order to minimise the error that may arise from the spatial variability of the elastic constants, a feature typical of most rock masses. The axis of each rock specimen extracted was chosen to be parallel to the vertical strain gauge direction unless visible weaknesses such as fractures or bedding planes were present in the core.

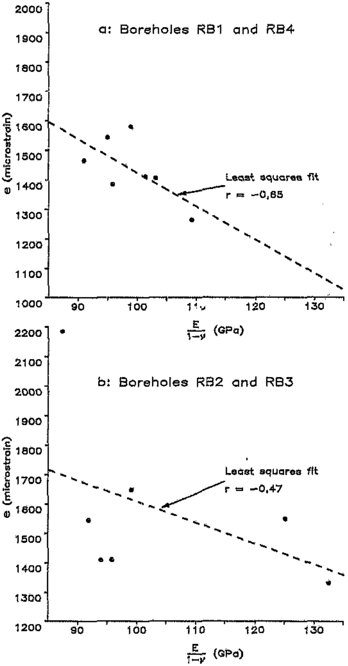

Figure 3.3
Scatter plots of planar strain invariants
versus elastic constants

In these cases the samples were extracted in directions which ensured that no weaknesses would be included. A typical overcored strain cell with sample extracted for testing is shown in Figure 3.4.

The samples were all 30 mm in diameter and 60 mm in height, because of the size restrictions imposed by the core diameter. This is not expected to influence the test results because it has been demonstrated on a number of occasions that neither the sample geometry nor the sample size influence the modulus values in the pre-failure range if the rock specimens are homogeneous and intact (Lama and Vutukuri, 1978). The test data derived from the rock specimens was received in the form of axial loads at regular intervals with the corresponding axial stress, axial strains and transverse strains. Each specimen was loaded to failure and the uniaxial compressive strength was recorded. The detailed results appear in Appendix B.

The average elastic constants were calculated to three significant figures as recommended by Brown (1981). In order to eliminate any bias that may arise in the calculations, the average slope of each stress strain curve was found by using the method of least squares. This was done using the data up to two-thirds of the uniaxial compressive strength of each sample because it is generally accepted that beyond this point the stress-strain relationship ceases to be linear. A typical axial and diametric stress strain curve together with the best-fit lines appears in Figure 3.5. The values of the elastic constants together with other information pertinent to each test specimen are listed in Table 3.5.

3.4 In Situ Stress Estimation

The boreholes were drilled in directions as close as possible to the principal stress directions determined by Leeman (1968) and Gay (1972). If it is assumed that at depth the regional stress tensor does not vary significantly laterally and that the mining

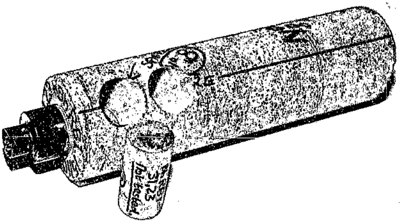

Figure 3.4

Typical overcored strain cell with
sample extracted for testing

Specimen No. : 10
Rock type : Hangingwall Quartzite
Length to diameter ratio : 2:1
Sample diameter : 30 mm
Sample mass : 116,8 g
Young's Modulus : 84,947 GPa
Poisson's Ratio : 0,176
Uniaxial Compressive Strength : 254,65 MPa

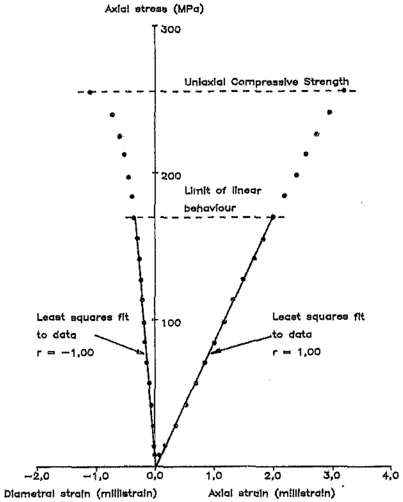

Figure 3.5

Example plot of stress versus strain

TABLE 3.5: ELASTIC CONSTANTS DETERMINED IN THE LABORATORY

BOREHOLE	DEPTH (m)	SAMPLE DIRECTION	E_{av} (GPa)	ν_{av} (GPa)	REMARKS
RB1	30,49	Vertical	86,494	0,209	Hangingwall quartzite Quartz-filled fracture in specimen
	30,89	Vertical	82,704	0,199	Hangingwall quartzite
	31,27	Vertical	81,648	0,176	Hangingwall quartzite
	32,59	Vertical	82,411	0,188	Hangingwall quartzite
	AVERAGES		83,314	0,193	Used for in-situ stress determination
RB2	21,31	Vertical	95,854	0,245	Hangingwall quartzite Quartz-filled fracture in specimen
	21,82	+120°	72,920	0,164	Hangingwall quartzite Quartz-filled fracture in specimen
	22,39	+135°	97,117	0,266	Hangingwall quartzite Quartz-filled fracture in specimen
	22,85	Vertical	80,408	0,188	Hangingwall quartzite
	AVERAGES		86,575	0,216	Used for in situ stress determination
RB3	10,19	+60°	71,841	0,217	Footwall quartzite. Specimen end chipped
	10,48	Vertical	75,335	0,197	Footwall quartzite
	10,75	Vertical	78,007	0,185	Footwall quartzite
	AVERAGES		75,061	0,200	Used for in-situ stress determination
RB4	9,15	Vertical	78,478	0,182	Footwall quartzite
	9,31	Vertical	75,478	0,206	Footwall quartzite
	9,50	Vertical	74,378	0,185	Footwall quartzite
	AVERAGES		76,111	0,191	Used for in-situ stress determination

TABLE 3.5: ELASTIC CONSTANTS DETERMINED IN THE LABORATORY

BOREHOLE	DEPTH (m)	SAMPLE DIRECTION	E_{av} (GPa)	v_{av} (GPa)	REMARKS
RB1	30,49	Vertical	86,494	0,209	Hangingwall quartzite Quartz-filled fracture in specimen
	30,89	Vertical	82,704	0,199	Hangingwall quartzite
	31,27	Vertical	81,648	0,176	Hangingwall quartzite
	32,59	Vertical	82,411	0,188	Hangingwall quartzite
	AVERAGES		83,314	0,193	Used for in-sitr stress determination
RB2	21,31	Vertical	95,854	0,245	Hangingwall quartzite Quartz-filled fracture in specimen
	21,82	+120°	72,920	0,164	Hangingwall quartzite Quartz-filled fracture in specimen
	22,39	+135°	97,117	0,266	Hangingwall quartzite Quartz-filled fracture in specimen
	22,85	Vertical	80,408	0,188	Hangingwall quartzite
	AVERAGES		86,575	0,216	Used for in situ stress determination
RB3	10,19	+60°	71,841	0,217	Footwall quartzite. Specimen end chipped
	10,48	Vertical	75,335	0,197	Footwall quartzite
	10,75	Vertical	78,007	0,185	Footwall quartzite
	AVERAGES		75,061	0,200	Used for in-situ stress determination
RB4	9,15	Vertical	78,478	0,182	Footwall quartzite
	9,31	Vertical	75,478	0,206	Footwall quartzite
	9,58	Vertical	74,378	0,185	Footwall quartzite
	AVERAGES		76,111	0,191	Used for in-situ stress determination

induced stress prior to the stress monitoring phase were insignificant, the method given by Pallister (1969) for boreholes drilled along principal stress directions can be applied.

3.4.1 Triaxial stress tensor estimate

In the case of the initial stress state, four simultaneous equations can be set up using the information from boreholes RB1 and RB2 *to solve for the principal stresses in the hangingwall quartzites* to the west of the Elf Fault. A similar procedure can be applied to the information derived from boreholes RB3 and RB4 situated in footwall quartzites to the east of the fault. The stress concentration factors selected for both cases were those given by Coates and Yu (1970) and Hocking (1976). The results are listed in Table 3.6, while the calculations are presented in Appendix C.

The most strikin feature of the results presented are the magnitudes of the estimated stress. In all the cases, σ_1 is far in excess of the theoretical overburden stress σ_{OB} = *75,8 MPa* as well as the total vertical stress at 80,2 MPa estimated for mining as at December 1984. The condition of all the underground excavations in the area showed no evidence to suggest that stresses of these magnitudes existed at that time. Furthermore, the excavations in the area were not heavily supported, and did not show any signs of duress aside from the fairly intense induced fracturing common to all such excavations at depth. Grouted pre-tensioned long-rope anchors together with wire mesh and lacing was installed about a year after the measurements when considerable additional mining induced stress had been imposed on the area. During the period prior to the installation of additional support few ground control problems were evident aside from two major falls of ground in 100/25 Replacement Crosscut North. These falls of ground could be attributed directly to the effects of overstoping the crosscut and not to high stress.

In the above argument it is assumed that the measured stresses are representative of the entire area. All the strain relief measurements considered in the analysis were made within 10 m of the inferred position of the fault surface and may therefore

TABLE 3.6: ESTIMATES OF INITIAL IN SITU STRESS USING DIFFERENT STRESS CONCENTRATION FACTORS

STRESS	WEST OF ELF FAULT – HANGINGWALL Magnitude (MPa)	% Error*	Plunge (degrees)	Direction (degrees)	EAST OF ELF FAULT – FOOTWALL Magnitude (MPa)	% Error*	Plunge (degrees)	Direction (degrees)	STRESS CONCENTRATION FACTORS a	b	c
σ_1	+125,5	3,7	90	–	+103,8	11,6	90	–	+1,35	0,0	-0,75
σ_2	+ 86,9	9,7	0	120	+ 66,8	32,5	0	30	After Coates and Yu (1970)		
σ_3	+ 72,6	11,6	0	30	+ 64,3	33,7	0	120			
σ_1	+113,5	5,7	90	–	+ 93,8	9,9	90	–	+1,35	0,0	-0,58
σ_2	+ 75,0	19,5	0	120	+ 56,1	37,1	0	30	After Hocking (1976)		
σ_3	+ 57,[illegible]	25,4	0	30	+ 52,8	39,4	0	120			

* Calculated by finding the 95% confidence level limit and dividing this value by the average stress, and expressing the result as a percentage.

represent a zone of high stress associated with it. The condition of 100/2 'C' Haulage West, 100 Reef Drive West and 100 Return Airway at the fault intersections suggest that no such zone of high stress exists.

Finally, the vertical stress calculated from a number of ground stress tensor determinations in deep Witwatersrand Gold Mines agree reasonably well with the theoretical overburden stress at each site (Gay, 1975). There is no reason to believe or evidence to suggest that the initial stress at the monitoring site should deviate from this pattern.

Effect of stress concentration factors

The next significant feature of Table 3.6 is the sensitivity of the results to changes in the stress concentration factors used in the calculations. The radial an' axial stress concentration factors determined by Hocking (1976) are 3% and 23% smaller in absolute terms than those given by Coates and Yu (1970). Their use results in a reduction of σ_1 and σ_3 to the west of the fault of 10% and 21% respectively. More significantly, the error of the determinations increases substantially if Hocking's results are used. Pallister (1969) demonstrated that small errors in the stress concentration factors a and c can result in large errors in the results especially if $a\sigma_1$ and $a\sigma_2$ are close in value to $c\sigma_3$. This is evident in the errors in the horizontal stress east of the fault, and it appears to become more pronounced if the absolute values of the factors are reduced, as demonstrated in Table 3.6.

3.4 2 Re-evaluation of stress concentration factors

A survey of the rock mechanics literature reveals that the values of the stress concentration factors are periodically subject to review and re-evaluation. Rahn (1984) lists the results of his analysis together with the results of others in chronological order. The results of the latest few analyses listed show remarkably good agreement, even though they were arrived at using different [illegible] The feature common to all the analyses are the underlying a[illegible]ions of a perfectly linearly elastic and continuous solid.

Unlike the others, Rahn considered the effect of anisotropy, and showed that it has a marked effect on the values of the stress concentration factors. No analysis which considers the effect of discontinuities has been carried out, even though it does appear that their effect can be considerable. Gay (1975) mentions that the stress concentration factors calculated for a continuous solid are not applicable to broken ground and have to be modified, but no guidelines are given.

It would appear therefore that the values of the stress concentration factors are subject to a number of influences, the most important being Poisson's ratio, anisotropy and the presence or otherwise of discontinuities. These three variables will assume different levels of importance from site to site, and must be taken into account when choosing the stress concentration factors for in situ stress estimation. In the case under study, Poisson's ratio was determined while it can be reasonably assumed that on the scale of the strain gauges the rock is isotropic. The effect of discontinuities is unknown quantitatively but the experience of other workers suggests that the absolute values of the stress concentration factors should be reduced in discontinuous rock (Gay 1975).

The radial stress concentration factor a, was therefore taken to be 1,30 for a fractured rock mass with Poisson's ratio of 0,2 (after Gay, 1975 and Rahn, 1984). The tangential stress concentration factor b was assumed to have a value of zero as this would not produce a large error in the calculations. The axial stress concentration factor c was also assumed to be zero for the purposes of the analysis in order to avoid the large errors that would result if a small value was chosen.

3.4.3 Biaxial stress tensor estimate

The estimates of both the initial and final in situ stress using the above values and the method outlined by Leeman (1965a) are presented in Table 3.7 together with other relevant details. The results are in far better agreement with the theoretical over-

TABLE 3.7: IN SITU STRESS STATE AT THE MONITORING SITE BEFORE AND AFTER THE STRESS MONITORING PERIOD

BOREHOLE	AXES* HORIZ.	VERT.	ε_1 ($\times 10^{-6}$)	ε_2 ($\times 10^{-6}$)	θ_1 (deg.)	E (GPa)	ν	σ_1 (MPa)	σ_2 (MPa)	θ (deg.)	σ_x (MPa)	σ_y (MPa)	γ_{xy} (MPa)	OVERALL Error %	DATE of Measurement
RB1	x1	y1	+1218	+197	-6	83,314	0,193	+ 83,6	+28,8	-6	+29,4	+ 83,0	+5,7	±11	Dec. '84
RB2	x2	y2	+1231	+445	-4	86,575	0,216	+ 92,7	+49,7	-4	+49,9	+ 92,5	+3,0	±16	Dec. '84
RB3	x3	y3	+1118	+333	+2	75,061	0,200	+ 71,2	+33,5	+2	+33,5	+ 71,2	-1,3	± 7	Dec. '84
RB4	x4	y4	+1179	+285	+5	76,111	0,191	+ 74,9	+31,0	+5	+31,3	+ 74,6	-3,8	±11	Dec. '84
RB7	x7	y7	+1610	+ 35	-6	84,945+	0,201+	+110,1	+24,4	-6	+25,3	+109,2	+8,9	-	Sept.'86

* The strains and stresses for each borehole are expressed in terms of the system of axes defined for that borehole as shown in Figure 3.1

\+ Average modulus of elasticity determined from the values quoted for boreholes RB1 and RB2 burden stress of 75,8 MPa. The vertical stress estimated by numerical methods for mining as at December 1984 is 80,2 MPa, which agrees very well with the average vertical stress measured in December 1984 of 80,3 MPa (see Table 5.2). The observed variation in the vertical stress can be ascribed to the lateral variation in the elastic constants as well as the fact that two rock masses with different constants abut against each other on the fault surface (Deacon and Swan, 1965). The average horizontal stress for December 1984 is 36,0 MPa and the ratio of horizontal to vertical stress k is 0,45.

Biaxial stress estimate error

The overall error listed in Table 3.7 is obtained from the spatial variation of the planar stress invariant which was calculated by Equation 3.3 using the data listed in Tables 3.4 and 3.5. The results were then averaged, and assuming a normal distribution, the 95% confidence limits were found and expressed as a percentage of the mean. The overall error serves purely as a measure of the error of the stress determination while taking into account the spatial variation of the elastic constants of the intact rock. Furthermore, it is a measure of confidence with which the overall stress state of the rock mass was measured in two dimensions in each borehole. The error for Borehole RB7 could not be calculated in the same way because laboratory tests were not carried out on the cores.

The inclusion of anomalous strains, especially in the data for Borehole RB2 has increased the uncertainty with which the measurements were made but reduced the amount of bias. Even so, the errors lie within the 20% margin which is usually expected for a fractured rock mass. The data presented in Table 3.6 was rejected while that in Table 3.7 was accepted because it represented so much more reasonably the conditions present at the site at the time.

3.5 Discussion and Conclusions

The initial and final stresses are presented in biaxial form as the assumptions about the initial stress state led to large errors in the calculation of the triaxial stress state. This has not led to a serious loss of information because the stress state on the Elf Fault Surface car be approximated from the results of boreholes RB2 and RB3 alone.

A prominent feature of all the stress estimates given is the difference between the stresses to the east and west of the fault. This difference can be explained if it is assumed that the strains are uniform on both sides of the fault. The average vertical strain to the west of the fault is about 6% larger than that to the east, a difference that is not considered to be significant. The 20% difference in stress magnitudes can therefore be accounted by the 13% difference in elastic modulus for footwall and hangingwall quartzites (Table 3.5) and the 6% difference in the strains (Table 3.4). The significance of these results is discussed in Chapter 6.

CHAPTER 4

STRESS CHANGE MONITORING RESULTS

Thirteen vibrating wire stressmeters were set in boreholes to monitor stress changes induced by the advance of the 100/38 Longwall towards the monitoring site. The object was to obtain measurements of changing stress conditions on the Elf Fault as it came under the influence of changing mining induced stresses.

The purpose of this chapter is to present the stress changes measured by the stressmeters and to use the results to calculate the total stress state on the Elf Fault Surface throughout the monitoring period. The potential for fault instability is then assessed by using the Excess Shear Stress criterion discussed by Ryder et al (1978). Thereafter, observations on seismicity experienced in the area as well as the results of a levelling survey to monitor fault movement are presented. Finally, the results are combined to show that the fault remained stable throughout the stress monitoring period.

4.1 General Considerations

Long term in situ stress monitoring commenced in boreholes RB3 and RB2 on 11 January and 4 February 1985 respectively. Stress induced damage to both boreholes RB1 and RB4 resulted in a three month delay before the vibrating wire stressmetres could be installed. Monitoring in these boreholes commenced on 12 April 1985 after the stressmeters had been set satisfactorily and given time to settle. During the intervening period the 100/38 Longwall had advanced steadily toward the stress monitoring site, but the mining induced stress changes measured in borehole RB2 and RB3 as well as those estimated by numerical methods were small. It was therefore possible to assume that the initial stress, measured in December 1985, was applicable as a starting point for mining induced stress changes measured in all four boreholes.

4.1.1 Stressmeter layout

The layout of the vibrating wire stressmeter clusters in Borehole RB1 to RB4 is illustrated in Figure 2.14. The arrangement permitted the biaxial determination of mining induced stress changes in the plane of each borehole. A single stressmeter, set to measure vertical stress changes was installed in borehole RB6 located approximately 110 m west of the monitoring site (Figure 2.1). Monitoring commenced here on 12 April 1985. The purpose of this stressmeter was to measure the mining induced stress changes in the far field where the rock mass conditions were not expected to change as a result of mining in the area. Finally, a stressmeter kept on surface for the duration of the project was used as a reference. The period of this vibrating wire stressmeter was measured and recorded on each occasion that those underground were measured.

4.1.2 Position of mining faces

As demonstrated in Section 4.2, the vibrating wire period changes can be attributed solely to the rock stress changes induced by the westward advance of the 100/38 Longwall, and the increasing areal extent of 100/25 Stope. It is therefore important to know the positions of these mining faces at specific times in order to make comparable stress change estimates by numerical means. The mine survey department measures all mining face positions monthly, and this information was used to draw up the positions of the advancing stope faces at eleven different times throughout the stress monitoring period (Figure 4.1)

Each position shown in Figure 4.1 is referred to as a mining step, and the shaded area in each step represents the areal extent of reef mined between the date of that step and the date of the preceding step. The eight mining steps, succeeding the initial conditions represented by the December 1984 Step, show fairly regular advances of the 100/38 Longwall towards the Elf Fault. The last two steps cover a period of final remnant extraction of reef to the east of the fault. Intermittent mining took place throughout the monitoring period to the west of the Elf Fault in 100/25 Stope.

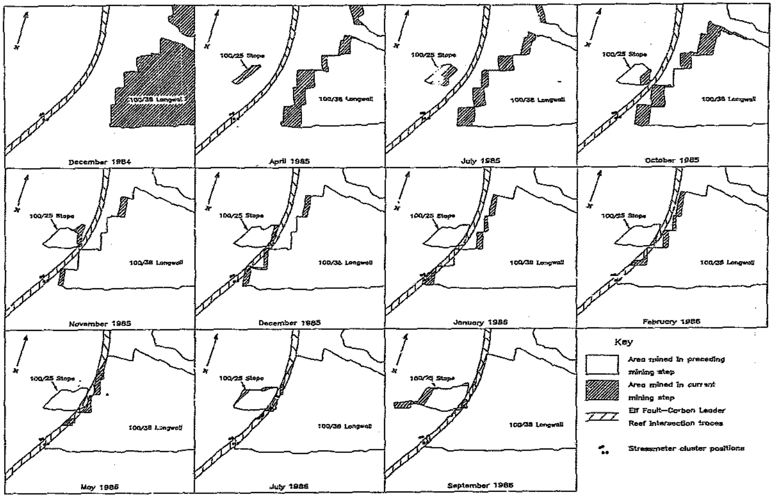

Figure 4.1

Progressive positions of the 100/38 Longwall and 100/25 Stope

Scale 1:5000

The mining face positions as shown for September 1986 in Figure 4.1 depict the final conditions at the end of the stress monitoring period.

4.2 Vibrating Wire Period Readings

Each set of vibrating wire period readings necessitated a trip underground. These were taken as often as possible, with smaller time intervals between readings when the mining induced stress changes were expected to be large. The initial period for each gauge was chosen as that point beyond which at least one of the three gauges in each borehole started registering consistent increases in the period (see Appendix D). This criterion was defined firstly because the stresses in the area were expected to increase and secondly, all the gauges showed decreases in the vibrating wire period as they settled into the boreholes after installation.

The vibrating wire period readings at eleven different times are presented together with the initial period T_o for each gauge in Table 4.1. The readings given were taken on the day or within a week of the day that the stope face positions were measured by the mine survey department. This enables comparisons to be made between the measured stress changes and the stress changes derived from the numerical analyses. The readings are listed in full in Appendix D.

The most remarkable feature of the table and of vibrating wire stressmeters in general is their long-term stability. The reference stressmeter is a good example to illustrate this point. It was kept in a cupboard in air-conditioned offices for the duration of the monitoring period, which lasted 21 months. The period of this stressmeter remained within a narrow range of 0,2 microseconds throughout the stress monitoring phase of the study with the observed variation attributable possibly to fluctuations in temperature. Since the virgin rock temperature at the stress monitoring site has probably remained unchanged for the duration of the study, it has been assumed that all the changes in vibrating wire period readings both in Table 4.1 and Appendix D can be ascribed purely

TABLE 4.1: SELECTED VIBRATING WIRE PERIOD READINGS COVERING THE ENTIRE MONITORING PERIOD

BOREHOLE NUMBER	DIRECTION	VIBRATING WIRE PERIOD READINGS ($x10^{-6}$) Initial* Reading T_o DEC'84	T APR'85	T JULY'85	T OCT'85	T NOV'85	T DEC'85	T JAN'86	T FEB'86	T MAY'86	T JULY'86	T SEPT'86
RB1	Horizontal	222,2	222,2	223,9	228,0	229,9	237,0	263,5	283,9	311,6	319,5	326,8
	45°	204,9	204,9	203,7	205,4	206,2	209,4	218,9	225,3	233,5	234,7	236,6
	Vertical	229,4	229,3	230,5	232,2	232,9	236,0	242,2	247,7	255,5	257,7	259,6
RB2	Horizontal	203,2	202,2	201,6	201,5	201,7	201,1	204,0	203,7	205,9	206,0	206,8
	45°	193,4	192,7	192,9	193,5	193,6	193,1	191,7	190,8	190,6	190,7	191,0
	Vertical	210,3	211,5	215,1	221,6	224,1	234,5	254,4	268,7	293,3	301,6	310,0
RB3	Horizontal	204,7	204,3	204,3	203,3	203,3	203,0	203,2	201,4	201,1	201,0	201,0
	45°	224,7	225,8	228,0	230,2	231,4	236,0	258,4	265,7	270,5	273,4	275,6
	Vertical	219,3	221,5	225,7	235,6	239,1	255,5	385,7	–	302,6**	280,1**	266,3**
RB4	Horizontal	221,3	221,3	219,8	220,7	221,3	219,1	–	–	–	–	–
	45°	201,1	201,1	201,3	201,8	201,9	201,6	–	–	–	–	–
	Vertical	197,7	197,8	199,4	203,2	204,9	217,7	–	–	–	–	–
RB6	Vertical	227,2	227,2	228,5	229,8	230,0	231,2	232,9	233,3	233,7	234,4	235,0
CONTROL	–	216,7	216,8	216,7	216,7	216,8	216,8	216,7	216,8	216,6	216,8	216,6

* The initial vibrating period readings, all obtained after December 1984 were assumed valid for December 1984 because of the small error involved.

** Readings probably unreliable

to stress changes in the rock.

Another feature of the stressmeters is their reliability. None of the instruments failed during the monitoring period, nor did any appear to provide unreliable readings except for the vertical stressmeter in Borehole RB3. The readings for Boreholes RB1 and RB2 were therefore taken to be acceptable for the entire stress monitoring period. The readings from Borehole RB3 were assumed unreli[illegible] after 9 January 1986 because the vertically orientated stressmeter was compressed beyond the specified range limit of 450 microseconds. This occurred when 100W1 Panel was stripped onto the Elf Fault almost directly above the borehole. Since then either [illegible] relaxation or borehole damage has caused the period read[illegible] to drop below the maximum limit while the horizontal and 45° stressmeters have continued to register increases. No readings were possible in borehole RB4 after 21 December 1985 because of blast damage to the borehole as 100W1 P[illegible]nel passed over it.

The readings from each stressmeter revealed well defined trends, with small changes in the periods while mining [illegible]s some distance away, and large changes as mining approached the fault. This trend was particularly true of the vertically orientated gauges and was in keeping with the expected in situ stress changes at the monitoring site as mining a[illegible]proached.

4.2.1 Potential sources of error

The vibrating wire period changes are the result of a complex interaction between the rock-stressmeter body-tensioned wire system when subjected to changing externally applied loads. Therefore the period changes cannot be treated in the same way as strain reliefs when considering error in the readings.

A discussion of the potential sources of error is considered more appropriate at this stage than converting the period changes to some form more amenable to error analyses. The potential sources of error listed below are similar to those for strain reliefs, but are recounted with reference to stressmeters:

i) spatial and directional variability of the elastic constants of the surrounding rock;

ii) non-linearity of the stress-strain relationship in the surrounding rock mass;

iii) changes in the rock type in areas where stressmeter clusters are installed;

iv) variations in rock structure in the areas where stressmeter clusters are installed;

v) the presence of stress gradients, both developed and changing in discontinuity-bounded intact rock material as a result of deformation mechanisms such as slip and rotation;

vi) spatial variation of magnitudes of mining induced stress changes at any one time;

vii) the influence that discontinuities close to or intersecting a borehole may have on its deformation;

viii) poor contact between the installed gauges and the borehole sidewalls;

ix) measuring equipment error;

x) error in stressmeter orientation;

xi) intrinsic errors in the stressmeters themselves.

The sources mentioned above are not listed in any particular order of importance but are grouped into two main categories. The first group, namely sources (i) to (vii), are characteristics particular to the sites where stress change measurements may be required. They are partly beyond the control of the investigator, and steps must be taken at the design stage of the project to minimise their effects. The second group of sources are related to stressmeter installation procedure and the proper care and maintenance of the equipment together with the proper use of experimental controls. In the case of (x) the crude means of orientating the stressmeters in the boreholes has resulted in errors that may be as large as 10°. Since no means of determining the error of orientation of the individual stressmeters is possible they are assumed to be orientated exactly in the direction specified for each stressmeter. An analysis of the error of comparable stress change estimates is carried out on the vertical stress changes in each borehole at a later stage.

4.3 In Situ Stress Change Estimates

The term stressmeter used by Hawkes and Hooker (1974) is something of a misnomer, because a reasonably accurate determination of the rock mass modulus of elasticity was found to be necessary before the in situ stress changes could be estimated. This is obvious in the fact that they included a stress sensitivity factor in the equation that relates vibrating wire period readings to uniaxial rock stress changes.

4.3.1 Estimates of effective elastic constants

If the laboratory determined modulus of elasticity is used to estimate the stress sensitivity factor the resulting stress change estimates tend to be too large when compared with the numerical estimates. More reasonable results are obtained when the rock mass discontinuities at the stress monitoring site are taken into account. This is justified by viewing the borehole and its stress-meter cluster as a structure in a discontinuum which undergoes deformations proportional to the effective elastic constants of the discontinuum. The method of estimating the effective modulus of elasticity of the rock mass at the monitoring site is that proposed by Fossum (1985). The calculations appear in Appendix E and the results are presented in Table 4.2.

The values of the stress sensitivity factor presented in Table 4.2 were used for the duration of the stress monitoring phase even though it was expected that mining induced fractures would develop in the rock mass at the stress monitoring site when the longwall was stripped onto the Elf Fault. This is an essentially dynamic process for which no viable means of measurement was considered possible. Consequently the measured stress changes were expected to be overestimates of the true stress changes towards the end of the study.

4.3.2 Uniaxial stress change estimates

The uniaxial stress changes were calculated using the initial vibrating wire reading T_o as the reference reading and Equation 2.2.

TABLE 4.2: ESTIMATES OF STRESS SENSITIVITY FACTORS

ROCK TYPE	APPLICABLE BOREHOLES	MODULUS OF ELASTICITY OF INTACT ROCK*(GPa)	EFFECTIVE MODULUS OF ELASTICITY (GPa)	STRESS SENSITIVITY FACTOR
Hangingwall Quartzite	RB1, RB2, RB6	86,662	62	4,9
Footwall Quartzite	RB3, RB4	75,586	55	5,4

* Averages from the laboratory test results, Table 3.5

The resulting uniaxial stress change evaluations are therefore total uniaxial stress changes that took place between December 1984 and the date in question. The standard rock mechanics notation applies to the data which means that a positive stress change denotes an increase in normal stress in a compressive sense. The uniaxial stress changes calculated for eleven selected times throughout the monitoring period from the data presented in Table 4.1 appear in Table 4.3 while the complete set of data appear in Appendix D.

Not much can be deduced from the uniaxial stress changes aside from the fact that the vertically orientated stressmeters registered the largest stress changes in each borehole with the exception of Borehole RB1, in which the horizontally orientated stressmeter registered the largest stress change. This result is surprising in view of the fact that vertical stress changes should be the largest in the situation under review, with horizontal stress changes being less prominent. This phenomenon can be linked to one of two possibilities. The first is that at the time of stressmeter installation the cables protruding from the borehole were somehow confused with each other, resulting in those from the horizontal and vertical gauges being erroneously labelled. At the time of installations extreme care was taken in labelling the cables correctly to avoid such a possibility. Subsequent checks of field notes covering the installations rule out any errors in labelling. The second possibility is that a small discontinuity-bounded volume of rock containing the stressmeters has undergone anomalous loading. This could occur through mechanisims of slip and rotation as explored by Chappell (1979). It is concluded that a phenomenon of this nature must have taken place in borehole RB1, illustrating vividly the need to monitor stress changes in a number of closely spaced parallel boreholes in order to make a reasonable assessment of stress changes in discontinuous rock masses.

4.3.3 Biaxial stress change estimates

In order to render the data in Table 4.3 amenable to analysis, the stress changes need to be resolved into their respective com-

TABLE 4.3: SELECTED UNIAXIAL STRESS CHANGE ESTIMATES COVERING ENTIRE MONITORING PERIOD

BOREHOLE	DIRECTION	UNIAXIAL STRESS CHANGES (MPa)										
		DEC'84	APR'85	JULY'85	OCT'85	NOV'85	DEC'85	JAN'86	FEB'86	MAY'86	JULY'86	SEPT'86
RB1	Horizontal	0,0	0,0	+0,8	+2,6	+3,3	+ 6,2	+14,7	+19,7	+25,0	+26,2	+27,3
	45°	0,0	0,0	-0,7	+0,3	+0,8	+ 2,5	+ 7,4	+10,3	+13,7	+14,2	+14,9
	Vertical	0,0	0,0	+0,5	+1,1	+1,4	+ 2,6	+ 4,9	+ 6,8	+ 9,2	+ 9,9	+10,5
RB2	Horizontal	0,0	-0,6	-1,0	-1,0	-0,9	- 1,3	+ 0,5	+ 0,3	+ 1,6	+ 1,6	+ 2,1
	45°	0,0	-0,5	-0,3	+0,1	+0,1	- 0,2	- 1,2	- 1,8	- 2,0	- 1,9	- 1,7
	Vertical	0,0	+0,6	+2,5	+5,6	+6,8	+11,1	+18,0	+22,0	+27,6	+29,2	+30,6
RB3	Horizontal	0,0	-0,2	-0,2	-0,8	-0,8	- 0,9	- 0,8	- 1,8	- 2,0	- 2,0	- 2,0
	45°	0,0	+0,4	+1,3	+2,1	+2,6	+ 4,2	+11,0	+12,8	+14,0	+14,6	+15,1
	Vertical	0,0	+0,9	+2,6	+6,3	+7,5	+12,5	+32,0	-	+22,5*	+18,3*	+15,2*
RB4	Horizontal	0,0	0,0	-0,6	-0,3	0,0	- 0,9	-	-	-	-	-
	45°	0,0	0,0	+0,1	+0,4	+0,4	+ 0,3	-	-	-	-	-
	Vertical	0,0	+0,1	+1,0	+3,1	+4,0	+10,2	-	-	-	-	-
RB6	Vertical	0,0	0,0	+0,6	+1,1	+1,2	+ 1,7	+ 2,4	+ 2,5	+ 2,7	+ 2,9	+ 3,2

* Results are probably unreliable.

ponents and expressed in the system of axes defined for each borehole. First the secondary principal stress changes and their directions were calculated for each set of uniaxial stress change readings using the relationships (after Hawkes and Hooker 1974):

$$\Delta\sigma_1 = 3/2a + 3/4b$$

$$\Delta\sigma_2 = 3/2a - 3/4b \qquad \ldots\ldots\ldots\ 4.1$$

$$\theta = \tfrac{1}{2}\sin^{-1}\left[\frac{a - \Delta\sigma_{45}}{b}\right]$$

where

$$a = \tfrac{1}{2}(\Delta\sigma_v + \Delta\sigma_h)$$

$$b = \sqrt{(\Delta\sigma_{45} - a)^2 + (\Delta\sigma_v - a)^2}$$

$\Delta\sigma_h$ = horizontal uniaxial stress change

$\Delta\sigma_{45}$ = 45° uniaxial stress change

$\Delta\sigma_v$ = vertical uniaxial stress change

The angle θ expressed above requires clarification in terms of the stressmeter arrangement employed for the stress monitoring phase. Looking up each borehole the stressmeter directions would appear as shown in Figure 2.14. This arrangement is a mirror image of that proposed by Hawkes and Hooker (1974) and it has the advantage that θ is interpreted in the same way as in the standard rock mechanics notation. Therefore, if θ is positive, $\Delta\sigma_1$ is displaced anticlockwise from the vertical stressmeter direction when viewed from the borehole collar.

The principal stress changes and their directions were then resolved into their normal and shear components. Neither this procedure nor the one before can be applied to Borehole RB6 because a single uniaxial stress change was measured. The data from borehole RB6 is therefore not included in the following discussion and analyses, but will be used at a later stage for comparative purposes.

The results of the above-mentioned calculations for eleven selected times throughout the monitoring phase are presented in Table 4.4

TABLE 4.4: BIAXIAL STRESS CHANGE COMPONENTS AT SELECTED TIMES THROUGHOUT THE STRESS MONITORING PERIOD

BOREHOLE	COMPONENT	BIAXIAL STRESS CHANGES (MPa) DEC'84	APR'85	JUL'85	OCT'85	NOV'85	DEC'85	JAN'86	FEB'86	MAY'86	JULY'86	SEPT'86
RB1	$\Delta\sigma_{y1}$	0,0	0,0	+1,1	+3,3	+4,2	+ 8,0	+18,4	+24,7	+31,6	+33,2	+34,7
	$\Delta\sigma_{x1}$	0,0	0,0	+0,9	+2,2	+2,8	[illegible]	+11,0	+15,0	+19,7	+21,0	+22,1
	$\Delta\tau_{x1y1}$	0,0	0,0	-1,0	-1,2	[illegible]	[illegible]	- 1,8	- 2,2	- 2,5	- 2,9	- 3,0
RB2	$\Delta\sigma_{y2}$	0,0	+0,5	+2,4	+5,9	[illegible]	[illegible]	+20,4	+24,9	+31,7	+33,5	+35,2
	$\Delta\sigma_{x2}$	0,0	-0,4	-0,2	+1,0	+1,5	+ 2,7	+ 7,3	+ 8,6	+12,2	+12,8	+13,8
	$\Delta\tau_{x2y2}$	0,0	-0,4	-0,8	-1,7	-2,1	- 3,8	- 7,8	- 9,7	-12,5	-13,0	-13,5
RB3	$\Delta\sigma_{y3}$	0,0	+0,9	+2,9	+6,8	+8,1	+13,7	+35,7	-	+24,6*	+19,8*	+16,4*
	$\Delta\sigma_{x3}$	0,0	+0,1	+0,7	+1,5	+1,9	+ 3,7	+11,1	-	+ 6,2*	+ 4,6*	+ 3,4*
	$\Delta\tau_{x3y3}$	0,0	0,0	+0,1	-0,5	-0,6	- 1,2	- 3,4	-	+ 2,8*	+ 4,8*	+ 6,4*
RB4	$\Delta\sigma_{y4}$	0,0	+0,1	+0,9	+3,4	+4,5	+11,1	-	-	-	-	-
	$\Delta\sigma_{x4}$	0,0	0,0	-0,3	+0,8	+1,5	+ 2,8	-	-	-	-	-
	$\Delta\tau_{x4y4}$	0,0	0,0	-0,1	-0,8	-1,2	- 3,3	-	-	-	-	-

* Results are probably unreliable

while the complete results are presented in Appendix D. The stress change components listed in the table and the appendix all show well defined trends. The normal stress changes for all the boreholes are consistently positive which means that the rock mass at the site was subject to an increase in compressive stress both in the horizontal and vertical directions. The shear stress changes for Boreholes RB2 and RB3 show reasonable agreement in that they indicate the rock mass loading took place from similar directions. This is not the case when comparing the shear stress changes in Boreholes RB1 and RB4 because a uniform loading direction should be expressed by shear stress changes of opposite sign. This effect is probably the result of discontinuities in the rock mass and the presence of the Elf Fault between the stressmeter clusters in each borehole.

Another feature of the data in Table 4.4 is the fact that the vertical stress changes are consistently the largest in all four boreholes. In the case of Borehole RB1 this was unexpected because of the anomalous results in Table 4.3. Nevertheless, the stress components as calculated for Borehole RB1 were the natural outcome of the substitution of the respective values into Equations 4.1 and then resolution into the repective components in terms of the system of axes defined for the borehole. It was found that the outcome was unaffected by swopping $\Delta\sigma_h$ and $\Delta\sigma_v$ around, because the value of b in Equations 4.1 is unaffected by the substitution. It was therefore concluded that first, when calculating b, the positive alternative would be chosen in all cases when the square root was found, and second, that the horizontal and vertical stress changes as measured would be correctly substituted into their respective positions in all cases. Any other procedure would introduce bias to the results.

Even so, the horizontal stress component changes measured in borehole RB1 are anomalously large when compared with those of other boreholes, and are therefore still consistent with the data and discussion of Table 4.3

4.3.4 Error of stress change estimates

The error in stress change estimates can be assessed by comparing two or more in the same direction. The vertical stress changes measured in each borehole are therefore suitable for analysis. The first requirement of such an analysis is that the measurements to be compared should be reasonably close to one another in order to avoid as far as possible spatial variations of induced stress changes that may occur. Secondly the measurements should come from geologically similar rock so that variation in estimates that arise when comparing measurements in different rock types are eliminated. For these reasons, the vertical stress changes measured in Boreholes RB1 and RB2 can be compared while those from Boreholes RB3 and RB4 are suitable for comparison. Since only two values can be considered at a time, a formal statistical error determination is not possible. Therefore, the definition of stress change error takes the form similar to the inherent error defined in Equation 3.1:

$$\xi = \frac{2\left[\Delta\sigma_{ya} - \Delta\sigma_{yb}\right]}{\Delta\sigma_{ya} + \Delta\sigma_{yb}} \quad \ldots\ldots\ldots \quad 4.2$$

where ξ is the stress change error, and $\Delta\sigma_{ya}$ and $\Delta\sigma_{yb}$ are the measured vertical stress changes in boreholes a and b respectively.

The stress change error is essentially transient in that it varies with time. The errors were calculated from the data in Table 4.4 and then plotted against time (Figure 4.2a). In the first half of the monitoring period the stress change errors for boreholes RB1 and RB2 as well RB3 and RB4 show errors well in excess of 20%. This is caused by the fact that, until December 1985, the mining induced stress changes were relatively small and stress change monitoring started in the different boreholes at different times. When the total stress changes induced by mining became large during and after December 1985, the errors between the measurements quickly dropped below 10%, and levelled out in the 1% to 3% range.

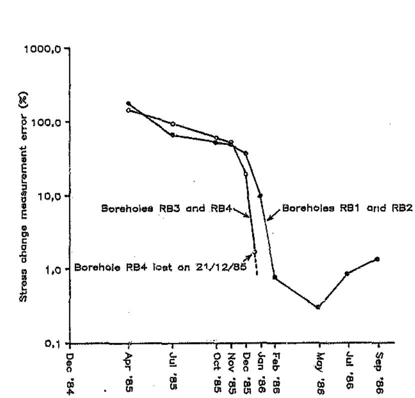

a: Plot of stress change error versus time

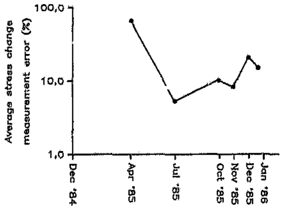

b: Plot of average stress change error versus time

Figure 4.2

Plots of stress change measurement error versus time

A similar plot of average vertical stress change error was plotted against time appears in Figure 4.2b. In this case the percent error is found from the average vertical stress changes calculated for Boreholes RB1 and RB2 and the average for RB3 and RB4. The curve drops quickly to a minimum in July 1985 and then rises slowly thereafter. The increase would appear to be caused by the fact that Boreholes RB3 and RB4 were closer to the advancing longwall, and were therefore subject to consistently greater mining induced stress changes than were Boreholes RB1 and RB2.

The major deductions to be made from the plots are that the vertical stress changes were measured with decreasing error as the magnitudes of the stress changes increased. This pattern held for the hangingwall quartzites to the west of the Elf Fault and the footwall quartzites to the east of the fault. The analysis also showed that when the stress changes became large, the agreement between the measurements was good. A similar analysis was not carried out for the horizontal stress change measurements because firstly, these changes were measured in different directions, thereby limiting the scope of the analysis, and secondly the horizontal stress changes were less prominent than the vertical changes, and therefore were measured with a lower degree of certainty.

4.3.5 Stability of the Elf Fault

The presence of the fault indicates that at some period in geological time the rock mass at the monitoring site was unstable, which initiated major shear deformation. The stress field responsible for the deformation appears to have dissipated resulting in a pre-mining virgin stress field that is primarily a product of gravity loading by the superincumbent strata. The fault is not known to be seismically active although the superposition of mining induced stress on the virgin stress field may make it so (Cook et al 1966). A check on potential fault instability from a stress point of view was monitored throughout the stress monitoring period by making use of the recently introduced criterion called Excess Shear Stress, first discussed by Ryder et al (1978).

The excess Shear Stress or ESS is defined as:-

$$\tau \text{ excess} = \tau_{nm} - (Co + \mu\sigma_n) \quad \text{.........} \; 4.3$$

where τ excess = Excess Shear Stress

τ_{nm} = resultant shear stress on oblique plane

Co = cohesive strength of oblique plane

μ = coefficient of friction on oblique plane

σ_n = normal stress acting on oblique plane.

If the ESS is negative it means that the plane for which it is calculated is stable. In cases where the ESS is found to be zero or positive, the plane is unstable and slip can occur.

The ESS on the Elf Fault surface can be found in two dimensions by considering the stress data obtained in the planes of Boreholes RB2 and RB3. In this case it is assumed that both boreholes are parallel and that their planes intersect the fault on true dip, as shown in Figure 4.3. First, the total stresses acting in each borehole are found by applying the principle of superposition which means that the stress change components listed in Table 4.4 are simply added to their corresponding initial stress components listed in Table 3.7. The resulting total stress components appear in Table 4.5. The absolute normal and shear stresses acting on the Elf Fault surface can be found from the total stress components by the relations given in all discussions of elementary stress analysis.

Table 4.6 contains the normal, shear and excess shear stress calculated for a plane with $C_o = 0$ and $\mu = \tan 30°$. The estimates of the ESS are conservative, that is they are closer to zero than they would otherwise have been had larger values for the cohesive strength and the coefficient of friction been chosen.

Nevertheless, the ESS was negative for the duration of the stress monitoring phase, indicating that the Elf Fault surface in the vicinity of the stress monitoring site was stable. The conclusion does not apply to the entire known extent of the fault as there

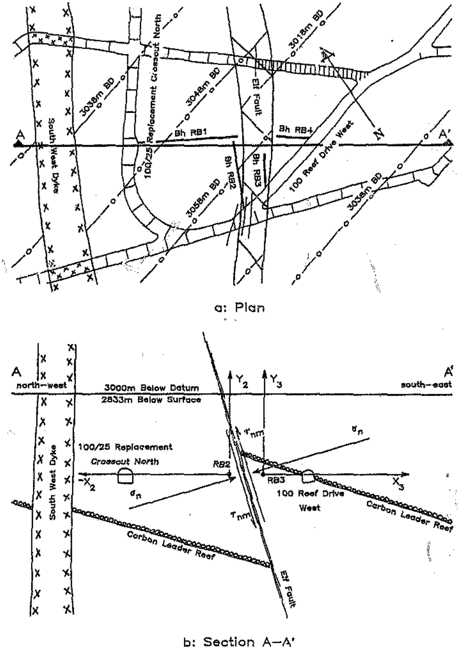

Figure 4.3

Dip section of fault at Boreholes RB2 and RB3

Scale 1:1000

TABLE 4.5: TOTAL STRESS COMPONENTS FOR RB2 AND RB3

BOREHOLE	COMPONENT	TOTAL STRESS COMPONENTS (MPa) INITIAL DEC'84	APR'85	JULY'85	OCT'85	NOV'85	DEC'85	JAN'86	FEB'86	MAY'86	JULY'86	SEPT'86
RB2	σ_y	+92,2	+92,7	+94,6	+98,1	+99,1	+104,2	+112,6	+117,1	+123,9	+125,7	+127,4
	σ_x	+49,9	+49,5	+49,7	+50,9	+51,4	+ 52,6	+ 57,2	+ 58,5	+ 62,1	+ 62,7	+ 63,7
	τ_{xy}	+ 3,0	+ 2,6	+ 2,2	+ 1,3	+ 0,9	- 0,8	- 4,8	- 6,7	- 9,5	- 10,0	- 10,5
RB3	σ_y	+71,2	+72,1	+74,1	+78,0	+79,3	+ 84,9	+106,9	-	+ 95,8*	+ 91,0*	+ 87,6*
	σ_x	+33,5	+33,6	+34,2	+35,0	+35,4	+ 37,2	+ 44,6	-	+ 39,7*	+ 38,1*	+ 36,9*
	τ_{xy}	- 1,3	- 1,3	- 1,2	- 1,8	- 1,9	- 2,5	- 4,7	-	+ 1,5*	+ 3,5*	+ 5,1*

* Results probably unreliable

TABLE 4.6: ABSOLUTE NORMAL, SHEAR AND EXCESS SHEAR STRESS ON THE ZLF FAULT SURFACE WITH TIME

CALCU-LATED FROM	COMPONENT	INITIAL DEC'84	APR'85	JULY'85	OCT'85	NOV'85	DEC'85	JAN'86	FEB'86	MAY'86	JULY'86	SEPT'86
RB2	σ_n	+55,7	+55,0	+54,9	+55,4	+55,5	+55,3	+56,1	+55,7	+56,7	+56,9	+57,5
	τ_{nm}	+13,2	+13,1	+13,1	+12,9	+12,7	+12,2	+ 9,7	+ 8,8	+ 7,2	+ 7,1	+ 6,8
	τ_{excess}	-19,0	-18,7	-18,6	-19,0	-19,3	-19,7	-22,7	-21,3	-25,5	-25,8	-26,3
AVERAGED STRESSES from RB2 & RB3	σ_n	+45,2	+44,9	+45,3	+45,7	+46,0	+46,6	+50,1	-	+50,8*	+51,0*	+51,4*
	τ_{nm}	+10,7	+10,8	+11,0	+11,1	+11,0	+11,0	+10,6	-	+11,3*	+11,7*	+12,0*
	τ_{excess}	-15,4	-15,2	-15,1	-15,3	-15,5	-15,9	-18,3	-	-18,1*	-17,8*	-17,7*

* Results probably unreliable.

is likely to be spatial variation of the total stress as a result of mining in the area. This variation is investigated at a later stage.

4.4 Effects of Stress Changes on the Elf Fault

Stress changes may induce stable or unstable shear deformation along the fault surface. This can be indentified by locating all seismic events that occur in the area, and by maintaining continuous observations of movement on the fault plane itself. The former was possible with the use of the mine-wide seismic location system while the latter was acheived by visual observation of the fault itself, and by a series of levelling surveys.

4.4.1 Seismic record

A record of the mining induced seismicity that took place in the monitoring area was kept for the duration of the project. The purpose of the record was to relate where possible any stress changes that may take place as a result of seismicity, and to provide a second set of independent observations about the stability of the fault.

A total of 64 seismic events were detected within a radius of approximately 300 m of the monitoring site for the period December 1984 to September 1986. The location and magnitude of each event was determined from information provided by the mine wide seismic monitoring system. A frequency histogram of the magnitude distribution of the seismicity is shown in Figure 4.4. More than half of the events detected had magnitudes of 1,0 or less on the Richter Scale and were not related with any damage to the mine workings. Of the rest, several caused damage, but none of the boreholes or the instruments were affected.

The seismic events with magnitudes bigger than 1,0 on the Richter Scale were plotted on a 1:1000 plan as they occurred in order to identify those that may have originated on the fault. The plots are shown in Figure 4.5. The depth of each location accompanies its plan position so that its spatial relationship with the inferred

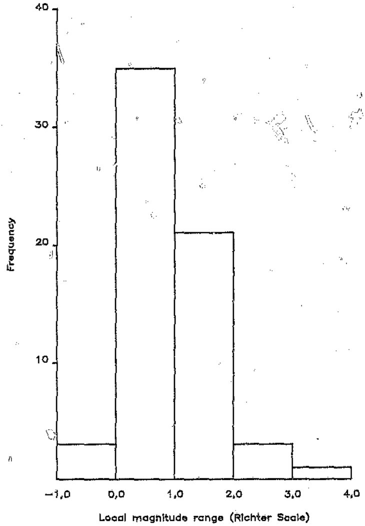

Figure 4.4

Frequency histogram of seismicity in the monitoring site area for the period December 1984 to September 1986

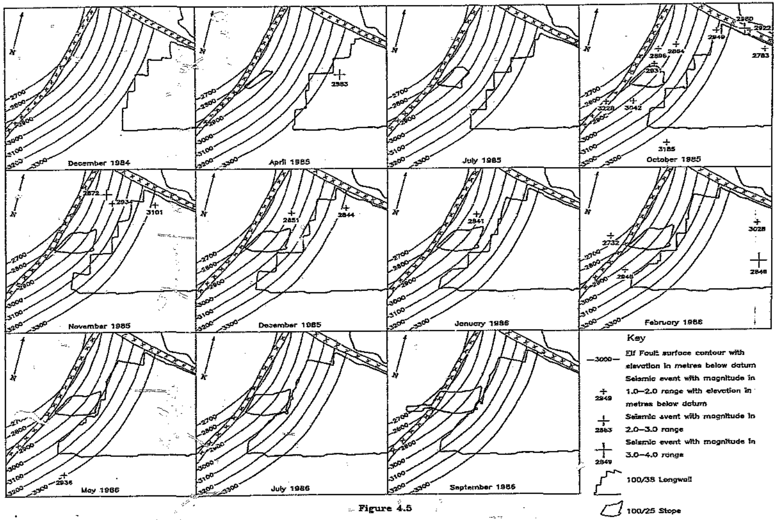

Figure 4.5

Locations of seismic events in the monitoring site area

Scale 1:5000

position of the fault is readily discernible. An underground trip was made on each occasion that the fault was suspected of being the source in order to look for signs of movement. Vibrating wire period readings were taken at the same time to check whether the stress state in the monitoring site area had been affected. On no occasion was the stress state found to be altered by seismic activity, nor were any signs of movement on the fault plane visible.

4.4.2 Levelling survey results

Levelling of a series of rock anchors set in the hangingwall above 100/2 'C' Haulage West was carried out during the stress monitoring phase. The largest movements occurred during the critical period from October 1985 to February 1986 when the longwall approached the fault. Movements before and after this period were small and are not considered in the analysis.

Vertical displacements were measured in relation to a datum, chosen as Levelling Station No.13 as it was most remote from the mining activity and therefore least affected. The absolute displacement, if any, of this station is not known. Relative displacements of each levelling station with respect to the datum are listed in Table 4.7 for October 1985 and February 1986, together with the changes in displacement.

The displacement changes appear to be affected by movements induced by the installation of support in the haulage, which took place concurrently with the project. Nevertheless, they show that no movement took place on the fault surface, an observation supported by the paint strips across the fault traces both in 100/2 'C' Haulage West and in 100/25 Stope.

4.5 Concluding Remarks

The stress change estimates reflect the expected patterns of small stress changes while the longwall was some distance away, and larger stress changes as it drew closer to the monitoring sits. The stress changes measured were universally compressive in nature, position of the fault is readily discernible. An underground trip was made on each occasion that the fault was suspected of being the source in order to look for signs of movement. Vibrating wire period readings were taken at the same time to check whether the stress state in the monitoring site area had been affected. On no occasion was the stress state found to be altered by seismic activity, nor were any signs of movement on the fault plane visible.

4.4.2 Levelling survey results

Levelling of a series of rock anchors set in the hangingwall above 100/2 'C' Haulage West was carried out during the stress monitoring phase. The largest movements occurred during the critical period from October 1985 to February 1986 when the longwall approached the fault. Movements before and after this period were small and are not considered in the analysis.

Vertical displacements were measured in relation to a datum, chosen as Levelling Station No.13 as it was most remote from the mining activity and therefore least affected. The absolute displacement, if any, of this station is not known. Relative displacements of each levelling station with respect to the datum are listed in Table 4.7 for October 1985 and February 1986, together with the changes in displacement.

The displacement changes appear to be affected by movements induced by the installation of support in the haulage, which took place concurrently with the project. Nevertheless, they show that no movement took place on the fault surface, an observation supported by the paint strips across the fault traces both in 100/2 'C' Haulage West and in 100/25 Stope.

4.5 Concluding Remarks

The stress change estimates reflect the expected patterns of small stress changes while the longwall was some distance away, and larger stress changes as it drew closer to the mc site. The stress changes measured were universally n nature,

TABLE 4.7: RESULTS OF LEVELLING SURVEY

LEVELLING STATION NUMBER	VERTICAL DISPLACEMENTS (mm)		
	OCT.1985	FEB.1986	DIFFERENCE
13	0	0	0
12	-1	-1	0
11	-1	+2	+3
10	+1	+7	+6
9	0	+7	+7
8	0	+7	+7
7	0	+6	+6
6	-2	-5	-3
5	-3	-5	-2
4	-3	-8	-5
3	+3	+21	+18
2	-3	-9	-6
1	-3	-8	-5
1A	-3	-9	-6

and resulted in a final stress state that was greater in a compressive sense than the initial stress state, both in the vertical and all horizontal directions.

The total stresses resulting from the initial stresses and stress changes never reached a condition sufficient to induce unstable equilibrium. This is reflected in the Excess Shear Stress calculated for the duration of the monitoring period, and borne out by the lack of movement on the *fault as* well *as* the fact that none of the located seismic events in the area could be irrefutably *ascribed to the* fault. It appears that the fault remained stable for the duration of the stress monitoring phase, especially in the areas where it is exposed. More detailed analysis of the fault behaviour is carried out in Chapter 6.

The results presented so far and the conclusions reached do indicate that the vibrating wire stressmeter is a reliable instrument that can be used to obtain reasonable stress change results in deep gold mines.

CHAPTER 5

RESULTS OF NUMERICAL ANALYSES

Stress and displacement data were *generated numerically* at selected points for comparison with the underground measurements. The MINSIM - D Phase 111 suite of programs was used for the *analysis*. This version is capable of calculating the Excess Shear Stress on planes having any orientation, a facility not available on earlier versions. The analyses were carried out by a Perkin Elmer 3230 computer system operated by the Anglo American Corporation *Rock Mechanics* Department in Welkom, Orange Free State.

The procedure and *analytical model* is outlined together with brief descriptions of some parameters necessary for the analysis. The results of the stress and displacement *analyses are then* presented. Finally, analysis error is dealt with briefly.

5.1 Analytical Model

The problem is approached by first digitizing the mine plans *in the area of interest* and entering via a user-friendly input program parameters such as rock elastic constants, depth, stoping width etc., required for the *analysis*. Closure and ride solutions are then found by running the SOLUTION program. Stresses, displacements and other variables are calculated at the *conclusion* of the analysis by running the BENCHMARK program, which operates on data generated by the SOLUTION program. The results may be obtained in the form of computer printouts, contour plots or other representations requested by the user, depending on the *computer* equipment available.

In the case *of the monitoring site*, the model consists of two reef planes parallel to each other and separated by a vertical distance of 40 m, Figure 5.1. The fault *surface* was *not* modelled

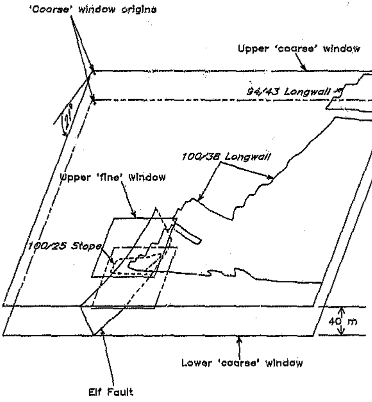

Figure 5.1

Perspective view of analytical model

Not to scale

because of its curvature. Both planes were inclined at the same angle as the reef dip observed at the monitoring site, and the depths below surface correspond to those at the site.

The major principal stress prior to min:.g in the area was assumed to be vertical and equal to the weight of the overlying strata given a density of 2700 kg/m^3. The corresponding intermediate and minor principal stresses were assumed to be equal, to lie in a horizontal plane and to have a magnitude of 0,45 times the major principal stress. This ratio was derived from the initial stress measurements in the area.

The outer or "coarse" window defined for each reef plane consists of a square area on reef broken up into 64 x 64 square elements (Chamber of Mines Research Organization, 1985). Each element is specified as being mined, partially mined or unmined, according to the mining geometry contained within the window. The element size for the coarse windows was set at 24 m which results in a window large enough to include mining on the entire 100/38 Longwall as well as the 94/43 Longwall to the north. The stoping patterns for these longwalls were digitized from 1:2500 scale mine plans and were defined on the upper reef plane window while that of the 100/25 Stope was defined on the lower reef plane, Figure 5.1. The mining excavations in the model therefore have the correct spatial relationship with each other.

Representative effective elastic constants of the rock were used in the analysis. They were obtained by averaging the laboratory test results presented in Table 3.5 and using the result in the method proposed by Fossum (1985). The calculations are presented in Appendix E. The effective elastic modulus was estimated to be 71 GPa and the effective Poisson's ratio, 0,20. These values are in good agreement with the widely accepted values of 70 GPa and 0,20 respectively used in analyses of this nature. Since the calculated values were so close to the widely accepted values, the latter were used in the analyses.

A stoping width of 1 m was used throughout. Closure and ride solutions were generated for eleven mining steps beginning with the measured longwall face positions for December 1984 and ending with those for September 1986, which appear in Figure 5.2. The intervening mining steps were taken as the surveyed longwall geometries as shown for the dates listed in Figure 4.1. Direct comparison of analytical results and underground measurements are therefore possible, although the numerical results are under-estimated because not all the mining was taken into account, as depicted in Figure 5.2.

A second set of closure and ride solutions were generated for each mining step by specifying a scaled "fine" window centered on the monitoring site within the original coarse windows, as shown in Figures 5.1 and 5.2. The fine windows effect a four-fold increase in resolution in the results obtained for the area of interest. Stresses and displacements were calculated from the "fine" solution data at a number of selected benchmark points.

5.2 Analysis Statistics

The computer system logged a total of 6 hours and 14 minutes of central processing unit time to solve the closures and rides for eleven mining steps. The benchmark processing required an additional 17 hours and 36 minutes of central processing unit time. These statistics emphasize the "number crunching" nature of the programs and therefore the cost of undertaking the analyses. For this reason, the analytical model was limited to the two coarse and two fine windows, which exclude the effects of mining further to the north, east and south-east of the monitoring site.

The benchmark statistics are listed in Table 5.1. Each benchmark point list contains 22 pieces of information which include the benchmark number, coordinates expressed in two coordinate systems, displacements, stresses and other variables requested by the user. In this analysis it amounts to 223146 pieces of information which, together with titles, headings and labels, occupy 378 pages of computer printout. The SOLUTION program log files occupy a further 152 pages. Listing all this information either in the text or an appendix is clearly impractical. Therefore only

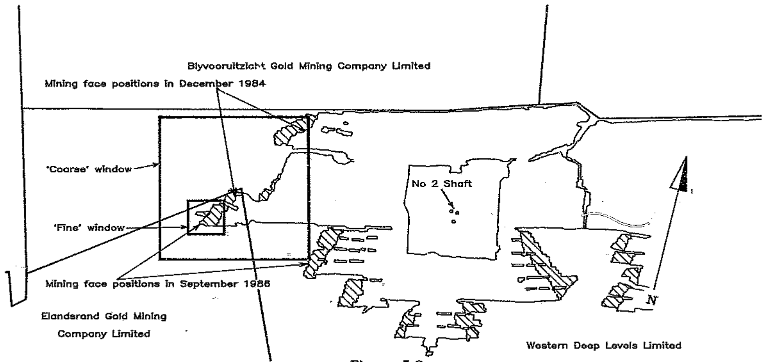

Figure 5.2

Plan showing analytical windows in relation to extent of mining

on the Carbon Leader Reef

Scale 1:30000

TABLE 5.1: LIST OF BENCHMARK POINTS GENERATED IN ANALYSIS

FEATURE MODELLED	NUMBER OF BENCHMARK POINTS	NUMBER OF MINING STEPS	TOTALS	OUTPUT
Stress Monitoring Boreholes	5	11	55	Principal Stresses
Final Stress Measurements	1	1	1	Principal Stresses
Elf Fault Surface	882	11	9702	Excess Shear Stress
Stress Profile	143	1	143	Principal Stresses
Levelling Survey	22	11	242	Displacements
Total benchmark points processed			10143	

an example of each is presented in Appendix F while the complete data are bound in separate volumes and kept in the Rockburst Project Library, Western Deep Levels, Limited. None of the output information was requested in graphic form.

5.3 Analysis Results

Five groups of data were generated in the analyses, as shown in Table 5.1. The standard engineering stress notation was adopted by the Chamber of Mines Research Organization when developing MINSIM-D which explains the fact that all the normal stresses represented in Appendix F have negative values. They were converted to the standard rock mechanics sign convention for presentation in the text.

In view of the volume of data to be considered, only small portions are presented in tabular form, such as the stresses and stress changes The rest is presented graphically or pictorially, whichever form is most effective.

5.3.1 Stresses and stress changes

Six benchmark points were specified at positions corresponding to the measuring positions of Boreholes RB1, RB2, RB3, RB4, RB6 and RB7. The numerically derived stresses are expressed as total principal stresses and their directions in three dimensions, Appendix F.

These results were converted to the plane of each borehole by plotting each principal stress direction on an equal angle stereonet together with the system of axes defined for the corresponding borehole as shown in Figure 3.1. The angle between each principal stress direction and borehole axis was determined stereographically and used to calculate the biaxial stress components in terms of the borehole system of axes. The results are presented in Table 5.2 while the calculations appear in Appendix G.

TABLE 5.2: NUMERICALLY DERIVED TOTAL STRESSES FOR THE STRESS MEASUREMENT BOREHOLE POSITIONS

BOREHOLE	TOTAL STRESS COMPONENTS (MPa)											
	COMPONENT	Dec'84	Apr'85	Jul'85	Oct'85	Nov'85	Dec'85	Jan'86	Feb'86	May'86	Jul'86	Sep'86
RB 1	σ_{y1}	+80,2	+80,9	+82,9	+84,9	+87,1	+90,3	+105,9	+108,0	+110,5	+111,5	+113,1
	σ_{x1}	+38,0	+38,7	+40,4	+41,3	+42,2	+43,7	+ 43,9	+ 44,9	+ 46,2	+ 47,0	+ 47,7
	τ_{x1y1}	− 0,3	− 0,3	− 0,7	+ 1,1	+ 2,1	+ 3,4	− 6,4	− 6,3	− 6,4	− 5,8	− 5,0
RB 2	σ_{y2}	+80,1	+80,9	+82,9	+84,9	+86,6	+89,1	+101,0	+102,6	+104,7	+105,8	+106,7
	σ_{x2}	+36,3	+36,7	+37,6	+37,8	+40,2	+40,3	+ 39,5	+ 39,9	+ 37,0	+ 39,3	+ 40,7
	τ_{x2y2}	− 0,5	− 1,9	− 2,5	− 2,1	− 3,1	− 2,2	− 4,7	− 3,8	− 3,8	− 7,8	− 8,4
RB 3	σ_{y3}	+80,2	+80,8	+82,8	+84,9	+87,2	+90,5	+113,6	+116,3	+118,7	+125,6	+129,0
	σ_{x3}	+35,9	+36,3	+36,9	+37,7	+38,7	+40,0	+ 35,5	+ 35,6	+ 35,2	+35,0	+ 36,6
	τ_{x3y3}	− 0,5	− 1,9	− 1,5	− 2,1	− 3,2	− 5,6	− 2,2	− 2,3	− 1,4	− 2,0	− 3,9
RB 4	σ_{y4}	+80,2	+80,9	+83,2	+85,5	+89,3	+97,0	*	*	*	*	*
	σ_{x4}	+38,7	+39,5	+42,4	+45,1	+48,1	+51,1	*	*	*	*	*
	τ_{x4y4}	+ 0,4	+ 0,4	−1,2	− 0,7	− 0,9	− 2,0	*	*	*	*	*
RB 6	σ_{y6}	78,8	79,0	79,5	79,9	80,0	80,2	80,4	80,6	80,9	81,1	81,6
RB 7	σ_{y7}	−	−	−	−	−	−	−	−	−	−	+ 91,3
	σ_{x7}	−	−	−	−	−	−	−	−	−	−	+ 42,6
	τ_{x7y7}	−	−	−	−	−	−	−	−	−	−	− 0,1

Notes: * Benchmark reliability flag was set because benchmark point less than 1 grid element size away from mined element.

− Benchmarks not requested.

TABLE 5.2: NUMERICALLY DERIVED TOTAL STRESSES FOR THE STRESS MEASUREMENT BOREHOLE POSITIONS

BOREHOLE	TOTAL STRESS COMPONENTS (MPa)											
	COMPONENT	Dec'84	Apr'85	Jul'85	Oct'85	Nov'85	Dec'85	Jan'86	Feb'86	May'86	Jul'86	Sep'86
RB 1	σ_{y1}	+80,2	+80,9	+82,9	+84,9	+87,1	+90,3	+105,9	+108,0	+110,5	+111,5	+113,1
	σ_{x1}	+38,0	+38,7	+40,4	+41,3	+42,8	+43,7	+ 43,9	+ 44,9	+ 46,2	+ 47,0	+ 47,7
	τ_{x1y1}	- 0,3	- 0,3	- 0,7	+ 1,1	+ 2,1	+ 3,4	- 6,4	- 6,3	- 6,4	- 5,8	- 5,0
RB 2	σ_{y2}	+80,2	+80,9	+82,9	+84,9	+86,6	+89,1	+101,0	+102,6	+104,7	+105,8	+106,7
	σ_{x2}	+36,3	+36,7	+37,6	+37,8	+40,2	+40,3	+ 39,5	+ 39,9	+ 37,0	+ 39,3	+ 40,7
	τ_{x2y2}	- 0,5	- 1,9	- 2,5	- 2,1	- 3,1	- 2,2	- 4,7	- 3,8	- 3,8	- 7,8	- 8,4
RB 3	σ_{y3}	+80,2	+80,8	+82,8	+84,9	+87,2	+90,5	+113,6	+116,3	+118,7	+125,6	+129,0
	σ_{x3}	+35,9	+36,3	+36,9	+37,7	+38,7	+40,0	+ 35,5	+ 35,6	+ 35,2	+35,0	+ 36,6
	τ_{x3y3}	- 0,5	- 1,9	- 1,5	- 2,1	- 3,2	- 5,6	- 2,2	- 2,3	- 1,4	- 2,0	- 3,9
RB 4	σ_{y4}	+80,2	+80,9	+83,2	+85,5	+89,3	+97,0	*	*	*	*	*
	σ_{x4}	+38,7	+39,5	+42,4	+45,1	+48,1	+51,1	*	*	*	*	*
	τ_{x4y4}	+ 0,4	+ 0,4	-1,2	- 0,7	- 0,9	- 2,0	*	*	*	*	*
RB 6	σ_{y6}	78,8	79,0	79,5	79,9	80,0	80,2	80,4	80,6	80,9	81,1	81,6
RB 7	σ_{y7}	-	-	-	-	-	-	-	-	-	-	+ 91,3
	σ_{x7}	-	-	-	-	-	-	-	-	-	-	+ 42,6
	τ_{x7y7}	-	-	-	-	-	-	-	-	-	-	- 0,1

Notes: * Benchmark reliability flag was set because benchmark point less than 1 grid element size away from mined element.

- Benchmarks not requested.

TABLE 5.3: NUMERICALLY DERIVED STRESS CHANGES FOR THE STRESS MEASUREMENT BOREHOLE POSITIONS

BOREHOLE	STRESS CHANGE COMPONENTS (MPa)											
	COMPONENT	Dec'84	Apr'85	Jul'85	Oct'85	Nov'85	Dec'85	Jan'86	Feb'86	May'86	Jul'86	Sep'86
RB 1	$\Delta\sigma_{y1}$	0,0	+0,7	+2,7	+4,7	+6,9	+10,1	+25,7	+27,8	+30,3	+31,3	+32,6
	$\Delta\sigma_{x1}$	0,0	+0,7	+2,4	+3,3	+4,8	+ 5,7	+ 5,9	+ 6,9	+ 8,2	+ 9,0	+ 9,7
	$\Delta\tau_{x1y1}$	0,0	0,0	-0,4	+1,4	+2,4	+ 3,7	- 6,1	- 6,0	- 6,1	- 5,5	- 4,5
RB 2	$\Delta\sigma_{y2}$	0,0	+0,7	+2,7	+4,7	+6,4	+ 8,9	+20,8	+22,4	+24,5	+25,6	+26,5
	$\Delta\sigma_{x2}$	0,0	+0,4	+1,3	+1,5	+3,9	+ 4,0	+ 3,2	+ 3,6	+ 0,7	+ 3,0	+ 4,4
	$\Delta\tau_{x2y2}$	0,0	-1,4	-2,0	-1,6	-2,6	- 1,7	- 4,2	- 3,3	- 3,3	- 7,3	- 7,9
RB 3	$\Delta\sigma_{y3}$	0,0	+0,6	+2,6	+4,7	+7,0	+10,3	+33,4	+36,1	+38,5	+45,4	+48,8
	$\Delta\sigma_{x3}$	0,0	+0,4	+1,0	+1,8	+2,8	+ 4,1	- 0,4	- 0,3	- 0,7	- 0,9	+ 0,7
	$\Delta\tau_{x3y3}$	0,0	-1,4	-1,0	-1,6	-2,7	- 5,1	- 1,7	- 1,8	- 0,9	-1,5	- 3,4
RB 4	$\Delta\sigma_{y4}$	0,0	+0,7	+3,0	+5,3	+9,1	+16,8	-	-	-	-	-
	$\Delta\sigma_{x4}$	0,0	+0,8	+3,7	+6,4	+9,4	+12,4	-	-	-	-	-
	$\Delta\tau_{x4y4}$	0,0	0,0	-1,6	-1,1	-1,3	- 2,4	-	-	-	-	-
RB 6	$\Delta\sigma_{y6}$	0,0	+0,2	+0,7	+1,1	+1,2	+ 1,4	+ 1,6	+ 1,8	+ 2,1	+ 2,3	+ 2,8
RB 7	$\Delta\sigma_{y7}$	0,0	-	-	-	-	-	-	-	-	-	+11,1*
	$\Delta\sigma_{x7}$	0,0	-	-	-	-	-	-	-	-	-	+ 4,6*
	$\Delta\tau_{x7y7}$	0,0	-	-	-	-	-	-	-	-	-	+ 0,2*

Notes: * Obtained by subtracting the initial stresses estimated numerically for Borehole RB1.

The stress changes, presented in Table 5.3, are obtained by subtracting the total stress components calculated for December 1984 from the total   ess components calculated for that and each subsequent date. These results are directly comparable with those of Table 4.4, and are discussed in Section 6.2.

Biaxial stress change components were not necessary in the case of Borehole RB6. Here, the vertical stress only was calculated from the numerical results and the vertical stress changes determined in the same way mentioned above. The initial and final absolute stresses are represented by the values listed in the first and last columns of Table 5.2 respectively.

5.3.2 Stress distribution on fault

The stress state on the Elf Fault surface was determined by defining the ESS at a series of benchmark points distributed over its known extent. The ESS distribution so determined provides a direct means of assessing the potential seismic hazard posed by the presence of the fault as well as the areas on the fault surface that are most likely to be unstable as a result of the given mining geometry.

Two assumptions are necessary for the benchmark point location. The first is that the fault dip is invariant at 75° for a distance 300 m above reef to 300 m below reef. The dip direction varies, producing the curved surface shown. The second assumption is that the inferred intersection of the Elf Fault and South West Dyke shown in Figure 2.2 is sufficiently remote from the mining excavations to have no effect.

Direct evaluation of the ESS at each point on the fault plane is achieved by rotating the x-axis of a benchmark sheet in a horizontal plane to a direction tangential to the fault surface at the sheet origin. The y-axis of the sheet is then rotated downwards through 75 degrees so that it lies on the fault surface for its entire length in the true fault dip direction. Only one benchmark point is defined in the x-axis direction, while

49 points are defined at 12,5 m intervals in the y-axis direction, as shown in Figure 5.3. A total of eighteen benchmark strings were defined in this manner, and shown as lines in Figure 5.4.

The ESS was calculated numerically at each point from the stress conditions arising from each mining step using the relation given by the Chamber of Mines Research Organization (1985). This equation is similar to Equation 4.3 aside from the fact that it is expressed in terms of the engineering stress sign convention. The cohesive strength of the plane being analysed is assumed to be zero. The ESS is given as two values, each corresponding to a coefficient of friction of tan 30° and tan 45°. The ESS value corresponding to the lower coefficient of friction is used in all cases.

The ESS distributions on the Elf Fault surface are shown in Figure 5.4 It is apparent that the potential for fault-generated seismicity increased during the course of the stress monitoring phase. This is especially true where the 100/38 Longwall and 100/25 Stope overlap. At the measuring positions, the fault plane is indicated to be stable.

The numerically derived ESS at the borehole measurement positions was calculated as the average for the six benchmark points closest to the instrument positions and listed in Table 5.4. The results show a consistent increase in the ESS as the mining approached the fault, except for the last mining step where the ESS is seen to decrease again. These results are compared with the measurement results in Section 6.4.3.

The ESS results given are conservative, that is, they are greater than they otherwise would have been because the fault surface is assumed to have no cohesive strength. Moreover, the coefficient of friction used is lower than the static value determined for quartzites of approximately tan 45° (Dieterich, 1972).

5.3.3 Stress distribution in vicinity of longwall

A vertically orientated benchmark sheet set parallel to reef

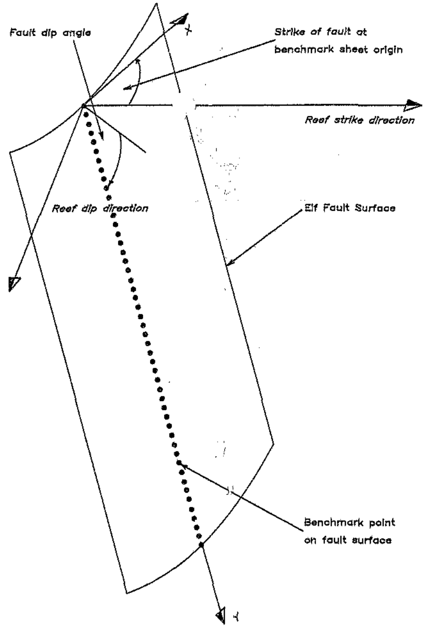

Figure 5.3
Diagram illustrating benchmark string definition
on fault surface
Not to scale

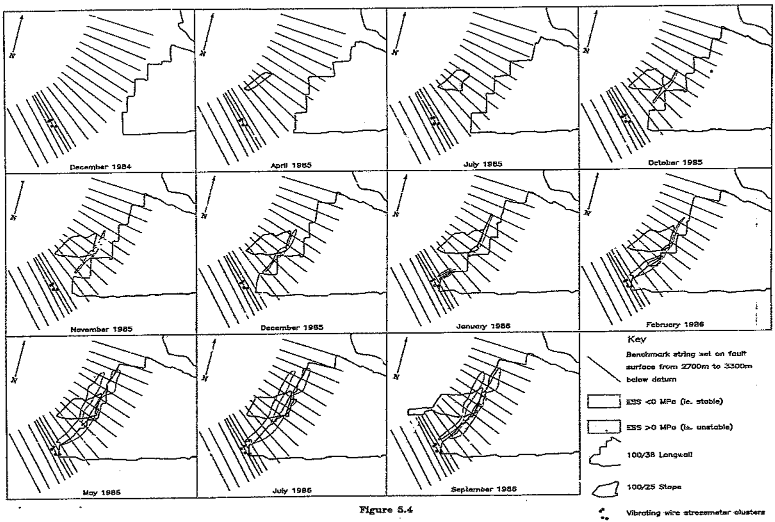

Figure 5.4

Excess Shear Stress distribution on the Elf Fault Surface

Scale 1:5000

TABLE 5.4: EXCESS SHEAR STRESS AT MEASUREMENT POSITIONS

BENCHMARK POINT NUMBER	EXCESS SHEAR STRESS (MPa)*										
	Dec'84	Apr'85	Jul'85	Oct'85	Nov'85	Dec'85	Jan'86	Feb'86	May'86	Jul'86	Sep'86
4.25	-10,0	-9,8	-9,2	-8,7	-8,2	-7,7	-6,0	-5,5	-4,9	-5,0	-5,5
4.26	-10,1	-9,9	-9,3	-8,6	-8,0	-7,4	-5,4	-5,0	-4,4	-3,9	-3,7
5.25	-10,1	-9,9	-9,3	-8,7	-8,2	-7,7	-7,2	-6,6	-5,9	-6,1	-7,7
5.26	-10,1	-9,9	-9,3	-8,6	-7,9	-6,8	-4,2	-3,7	-2,9	-1,9	-0,8
6.25	-10,1	-9,9	-9,3	-9,0	-8,7	-8,1	3,3**	-2,4**	-1,2**	-4,0**	-3,4**
6.26	-10,1	-9,9	-9,3	-8,7	-7,7	-6,0	-9,7	-9,3	-8,7	-1,3	-5,4
Averages	-10,1	-9,9	-9,3	-8,7	-8,1	-7,3	-6,0	-5,4	-4,7	-3,7	-4,4

* Calculated assuming cohesion is zero and μ = tan 30

** Benchmark point less than one grid width from mined element - values may be unreliable.

strike was requested in order to gain an idea of the effect of overstoping on boreholes RB3 and RB4. The stresses were resolved into their respective biaxial components in the plane of the sheet by the method given in Appendix G. The results are probably unreliable because off-reef benchmarks were requested too close to the reef plane, (Chamber of Mines Research Organization, 1985).

Nevertheless, the results did indicate that the vertical stress measured by Borehole RB3 should have remained at about 110 MPa for the mining face positions as at July 1986. The distribution together with the borehole positions and the mining face positions are shown in Figure 5.5.

5.3.4 Mining induced displacements

A string of 22 benchmark points were set about 2,5 m above 100/2 'C' Haulage West at 10 m intervals in order to determine the vertical displacements at points in the rock mass comparable with those measured in the underground levelling survey. The benchmark points and levelling stations are shown in Figure 5.6. Not all points coincide with the levelling stations, and in these cases either the closest benchmark point is used for comparison or the average displacement of the two benchmark points on either side of the levelling station is found.

The period in which the fault was most likely to become unstable was October 1985 to February 1986, when the 100/38 Longwall drew close to, and finally reached the Elf Fault. Although mining induced displacements were determined for each of the eleven mining steps, the displacement changes before and after this critical period are negligible, and are therefore not included in the analyses.

The displacements, together with the changes in displacement are listed opposite the benchmark point numbers and corresponding underground levelling station number in Table 5.5. The benchmark points in the western half of the traverse show the smallest movements as they are the most remote from mining. Benchmark Point No. 21, which corresponds to the westernmost Levelling

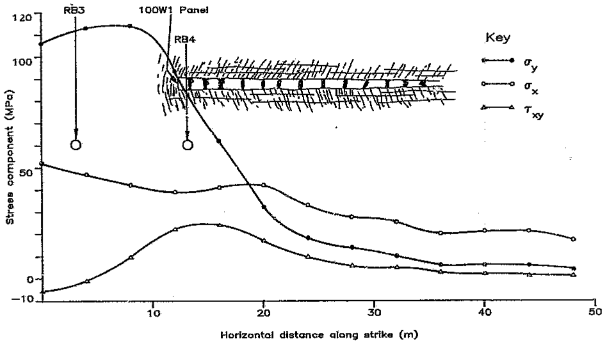

Figure 5.5

Section along strike through 100W1 Panel with plots of stresses superimposed

Scale: As shown

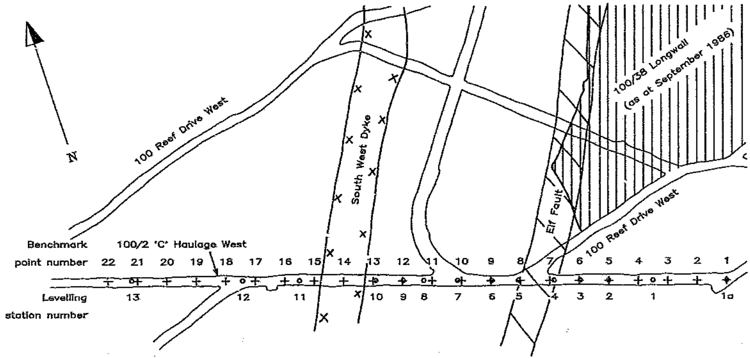

Figure 5.6

Benchmark point positions for displacement estimates in 100/2 'C' Haulage West

Scale 1:1000

TABLE 5.5: NUMERICALLY DERIVED VERTICAL DISPLACEMENTS IN 100/2 'C' HAULAGE WEST

BENCHMARK POINT NUMBER	LEVELLING STATION NUMBER	VERTICAL DISPLACEMENTS (mm) OCT 1985	FEB 1986	DIFFERENCE
21	13	0	0	0
17 & 18	12	0	-1	-1
15 & 16	11	0	0	0
13	10	0	0	0
12	9	0	0	0
11	8	0	0	0
10	7	+1	+1	0
9	6	+1	+1	0
8	5	+1	+1	0
7	4	+1	+2	+1
6	3	+2	+2	0
5	2	+2	+3	+1
3 & 4	1	+2	+4	+2
1	1A	+3	+5	+2

Notes: i) Two benchmark points indicate levelling station lies midway between them, and averages are quoted.

ii) Positive displacements are downward.

Station No. 13 is therefore chosen as the datum. Since this point is stable throughout the period considered, the displacement differences calculated are of an absolute nature in relation to it, and can be compared directly from the relative displacement changes obtained from the underground levelling survey. The numerically derived and measured data are compared in Section 6.4.2.

5.4 Analysis Error

Ryder and Napier (1985) describe the errors common to boundary element modelling techniques as well as a means of minimising these errors. MINSIM-D features these improvements, and it is expected for the model under consideration, the analysis error will be relatively small.

Other analytical errors arise from the assumptions that the rock mass is linearly elastic, homogeneous, isotropic and intact. These assumptions have been shown to be reasonable by Ryder and Officer (1965) as well as Ortlepp and Nicoll (1965) when considering the quartzites of the Witwatersand Basin. However, they are invalid where rock behaviour is inelastic, such as in the zones surrounding extensive excavations at depth where the rock is in a state of failure. At present no analytical technique can take these zones into account adequately, and the errors that result from applying elastic analyses in these regions are still undetermined.

The failed regions surrounding mining excavations at depth assumed increasing importance in the latter stages of the stress monitoring phase because numerical estimates of stress were made at points close to the mining excavations. Nevertheless, the results are considered acceptable because the stress field is universally compressive in the region of interest, and intensely fractured rock is capable of exhibiting linearly elastic properties in these conditions even though its modulus of elasticity may be reduced (Lama and Vutukuri, 1978).

The mining induced stresses are underestimated in the area of interest by not including in the analysis extensive excavations to the north, east and south-east of the coarse window, shown in Figure 5.2. Although no quantification of the error has been attempted, it is expected to be small in the area of interest.

5.5 *Concluding Remarks*

The MINSIM-D suite of programs was used to model the conditions at the monitoring site area. The data generated requires in some instances modification for direct comparison with the underground measurements. The results form a background against which the underground measurements were made. This provides an indication of conditions along the known extent of the Elf Fault Surface, which could not be achieved by the underground measurements alone.

The results are presented in a summarized form for comparison with the underground measurements which were presented in Chapters 3 and 4. The information from this, and the preceding two chapters is gathered together, compared, and the significance of the findings discussed in Chapter 6.

CHAPTER 6

DISCUSSION AND INTERPRETATION OF RESULTS

As far as the author can determine, the vibrating wire stressmeter had never been used for stress change measurements in deep gold mines before this study. Because of their unknown performance in this type of environment, detailed assessment of their behaviour was considered essential before an interpretation of the stress change results could be carried out. The chapter begins with an outline of the initial stress state as determined from the measurements, and is followed by a discussion of mining induced stress changes. The latter are described with comparisons between numerically estimated stress changes and those measured by the stressmeter. Several factors which affect the accuracy of stressmeter measurements are covered and those areas requiring further research are highlighted. The final stress state is described briefly and the possibility that the stress discontinuity still existed is mentioned. An analysis of the behaviour of the Elf Fault is lastly covered in some detail.

6.1 Initial Stress State

The Elf Fault exerted considerable influence over the initial stress state at the monitoring site. Firstly, the natural rock mass fracture frequency increases in the vicinity of the fault, thereby increasing the error of strain relief measurements. The second effect arises from the fact that two rock masses with differing elastic constants abut against each other at the fault surface. This results in a stress discontinuity which was observed at the site. The significance of the influences are discussed in more detail below.

6.1.1 Discontinuity frequency

Rock mass discontinuities affected the overall error of the initial stress measurements presented in Table 3.7. In order to demonstrate this affect, a curve relating the two variables is presented in Figure 6.1. The relationship shows that a larger stress estimate

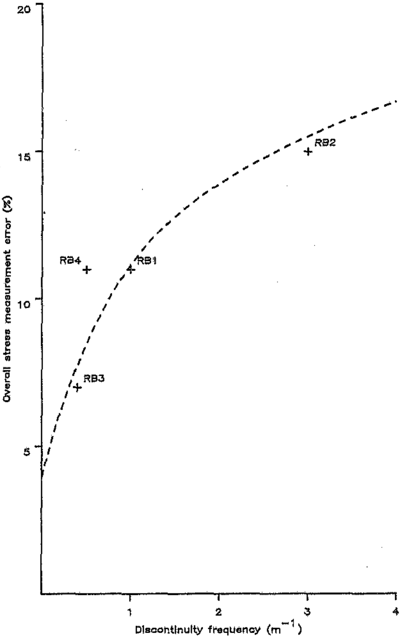

Note: Mining induced fractures are not included in the analysis

Figure 6.1

Plot of overall stress measurement error versus average discontinuity frequency error may be expected in more intensely fractured rock. The curve is characteristic of conditions at the monitoring site and may therefore not be directly applicable elsewhere.

6.1.2 Presence of the Elf Fault

The fault resulted in a clearly defined stress discontinuity at the monitoring site. A difference of the 14,9 MPa was observed between the average vertical stress measured to the west of the fault when compared with the east, Table 3.7. The horizontal stresses acting across the fault surface, obtained from boreholes RB2 and RB3, differ by 16,4 MPa.

These figures do not suggest that the fault surface is not in equilibrium, they highlight instead the complex stress field that exists in the vicinity of the fault. Observations of the fault exposure underground suggested that it was stable with seismic data for December 1984 giving further support. The stress discontinuity was therefore not sufficient to cause fault instability and may therefore have been smaller than the stress measurements show.

The averaged vertical stress for all four boreholes is equal to that estimated numerically. This indicates that the two major factors controlling the initial vertical stress were the overburden weight and mining. The average horizontal to vertical stress ratio of 0,45 was in reasonably good agreement with the accepted ratio of 0,5 for the average gold mine at depth (Gay, 1975, p.449).

A reverse fault such as the Elf Fault represents crustal shortening, which takes place when the horizontal stress exceeds the vertical stress. Since the horizontal stresses were found to be about half the vertical stresses, the conditions that resulted in the formation of the Elf Fault can no longer exist. Therefore the tectonic stress field responsible has slowly dissipated through geological time, leaving a displaced rock mass, some minor stress discontinuities of local significance only and a stress field that is primarily the result of the gravity loading by the superincumbent strata. These findings are in agreement with those of Gay (1972) who concluded that at his "deep" site, the effect of residual stress was small and that the maximum principal stress was approximately equal to the stress resulting from the weight of the existing overburden.

6.2 Mining Induced Stress Changes

The stress changes measured at the monitoring site are compared with the corresponding numerical estimates. The data came from Tables 4.3, 4.4, 4.6, 5.3 and 5.4.

6.2.1 Vertical stress changes

The vertical stress changes were largest and measured with the least error. They are plotted with the numerical estimates against time in Figure 6.2, which shows that agreement is good in all cases. Both the numerical results and the stressmeters revealed accelerated stress changes from October 1985 to February 1986 when the 100/38 Longwall drew near to the monitoring site. This change was also detected in Borehole RB6, but not supported by the numerical modelling. The differences between the two curves plotted for each borehole in Figure 6.2 arise from rock mass conditions at the stressmeters and their influence on borehole deformation, as explained below.

Changes in the effective modulus of elasticity

From January 1986 onwards, stress change measurements in Boreholes RB1 and RB2 exceeded the numerical estimates, which led to over-estimated stress changes towards the end of the period. This occurred when both stressmeter clusters were less than 10 m away from 100W1 Panel, which had stripped onto the Elf Fault in January 1986, and remained static thereafter. In these conditions the increases in stress may represent the time-dependent development of mining induced fracturing in the immediate vicinity of the stressmeter positions.

This process would result in the reduction of the effective elastic modulus, which would be expressed as an increase in stress even though the true stress changes at the stressmeters were small. This effect was not taken into account in the calculations because the changing fracture intensity could not be measured.

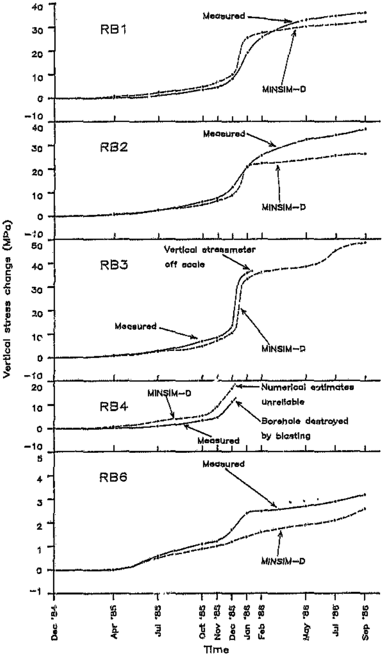

Figure 6.2

Comparison of vertical stress change measurements with numerical estimates

The same result may be produced by the stress induced scaling of the borehole surfaces. No definite evidence of scaling was found, even at the collar of Borehole RB4, when it was only one metre ahead of 100W1 Panel. Borehole scaling at the stressmeter clusters could not be monitored and therefore it cannot be excluded as a possible cause.

A third origin of the stress increases may be the time dependent transfer of load from more highly stressed vo[illegible]es to less stressed volumes of rock by creep. Although Briggs (1982) and others have found that quartzites are not prone to creep, these findings are based on the laboratory testing of intact rock specimens, which may not truly reflect the behaviour of a discontinuous rock mass in situ. The causes listed above may act singly or in combination with each other and may also pool with some of the sources of error listed in Section 4.2.1.

Borehole-rock mass deformations
It appears from the curves in Figure 6.2 that the effective rock mass modulus was over-estimated for Boreholes RB2, RB3 and RB6, and more less correctly estimated for RB1 and RB4. This is evident in the fact that for Boreholes RB1 and RB4 the stress changes were initially slightly under-estimated and then later over-estimated in the case of RB1 when changing rock conditions brought about a reduction in the effective rock modulus.

Over-estimates of the effective modulus are possible for RB6, but unlikely for RB2 and RB3 where the intact rock modulus and fracture frequencies are fairly well known. The reason for excessive stress change estimates may be that the boreholes lie more or less parallel to the fault as well as the major discontinuity direction, determined by Heunis (1976) As a result, the deformation in Boreholes RB2 and RB3 may be more pronounced for the same stress changes than for RB1 and RB4, which were drilled perpendicular to the major discontinuity trend.

This suggests that borehole deformation behaviour may depend on the borehole direction and the major discontinuity trends in a jointed rock mass. As far as is known, the effect of a discontinuous solid on borehole deformation has not been investigated, either in situ or by numerical modelling techniques. Further investigation of this phenomenon is necessary not only because the above observation requires confirmation, but also because the results will have an important bearing on all in situ stress and stress change measurements using borehole mounted devices.

6.2.2 Stress change components

Graphic comparisons of each stress change component for Boreholes RB1 and RB4 appear in Figures 6.3 to 6.6, where they appear plotted against the corresponding numerical estimate. Perfect agreement between each set of variables would be expressed as a straight line with a slope of unity passing through the origin, as shown in each figure.

The plots show that for the vertical stress changes, which are greatest, the agreement is best. Neither of the plots for the horizontal and shear stress changes show as good agreement. Both tend to be more erratic, probably because they are relatively small when compared with the vertical stress changes.

The overall correlation coefficients and regression constants for each stress component are presented in Table 6.1. The observed and estimated vertical stress components show by far the best correlation, while the measured horizontal and deduced shear stress changes are relatively poorly correlated with their numerically estimated counterparts. The constant a represents the slope of the least squares fit regression line while b is the value of the intercept on the vertical axis of each plot. The significance of these values is that the vertical stresses tended to be overestimated on average by the stressmeters beyond stress changes of about 6,0 MPa. The horizontal stress changes were over-estimated and the shear stress changes, deduced from the normal stress changes, were under-estimated by the instruments throughout the monitoring period.

The comparisons show that while general agreement between the measured

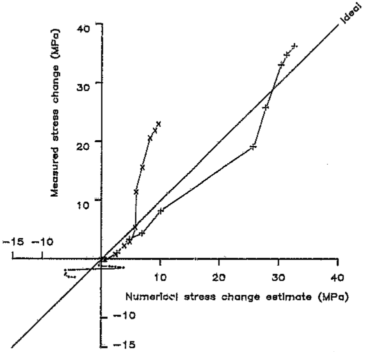

Key to curves and table of coefficients
for least square best fit lines to data

Key	Stress compt.	r	a	b
+——+	$\Delta\sigma_y$	0,98	1,08	−1,80
x——x	$\Delta\sigma_x$	0,93	2,69	−4,41
·——·	$\Delta\tau_{xy}$	0,44	0,11	−1,54

Notes: 1) r is the correlation coefficient
2) a and b are constants such that
$y = ax + b$ in which
y = measured stress change component
x = numerically estimated stress change component

Figure 6.3

Plot of measured stress change components versus corresponding numerical estimates for Borehole RB1

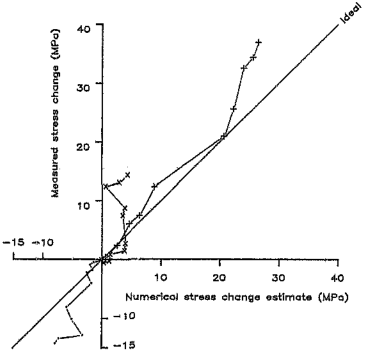

Key to curves and table of coefficients
for least square best fit lines to data

Key	Stress compt.	r	a	b
+——+	$\Delta\sigma_y$	0,99	1,30	−0,58
x——x	$\Delta\sigma_x$	0,44	1,57	1,78
·——·	$\Delta\tau_{xy}$	0,87	1,88	0,49

Notes: 1) r is the correlation coefficient
2) a and b are constants such that
$y = ax + b$ in which
y = measured stress change component
x = numerically estimated stress change component

Figure 6.4

Plot of measured stress change components versus corresponding numerical estimates for Borehole RB2

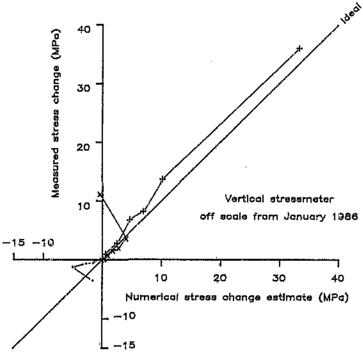

Key to curves and table of coefficients
for least square best fit lines to data

Key	Stress compt.	r	a	b
+——+	$\Delta\sigma_y$	1,00	1,07	0,85
x——x	$\Delta\sigma_x$	−0,18	−0,43	3,35
·——·	$\Delta\tau_{xy}$	0,25	0,25	0,08

Notes: 1) r is the correlation coefficient
2) a and b are constants such that
$y = ax + b$ in which
y = measured stress change component
x = numerically estimated stress change component

Figure 6.5

Plot of measured stress change components versus corresponding numerical estimates for Borehole RB3

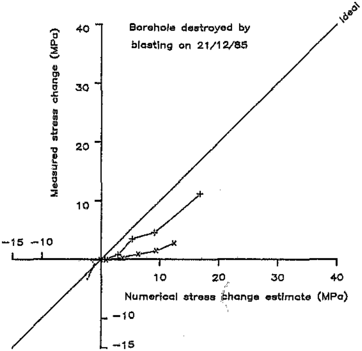

Key to curves and table of coefficients
for least square best fit lines to data

Key	Stress compt.	r	a	b
+——+	$\Delta\sigma_y$	0,99	0,67	−0,53
x——x	$\Delta\sigma_x$	0,97	0,21	−0,25
·——·	$\Delta\tau_{xy}$	0,78	1,05	0,24

Notes: 1) r is the correlation coefficient
2) a and b are constants such that
$y = ax + b$ in which
y = measured stress change component
x = numerically estimated stress change component

Figure 6.6

Plot of measured stress change components versus corresponding numerical estimates for Borehole RB4

TABLE 6.1: OVERALL CORRELATION COEFFICIENTS AND REGRESSION CONSTANTS FOR THE STRESS CHANGE COMPONENTS

PARAMETER	VERTICAL STRESS CHANGES	HORIZONTAL STRESS CHANGES	SHEAR STRESS CHANGES
r	+0,9689	+0,5147	+0,6301
a	+1,1256	+1,1023	+0,9058
b	-0,7156	+1,4681	-0,7037
n	35	35	35

Notes: i) r = correlation coefficient

ii) $y = ax + b$
where y is the measured stress component
x is the estimated stress component

iii) n = number of data points in the analysis.

TABLE 6.1: OVERALL CORRELATION COEFFICIENTS AND REGRESSION CONSTANTS FOR THE STRESS CHANGE COMPONENTS

PARAMETER	VERTICAL STRESS CHANGES	HORIZONTAL STRESS CHANGES	SHEAR STRESS CHANGES
r	+0,9689	+0,5147	+0,6301
a	+1,1256	+1,1023	+0,9058
b	-0,7156	+1,4681	-0,7037
n	35	35	35

Notes: i) r = correlation coefficient

ii) y = ax + b
where y is the measured stress component
x is the estimated stress component

iii) n = number of data points in the analysis.

and numerically estimated stress changes exists, the vertical stress changes were measured with the smallest error, because they were the largest. Nearly all the measured values lie within about 15% of the ideal situation of perfect agreement, which for a faulted rock mass, and data from only four boreholes, is very encouraging. It is concluded that the results from the stressmeters are reasonable and that the instrument is suitable for long term stress change measurement in deep gold mines.

6.3 Final Stress State

Three measurements of the final stress state are available. These are the total stresses measured in Boreholes RB1, RB2 and RB7, all to the west of the fault. They are compared with their numerical counterparts estimated for the same points in Table 6.2. The measured vertical and horizontal stress components are larger than the numerical estimates in all cases except for the horizontal stress measured in RB7, which is smaller than the numerical estimate. The pattern is typical of the initial numerical stress estimates, which also were smaller than their measured counterparts to the west of the fault.

The drop in stress measured in Boreholes RB3 after January 1986 does not agree with the numerical results because either rock failure or stressmeter - rock contact failure occurred in the borehole. This led to the spurious vertical stressmeter output since that date which showed that an apparent decrease in stress took place while the numerical results, themselves questionable, showed an increase in stress. Figure 5.5 nevertheless shows that such a decrease in stress follows once the borehole is overstoped, as in the case for RB4. The results from these boreholes and the numerical analyses indicate the limitations of both stress measurements and analytical techniques at points close to extensive mining excavations at depth. Because of these limitations, no direct information about the stress state to the east of the fault existed once the 100/38 Longwall had reached it.

The results from Boreholes RB1, RB2 and RB7, although unsupported

TABLE 6.2: COMPARISON OF THE MEASURED TOTAL STRESS COMPONENTS WITH THEIR NUMERICALLY ESTIMATED COUNTERPARTS

BOREHOLE	*STRESS* COMPONENT	SOURCE MEASURED	ESTIMATED
RJ1	σ_y	+117,7	+112,8
	σ_x	+ 51,5	+ 47,7
	τ_{xy}	+ 2,7	- 4,8
RB2	σ_y	+127,4	+106,7
	σ_x	+ 63,7	+ 40,7
	τ_{xy}	- 10,5	- 8,4
RB7	σ_y	+109,2	+ 91,3
	σ_x	+ 25,3	+ 42,6
	τ_{xy}	+ 8,9	- 0,1

by RB3 and RB4, suggest that the stress discontinuity still existed at the end of the stress monitoring period. This could not be confirmed by absolute stress measurements to the east of the fault because they would have been undertaken in de-stressed, overstoped ground. The possibility that the stress discontinuity still existed is discussed in Section 6.4.1.

6.4 Analysis of Elf Fault Behaviour

The response of the fault to the mining induced stress changes is examined from several points of view. The aspects considered are the effect of the fault on stress changes induced by mining, fault stability using the ESS criterion, displacements on the fault surface as well as the rock mass in general, and mining induced seismicity. The information used for the analyses comes from Tables 4.4, 4.6, 4.7, 5.3, 5.4 and 5.5. The analyses of mining induced seismicity is based on the information contained in Figures 4.5 and 5.4.

6.4.1 Stress transmission across fault

By far the greater part of the mining induced stress changes were generated by the 100/38 Longwall situated to the east of the fault. The question of how those stress changes were transmitted to the rock mass west of the fault are crucial to any assessment of its stability. The vertical stress changes measured in the four stress monitoring boreholes are most appropriate because they are the largest of all the stress changes measured.

A way of accomplishing a visual assessment is to plot the stress changes measured in RB1 against those in RB4, and to repeat the procedure with the corresponding numerical estimates, as shown in Figure 6.7a. Figure 6.7b is a similar set of curves for RB2 and RB3. If the trajectories of both curves are similar in each case, stress must be transmitted across the fault, because in the numerical model, mining induced stress changes are perfectly transmitted to all parts of the hypothetical solid.

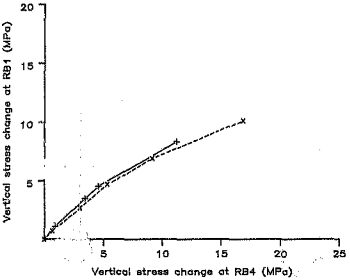

a: Comparison of stress changes at RB1 and RB4

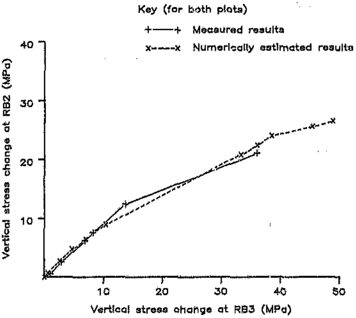

b: Comparison of stress changes at RB2 and RB3

Figure 6.7

Curves showing the effect of the Elf Fault on the transmission of mining induced stress changes

Since both curves are reasonably close to each other for all the stress change measurements, it is concluded that the presence of the fault has no influence on the transmission of mining induced stress changes. This observation is significant in the case under study because it eliminates one variable in discontinuity behaviour that would contribute to an erroneous assessment of rock mass stability using the ESS criterion. The observation also supports the supposition made in Section 5.4, that elastic analyses are still valid in intensely fractured rock masses provided that the discontinuities are adequately confined.

6.4.2 Levelling survey results

The displacements measured underground and those estimated numerically are presented in Tables 4.7 and 5.5 respectively. The data have been combined and presented for comparison in Figure 6.8. The displacement change plots show no agreement at all, and this arises from two important factors.

The first is that the rock anchors used for levelling were installed in 2,8 m deep holes drilled vertically upwards from the 100/2 'C' Haulage West roof. It appears that these anchors were too short to allow for the measurement of rock mass movements because the excessive sag measured between the South West Dyke and the Elf Fault. This suggests that the anchors may be fixed in rock whose movements are still affected by bedding separation.

The second factor important to the results was that a major re-supporting program was underway at the time of the measurements. The support medium employed in 100/2 'C' Haulage West was 4,5 m long pre-tensioned and grouted rope anchors set at 3 m centres with wire mesh and lacing. The conditions in the haulage were such that tensioning of the rope anchors may have been sufficient to induce the upward displacement of rock by as much as 6 mm. This is the only explanation for the generally upward movement of the rock between 120 to 2[illegible]0 m from the datum levelling station.

Nevertheles, the measurements show a downward displacement of the

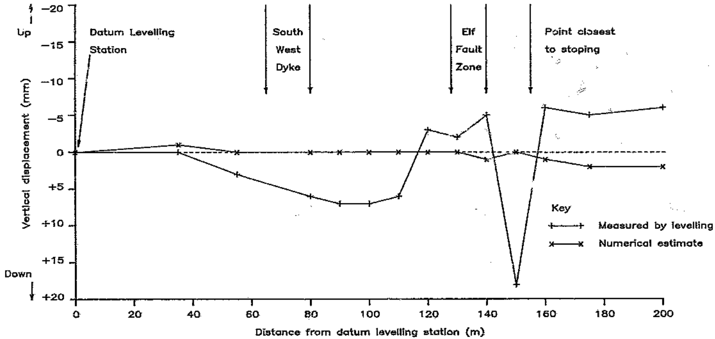

Figure 6.8

Comparison of measured and numerically derived estimates of mining induced displacement changes for the period October 1985 to February 1986 rock mass to the west of the fault, which is partly in keeping with expectations. Only insignificant displacement across the fault surface was measured and is more likely to be minor local movement than fault slip. Undisplaced paint strips across the fault traces lend further support to this observation. The results are therefore in general agreement with other findings, even if they do not coincide with the numerical predictions of displacement.

6.4.3 Mining induced seismicity

The seismic activity that took place during the monitoring period is described in Section 4.4.1, but spatial relationships between seismicity and geological structure, mining, and the Excess Shear Stress distribution on the fault surface were not discussed. In spite of the fact that only twenty-five seismic events with a magnitude of greater than 1,0 on the Richter Scale were detected in the area, some patterns do emerge. These are presented and discussed below.

Spatial relationship with geology and mining

The plan position of each seismic event that occurred in the monitoring area is shown in Figure 4.5. The minimum distance of each seismic event location from a geological structure surface was found by projecting perpendicular lines to each surface from a given event and finding their respective lengths. The results were then classed into different distance groups, for example 0-25 m, 25-50 m, etc. from a particular geological structure. The seismic frequencies were then counted in each distance class for a particular structure and a frequency histogram was constructed. The Elf Fault, the South West Dyke, the Georgette Dyke and the Carbon Leader Reef plane were each considered for the distance-seismic frequency histograms that appear in Figure 6.9.

The histogram for the Elf Fault shows some clustering of seismicity within 25 m of the fault surface. The frequency peak is prominent and shows that nine of the twenty-five seismic events located within 25 m of its projected surface position. A second peak is present about 125 m to the east of the fault. This is the result of seismicity associated with the Georgette Dyke and mined out areas.

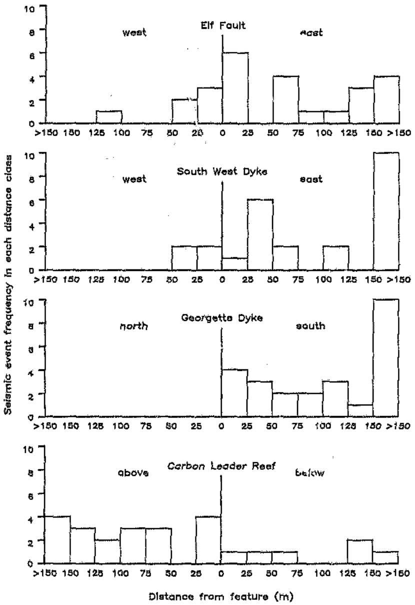

Figure 6.9

Frequency histograms showing spatial relationships of seismicity with geological features and mining

The South West Dyke is revealed to have little control over seismic locations in the area. A peak, probably associated with the Elf Fault, lies 50 m to the east of the dyke, while a second very prominent peak exists for events located at distances greater than 150 m from the dyke. The second peak is not associated with any particular structure but is an artefact of the distance interval chosen.

The Georgette Dyke shows a mild peak which means that minor clustering of seismicity occurred around it. The seismic frequency then tapers off to the south with a prominent peak for events greater than 150 m away. Again, this is the result of the class interval used. The histogram is one-sided because only events to the south of the Georgette Dyke were considered in the analysis.

The frequency histogram plotted for the Carbon Leader Reef plane shows that a majority of the events were located in the hangingwall. A minor peak lies immediately above the reef plane, a feature typical of seismic activity associated with mining, while a smaller peak exists in the deep footwall. The pattern shows that most of the seismicity located away from the reef plane, sometimes in the remote hangingwall and footwall, which appears typical of the geologically controlled seismicity observed in the Klerksdorp Goldfield (Gay et al, 1984).

The frequency histograms show that a significant portion of the seismicity clustered around the Elf Fault and that the other structures were associated with relatively smaller portions. The Elf Fault is therefore considered to be seismically active when exposed to mining induced stress changes.

Seismic location control by Excess Shear Stress

Zones of positive ESS developed on the Elf Fault surface when mining approached it from the east and west. These zones represent numerically predicted potential fault instability, which should coincide loosely with the seismic activity that was located at or near the fault surface. Of the nine seismic events that plotted within 25 m of the fault, eight have been re-plotted in Figure 6.10, together with the zones of positive ESS for the respective mining

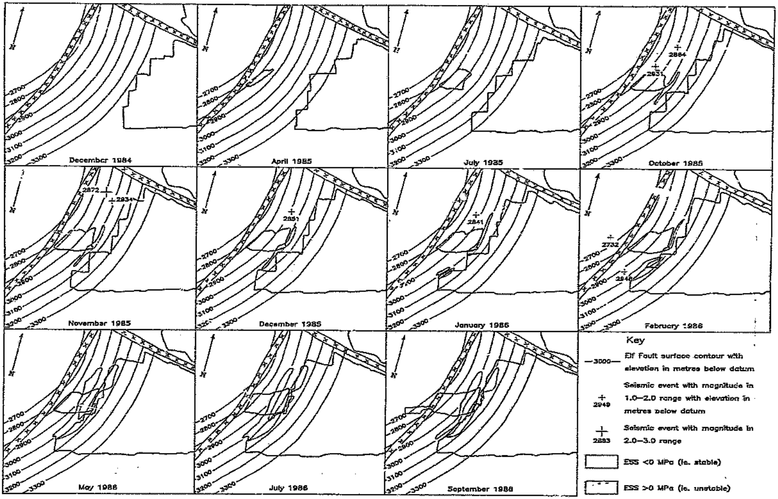

Figure 6.10

Spatial relationship of ESS distribution with mining induced seismicity

Scale 1:5000

steps. The ninth seismic event plots outside the field of view for October 1985 and was not included.

The fault-controlled seismicity occurred from September-October 1985 to February 1986, when the 100/38 Longwall approached the fault from the east. All except one of the seismic events plotted well away from the zone of positive ESS and six clustered in an area to the north and north-east of 100/25 Stope. No seismic events occurred in this region from May to September 1986 when a zone of positive ESS extended into it.

This behaviour is explained if the portion of the Elf Fault surface to the north of 100/25 Stope is considered potentially unstable as a result of some local stress anomaly. This condition quickly approached a state of unstable equilibrium while the 100/38 Longwall was still some distance away in September 1985. Further mining precipitated two [illegible] period ending in October 1985, followed by another four [illegible]ceding three months. The release of seismic energy in t[illegible] left the fault surface and surrounding rock mass stable, even when a zone of positive ESS penetrated it in May 1986.

One seismic event, in February 1986, plotted near to the southern edge of a zone of positive ESS associated with 100W1 Panel. This was the only seismic event that appears to be associated with positive ESS. An underground visit following the occurrence revealed no visible slip at the fault exposures nor were the overall trends of stress change measured at the stressmeters disturbed. No closure associated with the seismic event was visible in 100W1 Panel, and no damage was reported in any of the mining excavations except for a fall of ground in 100/25 Replacement Crosscut North.

No seismic events were located in the zone of instability extending below the 100/38 Longwall. This was considered to be one of the more critical zones when considering the work of Ryder (1986). It appears that the opposite was true. Furthermore the ESS calculated from the measurements at the monitoring site was in general much lower than the comparable numerical estimates.

The two sets of data are plotted against each other in Figure 6.11. It is clear that no agreement exists except that both sets of data are negative. No common trends are visible and the overall trajectory of the data is at variance with the ideal curve representing perfect agreement. The disparity between the numerical and measured ESS lies in the following probable sources:-

i) a stress discontinuity, not accounted for in the numerical analysis, tended to reduce the ESS values in the measured results;

ii) the measurements were not undertaken at the fault surface, but about five metres from it.

The presence of the stress discontinuity is considered an important agent in reducing the potential for seismic activity in the footwall below 100/38 Longwall. If the measured ESS values are correct for the zone, then a further 10 MPa may be subtracted from the numerically predicted zone of positive ESS, largely eliminating it and bringing numerical predictions into line with observations.

6.5 Summary of Results

The vibrating wire stressmeter is shown to be a reliable instrument capable of long term stress change measurement in harsh underground conditions. The results obtained from it can be used with assurance when the effective rock mass modulus of elasticity is known with good accuracy. Stress change measurement errors would be reduced further if the effect of discontinuities on borehole deformation could be determined.

The initial stress measurements revealed that a well defined stress discontinuity existed at the Elf Fault. The stress change measurements, which agreed reasonably well with the numerical estimates, showed that the discontinuity persisted throughout the stress monitoring period.

Spatial analysis of the seismic event locations showed the Elf Fault to be seismically active in a region not predicted by numerical analyses. The observed departure from elastic predictions can

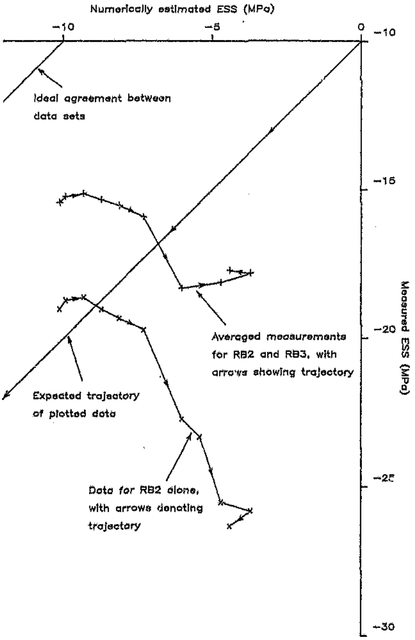

Figure 6.11

Plot of measured ESS versus numerically estimated ESS onl/ be explained by the existence of a stress anomaly. Since the fault was found to have such a strong influence on the stress field at the monitoring site, the presence of another stress anomaly elsewhere is possible. As the stress anomaly enhanced seismicity to the north of 100/25 Stope, so the stress discontinuity at the monitoring site may have suppressed seismicity on the Elf Fault below the 100/J8 Longwall.

CHAPTER 7

CONCLUSIONS

A more thorough knowledge of stress distributions in rock masses would help to clear away some of the unknowns of mining induced seismicity and rock bursts, and perhaps lead to a more effective solution to the problem. To this end an underground study of the stress state of a faulted rock mass, while it was subjected to changing mining induced stresses, was undertaken. The measurements consisted of absolute stress measurements at the beginning and end of a period of stress change monitoring which spanned nearly two years. The stress and stress change data were supplemented with rock mass displacement measurements, seismic observations, and numerical stress and displacement analyses.

The initial stress state measured at the monitoring site agrees well with the numerical estimate, which shows that it is predominantly the result of the overburden weight and a small mining induced stress component. No evidence of the stress field responsible for the formation of the fault was found. The presence of the fault creates a stress discontinuity as a result of the footwall and hangingwall quartzites coming into contact with each other across the fault surface. This produces a complex stress field in the vicinity of the fault, and appear to have had a strong influence over its seismic behaviour. This effect requires more detailed study.

Vibrating wire stressmeters were used to monitor the stress changes induced by mining during the course of the study. Their performance was assessed in detail because as far as could be determined, they had never been used in deep gold mines before. They proved to be reliable throughout the study with all the stress change results derived from them agreeing reasonably well with the numerical predictions. The stress change estimates both from the stressmeters and the stress analyses were used to assess the stability of the fault while it was subjected to changing mining induced stresses.

The seismic observations, stress monitoring results and numerical analyses all show that the fault surface at the monitoring site remained stable throughout the study. This evidence was supported by underground observations, but cannot be extended to the entire known extent of the fault surface.

An estimate of stability was extended to the known extent of the fault surface by calculating numerically the Excess Shear Stress distribution. These results showed the greatest disparity with observations. While the fault was expected to become unstable above and below the approaching 100/38 Longwall, no such instabilit was observed underground. This has been ascribed to the presence of the stress discontinuity which persisted throughout the study and appears to have had a stabilizing effect. This highlights the inability of present numerical analysis techniques to take account of rock mass history, structure and composition, and therefore the complex natural stress fields that arise.

The conclusions drawn from the study are listed below:-

i) the overall initial stress state at the monitoring site was controlled by the gravitational loading of the overlying strata and a small mining induced stress component;

the stress field responsible for the formation of the Elf Fault appears to have dissipated through geological time;

iii) a stress discontinuity existed at the fault surface at the beginning of the study and persisted to the end, resulting in a complex stress field in the vicinity of the fault;

iv) the vibrating wire stressmeter is suitable for long term stress change monitoring at depth;

v) the largest stress changes, in this case vertical, were measured with the smallest percentage error;

vi) the horizontal and shear stress changes were measured with relatively lower levels of confidence than the vertical stress changes;

vii) the effect of discontinuities on the stress concentration factors calculated for the flattened end of a borehole and discontinuity effects on borehole deformation, should be investigated;

ix) the underground stress measurements showed reasonably good agreement with the numerical analyses;

x) there was poor agreement between the numerical analyses and underground measurement of displacement and the Excess Shear Stress;

xi) the Elf Fault proved to be seismically active, but only in a region to the north of 100/25 Stope;

xii) the stress discontinuity appears to have a strong influence over the seismic behaviour of the fault;

xiii) current numerical stress analyses techniques are effective in cases where rock mass conditions do not deviate from the simplifying assumptions;

xiv) more must be discovered of natural stress distributions in rock masses in order to provide guidelines towards making the present stress analysis techniques applicable to a wider range of rock mass conditions.

The outcome of the measurements and analyses indicate that the influence of the pre-existing stress field on the Elf Fault is of paramount importance in the determination of its subsequent response to the imposition of mining induced stresses. This observation calls for the review of the questions concerning the seismic and rock burst mechanisms that appear in Chapter 1. These are relisted here:

i) what exactly is the seismic source mechanism?

ii) which factors are most important in bringing about a seismic event?

iii) how large are the stresses that drive it?

iv) what happens to the stress state at the initiation, during and after a seismic event?

v) why do some seismic events cause rock bursts while others do not?

vi) why are some faults and some dykes seismically active when exposed to mining induced stresses while others are not?

Reviewing these questions reveals that the influence of the total stress field on the behaviour of the Elf Fault sheds some light on the answers to questions ii) and vi). The stability of the fault eliminated the potential of the study to provide answers to questions ii), iii) and iv). The overall outcome of the study shows that more must be known of natural stress fields in rock masses and that more versatile methods of numerical stress analysis be developed before a complete unravelling of the mysteries of the seismic and rock burst mechanisms becomes possible.

fault eliminated the potential of the study to provide answers to questions i), iii) and iv). The overall outcome of the study shows that more must be known of natural stress fields in rock masses and that more versatile methods of numerical stress analysis be developed before a complete unravelling of the mysteries of the seismic and rock burst mechanisms becomes possible.

APPENDIX A

Borehole logs

Engineering Geological Log: General Borehole Details and Descriptive Codes

a: General Borehole Details

Borehole Number: RB1

Company: WESTERN DEEP LEVELS LIMITED

Location: 100/25 Replacement Crosscut North

Collar Co–ordinates
(Mine co–ordinate system, metres)
x: + 28760,2
y: – 37730,9
z: + 3028,2

Borehole Direction
Bearing: 121°
Inclination: +1°

Drilling method: Diamond coring
Borehole diameter (mm): 92,2
Core diameter (mm): 72,0
Drilling machine: Kempe
Drilling contractor: Boart Drilling

Date commenced: 13/8/1984
Date completed: 19/11/1984
Logged by: M.F. Handley
Date: 24th August 1984

b: Descriptive Codes Used on Log

1: Discontinuities

Spacing

>1000mm: very widely	vw
300–1000mm: widely	w
100–300mm: medium	m
30–100mm: closely	c
10–30mm: very closely	vc

Roughness

smooth	s
slightly rough	sr
medium rough	mr
rough	r
very rough	vr

Type of discontinuity

mining induced fracture	m
drilling fracture	d
joint	j
bedding plane	b
fault	f
geological contact	g

2: Material Properties

Fill consistency

very soft	s1
soft	s2
firm	s3
stiff	s4
very stiff	s5

Rock hardness

very soft rock	r1
soft rock	r2
hard rock	r3
very hard rock	r4
extremely hard rock	r5

3: Visual Symbols

RQD (Deere, 1964)

20%
40%
60%
80%
100%

Note: All descriptions conform to the recommendations of the Core Logging Committee of the South Africa Section of the Association of Engineering Geologists (1976)

Engineering Geological Log of Recovered Borehole Cores

Borehole number: RB1

Page 1 of 4

Logged by: MF Handley

Date: 9th August 1984

Progress (m)	Core Recovery: Material recovery (%)	Core Recovery: Whole core recovery (%)	Core Recovery: RQD (%)	No. of sets	Inclination (degrees)	Type	Spacing	Roughness	Fill type	Fill thickness (mm)	Fill consistency	No. of discontinuities per set	Fracture frequency (m^{-1})	Depth (m)
0,00	90	39	30	2	10	m	c	r	–	–		27	28	0,00
					45	j	vw	mr	–	–	–	1		
2,10				2	10	m	vc	mr	–	–	–	30+	30+	
3,10	73	24	0	2	10	m	vc	mr	–	–	–	30+	30+	
	93	61	61	2	10	m	c	mr	–	–	–	19	19	
				1	10	m	c	mr	–	–	–	19	19	
6,00				2	10	m	vc	mr	–	–	–	30+	30+	
	91	71	59	1	10	m	vc	mr	–	–	–	16+	16+	
				1	10	m	vc	mr	–	–	–	20+	20+	
				1	10	m	vc	mr	–	–	–	20+	20+	
9,90				1	10	m	vc	mr	–	–	–	20+	20+	10,00

Geological Description

WITWATERSRAND SUPERGROUP
CENTRAL RAND GROUP
Johannesburg Subgroup
Randfontein Formation

Unweathered dark greenish grey medium bedded closely to very closely fractured medium grained very hard rock quartzite. Hangingwall quartzite, Carletonville Member. *Core broken into disks, suggesting high levels of stress* in the area.

Rockmass Classification and General Comments

Poor quality *rockmass from* 0,00 – 10,07 m

Core discing

0,42 – 2,97 m
3,66 – 385 m
4,56 – 4,81 m
5,10 – 6,00 m
6,09 – 6,22 m
7,57 – 7,67 m
7,93 – 8,36 m
9,27 – 9,72 m
9,91 – 10,07 m

Biaxial stress measurement at *9,90 m*

Engineering Geological Log of Recovered Borehole Cores

Borehole number: RB1
Page 2 of 4

Logged by: M F Handley
Date: 26th September 1989

Progress (m)	Material recovery (%)	Whole core recovery (%)	RQD (%)	No. of sets	Inclination (degrees)	Type	Spacing	Roughness	Fill type	Fill thickness (mm)	Fill consistency	No. of discontinuities per set	Fracture frequency (m⁻¹)	Depth (m)	Geological section notes
														10,00	
	100	80	59	1	10	m	c	mr	–	–	–	14	4		
				2	10	m	m	mr	–	–	–	9	11		
					60	b	w	sr	sericite	1	r2	2			
12,94				1	10	m	m	mr	–	–	–	5	5		
	100	81	65	1	10	m	m	mr	–	–	–	4	4		
				2	10	m	c	mr	–	–	–	10	11	14,20	Pebble band
					70	b	vw	sr	sericite	1	2r	1		15,00	Slickensiding on fracture dip 70°
				2	10	m	m	mr	–	–	–	6	9		
					65	b	w	sr	sericite	1	r2	3		15,62	Pebble band
16,53	98	92	86	1	10	m	m	mr	–	–	–	6	6		
				3	10	m	m	mr	–	–	–	4	6		
					10	f	vw	s	–	–	–	1			
					65	b	vw	sr	sericite	1	r2	1		18,00	Fault dip 5°
				[illegible]	[illegible]	m	w	mr	–	–	–	3	3	18,66	Minor slickensiding
														18,86	Pebble band
				2	10	m	w	mr	–	–	–	3	7		20 cm sericite quartzite
					30	[illegible]	m	mr	–	–	–	4		19,44	5 cm pebble band
														20,00	

Geological Description

WITWATERSRAND SUPERGROUP
Central Rand Group
Johannesburg Subgroup
Randfontein Formation

Dark greenish grey becoming light grey unweathered medium bedded closely fractur[illegible] becoming medium to widely fract[illegible] with depth, medium to coarse gra[illegible] very hard rock quartzite. Occasional pebble bands, scattered pebbles and sericite quartzite bands occur. Hangingwall quartzite, Carletonville Member.

RQD (%): 20 40 60 80

Rockmass Classification and General Comments

Fair to good quality rockmass from 10,07 m to 20,00 m.

Engineering Geological Log of Recovered Borehole Cores

Borehole number: 181
Page 3 of 4

Logged by: MF Handley
Date: 26th September 1984

Core Recovery

Progress (m)	Material recovery (%)	Whole core recovery (%)	RQD (%)
20,28			
23,92	98	93	87
27,74		90	74
	99	84	54

Discontinuity Description

No. of sets	Inclination (degrees)	Type	Spacing	Roughness	Fill type	Fill thickness (mm)	Fill consistency	No. of discontinuities per set	Fracture frequency (m⁻¹)
1	10	d	m	sr	-	-	-	6	6
2	10	d	m	r	-	-	-	6	7
	55	b	vw	sr	sericite	3	r2	1	
1	10	d	m	mr	-	-	-	6	6
2	10	d	m	mr	-	-	-	7	8
	55	b	vw	sr	sericite	60	r2	1	
1	10	d	m	mr	-	-	-	4	4
1	10	d	m	mr	-	-	-	5	5
2	10	d	mc	mr	-	-	-	6+	7+
	55	b	vw	sr	sericite	1	r2	1	
2	10	d	c	r	-	-	-	15	17
	55	b	w	sr	sericite	1	r2	2	
2	10	d	mc	r	-	-	-	8	[illegible]
	55	b	vw	sr	sericite	1	r2	1	
3	10	d	w	r	-	-	-	3	11
	20	j	c	r	quartz	1	r4	7	
	55	b	vw	sr	sericite	1	r2	1	

Depth (m): 20,00; 21,74; 23,20; 23,69; 30,00

Geological Description

21,74 – 3 mm sericite parting

23,69 – 8 cm sericitic quartzite

WITWATERSRAND SUPERGROUP
Central Rand Group
Johannesburg Subgroup
Randfontein Formation

Unweathered dark grey medium bedded, medium to very widely fractured very hard rock conglomeratic quartzite. Pyrite mineralization is associated with the conglomerates, and sericitic quartzite partings occur. Hangingwall quartzite, Carletonville Member.

As above, but becoming yellowish grey and less pebbly

RQD (%) 20 40 60 80

Rockmass Classification and General Comments

Biaxial stress measurement at 21,12 m

Fair to good quality rockmass from 20,00 - 30,00 m

Engineering Geological Log of Recovered Borehole Cores

Borehole number: RB1
Page 4 of 4

Logged by: M F Handley
Date: 25th September 1984

Progress (m)	Core Recovery: Material recovery (%)	Core Recovery: Whole core recovery (%)	Core Recovery: RQD (%)	Discontinuity Description: No. of sets	Inclination (degrees)	Type	Spacing	Roughness	Fill type	Fill thickness (mm)	Fill consistency	No. of discontinuities per set	Fracture frequency (m^{-1})	Depth (m)	Geological section		Geological Description	RQD (%) 20 40 60 80	Rockmass Classification and General Comments
30,46				-	-	-	-	-	-	-	-	-	-	30,00 30,46		Last normal drilling run	WITWATERSRAND SUPERGROUP Central Rand Group Johannesburg Subgroup Randfontein Formation Yellowish grey unweathered medium to widely fractured coarse grained very hard rock quartzite. Hangingwall quartzite, Carletonville Member.		Fair to good quality rockmass from 30,00 to 34,26 m Biaxial stress measurement at 30,46 m 30,86 m 31,23 m 31,54 m 32,56 m. UCS, Young's modulus and Poisson's ratio determined at 30,49 m 30,89 m 31,27 m 32,59 m Vibrating wire stress meters installed at:- h : 33,51 m 45° : 33,71 m V : 33,91 m
	-	-	-																
32,91														32,91		End NXC borehole Start EX borehole	Notes: 1) A detailed engineering log of *cores from 30,46 to 32,56 m not* possible because of the core losses associated with in situ stress measurements 2) An EX sized extension to the NXC borehole was drilled to accommodate vibrating wire stressmeters		
	-	-	-																
34,26														34,26		End of hole			

Engineering Geological Log: General Borehole Details and Descriptive Codes

a: General Borehole Details

Borehole Number: RB2

Company: WESTERN DEEP LEVELS LIMITED

Location: 100 Reef Drive West

Collar Co-ordinates
(Mine co-ordinate system, metres)
x: +28739,1
y: -37748,8
z: +3028,0

Borehole Direction
[illegible]: 025°
[illegible]: +1°

[illegible] method: Diamond coring
Borehole diameter (mm): 92,2
Core diameter (mm): 72,0
Drilling machine: Kempe
Drilling contractor: Boart Drilling

Date commenced: 18/9/1984
Date com[illegible]ated: 23/11/1984
Logged by: MF Handley
Date: 26th September 1984

b: Descrip[illegible]e Codes Used on Log

1: Discontinuities

Spacing

[illegible] widely	vw
[illegible]	w
[illegible]00mm: medium	m
30–[illegible]00mm: closely	c
10–30mm: very closely	vc

Roughness

smooth	s
slightly rough	sr
medium rough	mr
rough	r
very rough	vr

Type of discontinuity

mining induced fracture	m
drilling fracture	d
joint	j
bedding plane	b
fault	f
geological contact	g

2: Material Properties

Fill consistency

very soft	s1
soft	s2
firm	s3
stiff	s4
very stiff	s5

Rock hardness

very soft rock	r1
soft rock	r2
hard rock	r3
very hard rock	r4
extremely hard rock	r5

3: Visual Symbols

RQD (Deere, 1964)

Note: All descriptions conform to the recommendations of the Core Logging Committee of the South Africa Section of the Association of Engineering Geologists (1976)

Engineering Geological Log of Recovered Borehole Cores

Borehole number: RB2
Page 1 of 3

Logged by: *MF Handley*
Date: *2nd September 1984*

Progress (m)	Core Recovery: Material recovery (%)	Whole core recovery (%)	RQD (%)	Discontinuity Description: No. of sets	Inclination (degrees)	Type	Spacing	Roughness	Fill type	Fill thickness (mm)	Fill consistency	No. of discontinuities per set	Fracture frequency (m^{-1})	Depth (m)
	86	21	0	7	–	m	vc	mr	–	–	–	30+	30+	0,00
				7	–	m	vc	mr	–	–	–	30+	30+	
				2	60	b	w	sr	sericite	1	r2	1	32+	
					0	m	vc	mr	–	–	–	30+		
				2	60	b	m	sr	sericite	1	r2	2	32+	
4,20					0	m	vc	mr	–	–	–	30+		
	98	42	0	2	20	f	vc	r	–	–	–	20+	27+	4,28
					0	b	m	mr	–	–	–	7		
				1	20	f	vc	r	–	–	–	30+	30+	
				2	20	f	m	r	–	–	–	5	25+	5,14
					0	m	vc	mr	–	–	–	20+		
				2	0	b	vc	mr	–	–	–	25	26	
8,20					90	j	vw	mr	–	–	–	1		
				1	0	m	vc	mr	–	–	–	23	23	
				1	0	d	c	mr	–	–	–	10	10	10,00

Geological Description

0,00 – 4,28

WITWATERSRAND SUPERGROUP
Central Rand Group
Johannesburg Subgroup
Randfontein Formation

Dark greenish grey unweathered very closely fractured, medium bedded very hard rock quartzite. Hangingwall quartzite, Carletonville Member.

4,28 – 5,14

Elf Fault

As above but close fracturing result of faulting, whereas above it is mining induced.

5,14 – 10,00

Dark greenish grey unweathered widely bedded closely fractured becoming medium fractured with depth very hard rock coarse grained pebbly quartzite. Hangingwall quartzite, Carletonville Member.

RQD (%): 20 40 60 80

Rockmass Classification and General Comments

Poor quality rockmass from 0,00 to 9,00 m

Fair to good quality rockmass from 9,00 to 10,00 m.

Engineering Geological Log of Recovered Borehole Cores

Borehole number: RB2
Page 2 of 3

Logged by: M F Hackley
Date: 4th September 1984

Progress (m)	Core Recovery: Material recovery (%)	Core Recovery: Whole core recovery (%)	Core Recovery: RQD (%)	Discontinuity Description: No. of sets	Inclination (degrees)	Type	Spacing	Roughness	Fill type	Fill thickness (mm)	Fill consistency	No. of discontinuities per set	Fracture frequency (m⁻¹)	Depth (m)	Geological section
	97	84	51	2	0	d	m	mr	–	–	–	8	9	10,00	
					60	b	vw	?r	–	–	–	1			
				1	0	d	m	mr	–	–	–	9	9		
12,20															
				1	0	d	m	mr	–	–	–	9	9		
				2	0	d	m	mr	–	–	–	8	9		
					75	b	vw	sr	sericite	5	r2	1			
	99	94	65	1	0	d	m	mr	–	–	–	5	5	14,20	10 mm sericitic quartzite band
				2	0	d	m	mr	–	–	–	5	6		
					75	b	vw	sr	sericite	20	r2	1		16,00	30 mm sericitic quartzite band
16,20															
				1	0	d	m	mr	–	–	–	7	7		
				1	0	d	m	mr	–	–	–	3	3		
				1	0	d	m	mr	–	–	–	4	4		
				1	0	d	m	mr	–	–	–	4	4	20,00	

Geological Description

WITWATERSRAND SUPERGROUP
Central Rand Group
Johannesburg Subgroup
Randfontein Formation

Dark greenish grey unweathered widely bedded medium fractured very hard rock coarse grained pebbly quartzite.
Hangingwall quartzite, Carletonville Member.

RQD (%)

Rockmass Classification and General Comments

Fair to good quality rockmass from 10,00 to 20,00 m

Engineering Geological Log of Recovered Borehole Cores

Borehole number: RB2

Page 3 of 3

Logged by: M F Handley

Date: 26th September 1984

Progress (m)	Core Recovery: Material recovery (%)	Whole core recovery (%)	RQD (%)	Discontinuity Description: No. of sets	Inclination (degrees)	Type	Spacing	Roughness	Fill type	Fill thickness (mm)	Fill consistency	No. of discontinuities per set	Fracture frequency (m^{-1})	Depth (m)	Geological section
				2	30	j	w	mr	–	–	–	2	5	20,00	
21,20	100	97	91		0	d	w	mr	–	–	–	3			
	–	–	–											22,60	Fault, 60 mm throw
23,00														23,00	End of NXC hole, start of EX hole
24,35	–	–	–											24,35	End of hole

Geological Description

WITWATERSRAND SUPERGROUP
Central Rand Group
Johannesburg Subgroup
Randfontein Formation

Dark greenish grey unweathered widely bedded medium fractured very hard rock coarse grained pebbly quartzite. Hangingwall quartzite, Carletonville Member.

Notes:
1) A detailed engineering log of cores from 21,20 to 23,00 m not possible because of the core losses associated with in situ stress measurements
2) An EX sized extension to the NXC borehole was drilled to accommodate vibrating wire stressmeters.

RQD (%): 20 40 60 80

Rockmass Classification and General Comments

Fair to good quality rockmass from 20,00 to 24,35 m

Biaxial stress measurements at:-
21,28 m
21,38 m
21,80 m
22,36 m
22,82 m

UCS, Youngs Modulus and Poison's ratio determined at:-
21,31 m
21,62 m
22,39 m
22,85 m

Vibrating wire stressmeters installed at:-
h : 23,25 m
45°: 23,85 m
v : 24,10 m

Engineering Geological Log: General Borehole Details and Descriptive Codes

a: General Borehole Details

Borehole Number: RB3

Company: WESTERN DEEP LEVELS LIMITED

Location: 100 Reef Drive West

Collar Co-ordinates
(Mine co-ordinate system, metres)
x: +2879,1
y: -37758,6
z: +3028,3

Borehole Direction
Bearing: 031°
Inclination: +1°

Drilling method: Diamond coring
Borehole diameter (mm): 92,2
Core diameter (mm): 72,0
Drilling machine: Kempe
Drilling contractor: Boart Drilling

Date commenced: 4/11/1984
Date completed: 16/12/1984
Logged by: MF Handley
Date: 24th January 1985

b: Descriptive Codes Used on Log

1: Discontinuities

Spacing

>1000mm: very widely	vw
300–1000mm: widely	w
100–300mm: medium	m
30–100mm: closely	c
10–30mm: very closely	vc

Roughness

smooth	s
slightly rough	sr
medium rough	mr
rough	r
very rough	vr

Type of discontinuity

mining induced fracture	m
drilling fracture	d
joint	j
bedding plane	b
fault	f
geological contact	g

2: Material Properties

Fill consistency

very soft	s1
soft	s2
firm	s3
stiff	s4
very stiff	s5

Rock hardness

very soft rock	r1
soft rock	r2
hard rock	r3
very hard rock	r4
extremely hard rock	r5

3: Visual Symbols

RQD (Deere, 1964)

20%
40%
60%
80%
100%

Note: All descriptions conform to the recommendations of the Core Logging Committee of the South Africa Section of the Association of Engineering Geologists (1976)

Engineering Geological Log of Recovered Borehole Cores

Borehole number: RB3

Page 1 of 2

Logged by: MF Hanckley

Date: 24th January 1985

Progress (m)	Core Recovery: Material recovery (%)	Core Recovery: Whole core recovery (%)	Core Recovery: RQD (%)	No. of sets	Inclination (degrees)	Type	Spacing	Roughness	Fill type	Fill thickness (mm)	Fill consistency	No. of discontinuities per set	Fracture frequency (m^{-1})	Depth (m)	
	84	33	0	2	45	m	m	mr	–	–	–	5	20+	0,00	
					–	d	vc	mr	–	–	–	15+			
				2	50	m	m	mr	–	–	–	4	14+		
					0	d	c	mr	–	–	–	20+			
				2	60	m	w	mr	–	–	–	1	16+		
3,10					0	d	c	mr	–	–	–	15+			
	100	91	58	1	0	d	c	mr	–	–	–	20+	20+		
				2	50	j	vw	r	–	–	–	1	9		
					0	d	m	mr	–	–	–	8		4,90	Pyrite stringer
				2	85	b	vw	sr	sericite	1	r2	1	11		
					0	d	m	mr	–	–	–	10		6,00	sericite parting
7,10				1	0	d	m	mr	–	–	–	10	10		
	98	65	53	2	85	b	vw	sr	sericite	1	r2	1	6		
					0	d	m	mr	–	–	–	5			
				2	30	j	vw	mr	–	–	–	1	7		
					0	d	m	mr	–	–	–	6			
				3	85	b	vw	sr	sericite	50	r2	1	8	9,25	fault dip 5°, 1 cm throw
					5	f	vw	sr	–	–	–	1			
					0	d	m	mr	–	–	–	6		10,00	

Geological Description

WITWATERSRAND SUPERGROUP
Central Rand Group
Johannesburg Subgroup
Randfontein Formation

Light greenish grey unweathered widely bedded, closely becoming medium fractured medium to *coarse grained gritty very hard rock quartzite.* Footwall quartzite, Carletonville Member.

RQD (%): 20 40 60 80

Rockmass Classification and General Comments

Poor quality rockmass from 0,00 to 4,00 m.

Fair to good quality rockmass from 4,00 to 10,00 m.

Engineering Geological Log of Recovered Borehole Cores

Borehole number: RB3
Page 1 of 2

Logged by: *M F Handley*
Date: *24th January 1985*

Progress (m)	Material recovery (%)	Whole core recovery (%)	RQD (%)	No. of sets	Inclination (degrees)	Type	Spacing	Roughness	Fill type	Fill thickness (mm)	Fill consistency	No. of discontinuities per set	Fracture frequency (m⁻¹)	Depth (m)	
				2	45	m	m	mr	–	–	–	5	20+	0,00	
					–	d	vc	mr	–	–	–	15+			
				2	50	m	m	mr	–	–	–	4	14+		
	84	33	0		0	d	c	mr	–	–	–	10+			
				2	60	m	w	mr	–	–	–	1	16+		
3,10					0	d	c	mr	–	–	–	15+			
				1	0	d	c	mr	–	–	–	20+	20+		
				2	50	j	vw	r	–	–	–	1	9		
					0	d	m	mr	–	–	–	8		4,90	Pyrite stringer
	100	91	58	2	85	b	vw	sr	sericite	1	r2	1	11		
					0	d	m	mr	–	–	–	10		6,00	sericite parting
7,10				1	0	d	m	mr	–	–	–	10	10		
				2	85	b	vw	sr	sericite	1	r2	1	6		
					0	d	m	mr	–	–	–	5			
				2	30	j	vw	mr	–	–	–	1	7		
	98	65	53		0	d	m	mr	–	–	–	6			
				3	85	b	vw	sr	sericite	50	r2	1	8	9,25	Fault dip 5°, 1 cm throw
					5	f	vw	sr	–	–	–	1			
					0	d	m	mr	–	–	–	6		10,00	

Geological Description

WITWATERSRAND SUPERGROUP
Central Rand Group
Johannesburg Subgroup
Randfontein Formation

Light greenish grey unweathered widely bedded, closely becoming medium fractured medium to coarse grained gritty very hard rock quartzite. Footwall quartzite, Carletonville Member.

RQD (%) 20 40 60 80

Rockmass Classification and General Comments

Poor quality rockmass from 0,00 to 4,00 m.
Fair to good quality rockmass from 4,00 to 10,00 m.

Engineering Geological Log of Recovered Borehole Cores

Borehole number: RB3
Page 2 of 2

Logged by: MF Handley
Date: 29th January 1985

Progress (m)	Core Recovery: Material recovery (%)	Core Recovery: Whole core recovery (%)	Core Recovery: RQD (%)	Discontinuity Description: No. of sets	Inclination (degrees)	Type	Spacing	Roughness	Fill type	Fill thickness (mm)	Fill consistency	No. of discontinuities per set	Fracture frequency (m^{-1})	Depth (m)	Geological section
10,10 – 11,03	-	-	-											10,10 – 11,03	End NXC borehole start EX borehole
11,03 – 12,13	-	-	-											11,03 – 12,13	End of hole

Geological Description

WITWATERSRAND SUPERGROUP
Central Rand Group
Johannesburg Subgroup
Randfontein Formation

Light greenish grey unweathered widely bedded medium fractured, medium to coarse grained, gritty very hard rock quartzite. *Footwall quartzite, Carletonville Member.*

Notes: 1) A detailed engineering log of cores from 10,10 m to 12,13 m not possible because of the core loss associated with in situ stress measurements.

2) An EX sized extension to the NXC borehole was drilled to accommodate vibrating wire stressmeters.

RQD (%) 20 40 60 80

Rockmass Classification and General Comments

Fair to good quality rockmass from 10,00 to 12,13 m

Biaxial stress measurements taken at:-
10,16 m
10,45 m
10,73 m

UCS, Young's Modulus and Poisson's ratio determined at:-
10,19 m
10,48 m
10,75 m

Vibrating wire stressmeters installed at:-
h : 11,10 m
45° : 11,35 m
v : 11,60 m

Engineering Geological Log: General Borehole Details and Descriptive Codes

a: General Borehole Details

Borehole Number: RB4

Company: WESTERN DEEP LEVELS LIMITED

Location: 100 Reef Drive West

Collar Co-ordinates
(Mine co-ordinate system, metres)
x: +28791,2
y: -37780,6
z: +3028,3

Borehole Direction
Bearing: 309°
Inclination: +1°

Drilling method: Diamond coring
Borehole diameter (mm): 92,2
Core diameter (mm): 72,0
Drilling machine: Kempe
Drilling contractor: Boart Drilling

Date commenced: 25/11/1984
Date completed: 16/12/1984
Logged by: M F Handley
Date: 24th January 1985

b: Descriptive Codes Used on Log

1: Discontinuities

Spacing

>1000mm: very widely	vw
300–1000mm: widely	w
100–300mm: medium	m
30–100mm: closely	c
10–30mm: very closely	vc

Roughness

smooth	s
slightly rough	sr
medium rough	mr
rough	r
very rough	vr

Type of discontinuity

mining induced fracture	m
drilling fracture	d
joint	j
bedding plane	b
fault	f
geological contact	g

2: Material Properties

Fill consistency

very soft	s1
soft	s2
firm	s3
stiff	s4
very stiff	s5

Rock hardness

very soft rock	r1
soft rock	r2
hard rock	r3
very hard rock	r4
extremely hard rock	r5

3: Visual Symbols

RQD (Deere, 1964)

20%
40%
60%
80%
100%

Note: All descriptions conform to the recommendations of the Core Logging Committee of the South Africa Section of the Association of Engineering Geologists (1976)

Engineering Geological Log of Recovered Borehole Cores

Borehole number: RB4
Page 1 of 2

Logged by: M F Handley
Date: 24th January 1985

Progress (m)	Material recovery (%)	Whole core recovery (%)	RQD (%)	No. of sets	Inclination (degrees)	Type	Spacing	Roughness	Fill type	Fill thickness (mm)	Fill consistency	No. of discontinuities per set	Fracture frequency (m^{-1})	Depth (m)
	100	68	42	1	45	m	c	mr	–	–	–	13	13	0,00
				2	45	m	w	mr	–	–	–	3	18+	
					0	d	c	mr	–	–	–	15+		
				2	40	j	w	mr	–	–	–	2	10	
					0	d	m	mr	–	–	–	8		
				2	40	j	m	mr	–	–	–	4	7	
4,00					0	d	w	mr	–	–	–	3		
	98	83	62	3	80	b	vw	sr	sericite	1	r2	1	10	
					60	f	vw	mr	–	–	–	1		
					0	d	m	mr	–	–	–	8		4,90
				2	80	b	vw	mr	sericite	1	r2	1	8	
					0	d	m	mr	–	–	–	7		
				2	0	d	w	mr	–	–	–	2	6	
					35	j	m	mr	–	–	–	4		
				1	80	b	vw	sr	sericite	1	r2	1	1	
8,08														
9,05	–	–	–	–	–	–	–	–	–	–	–	–	–	
9,80	–	–	–											9,80
														10,00

Geological section:

Fault, dip 60°

End of NXC borehole

Start of BX borehole

Geological Description

WITWATERSRAND SUPERGROUP
Central Rand Group
Johannesburg Subgroup
Randfontein Formation

Light yellowish to greenish grey unweathered widely bedded medium fractured medium to coarse grained, gritty very hard rock quartzite. Footwall quartzite, Carletonville Member.

RQD (%) 20 40 60 80

Rockmass Classification and General Comments

Poor quality rockmass from 0,00 m to 2,00 m.
Fair to good quality rockmass from 2,00 m to 10,00 m.

Biaxial stress measurements taken at:–
9,11 m
9,25 m
9,55 m

UCS, Young's Modulus and Poisson' ratio determined at:–
9,15 m
9,31 m
9,58 m

Engineering Geological Log of Recovered Borehole Cores

Borehole number: RB4
Page 2 of 2

Logged by: MF Handley
Date: 24th January 1985

Progress (m)	Core Recovery: Material recovery (%)	Core Recovery: Whole core recovery (%)	Core Recovery: RQD (%)	Discontinuity Description: No. of sets	Inclination (degrees)	Type	Spacing	Roughness	Fill type	Fill thickness (mm)	Fill consistency	No. of discontinuities per set	Fracture frequency (m^{-1})	Depth (m)	Geological section	Geological Description	RQD (%) 20 40 60 80	Rockmass Classification and General Comments
11,05	-	-	-											11,05	End of hole	WITWATERSRAND SUPERGROUP Central Rand Group Johannesburg Subgroup Randfontein Formation Light yellowish to greenish grey unweathered widely bedded, medium fractured, medium to coarse grained, gritty, very hard rock quartzite. *Footwall quartzite, Carletonville Member.* Notes: 1) A detailed engineering log of cores from 9,05 m to 9,80 m not possible because of the core loss associated with in situ stress measurements. 2) An EX sized extension to the NXC borehole was drilled to accommodate vibrating wire stressmeters.		Fair to good quality rockmass from 10,00 to 11,05 m. Vibrating wire stress meters installed at:- h : 10,23 m 45° : 10,48 m v : 10,80 m

Engineering Geological Log: General Borehole Details and Descriptive Codes

a: General Borehole Details

Borehole Number: RB5	Company: WESTERN DEEP LEVELS	Location: 100/2 'C' Haulage West	
Collar Co-ordinates (Mine co-ordinate system, metres) x: +28759,5 y: -37978,3 z: +3029,6	Borehole Direction Bearing: - Inclination: -90°	Drilling method: Diamond coring Borehole diameter (mm): 74,0 mm Core diameter (mm): 54,0 mm Drilling machine: Kempe Drilling contractor: Boart Drilling	Date commenced: 8/8/1984 Date completed: 13/8/1984 Logged by: MF Handley Date: 9th August 1984

b: Descriptive Codes Used on Log

1: Discontinuities

Spacing	
>1000mm: very widely	vw
300–1000mm: widely	w
100–300mm: medium	m
30–100mm: closely	c
10–30mm: very closely	vc

Roughness	
smooth	s
slightly rough	sr
medium rough	mr
rough	r
very rough	vr

Type of discontinuity	
mining induced fracture	m
drilling fracture	d
joint	j
bedding plane	b
fault	f
geological contact	g

2: Material Properties

Fill consistency	
very soft	s1
soft	s2
firm	s3
stiff	s4
very stiff	s5

Rock hardness	
very soft rock	r1
soft rock	r2
hard rock	r3
very hard rock	r4
extremely hard rock	r5

3: Visual Symbols

RQD (Deere, 1964)

20%
40%
60%
80%
100%

Note: All descriptions conform to the recommendations of the Core Logging Committee of the South Africa Section of the Association of Engineering Geologists (1976)

Engineering Geological Log of Recovered Borehole Cores

Borehole number: RB5
Page 1 of 3

Logged by: M F Handley
Date: 14th August 1984

Progress (m)	Material recovery (%)	Whole core recovery (%)	RQD (%)	No. of sets	Inclination (degrees)	Type	Spacing	Roughness	Fill type	Fill thickness (mm)	Fill consistency	No. of discontinuities per set	Fracture frequency (m^{-1})	Depth (m)
	91	70	61	2	10	d	vc	mr	–	–	–	30+	31+	0,00
					45	b	vw	sr	sericite	1	r2	1		
				1	5	d	c	mr	–	–	–	8+	8+	
				2	5	d	m	mr	–	–	–	5	12	
					15	b	m	sr	–	–	–	7		2,93
				1	15	b	m	sr	–	–	–	9	9	
4,20	99	95	82	2	5	d	w	mr	–	–	–	3	9	4,58
					15	b	m	sr	–	–	–	6		4,71
				1	5	d	w	r	–	–	–	5	5	
				1	5	d	m	r	–	–	–	7	7	
7,05	98	95	89	2	5	d	m	mr	–	–	–	5	9	7,22
					15	b	m	sr	–	–	–	4		7,62
				2	5	d	m	mr	–	–	–	6	7	
					15	b	w	sr	sericite	1	r2	1		
				2	5	d	w	mr	–	–	–	1	4	
					15	b	w	sr	sericite	1	r2	3		10,00

RQD (%) 20 40 60 80

Geological Description

WITWATERSRAND SUPERGROUP
Central Rand Group
Johannesburg Subgroup
Sandfontein Formation
Dark greenish grey unweathered medium to closely bedded very hard rock quartzite. Hangingwall quartzite, Carletonville Member.

Dark olive streaked black unweathered very intensely laminated hard rock chloritoid shale. Green Bar, Carletonville Member.

5cm conglomerate

Light yellowish grey streaked black unweathered medium bedded very hard rock siliceous quartzite. Carbon Leader Reef Zone quartzite, Carletonville Member.

Dark grey streaked and speckled black unweathered medium to closely bedded very hard rock quartzite and conglomerate with pyrite mineralization. Carbon Leader Reef, Carletonville Member.

Light yellowish grey unweathered closely bedded very hard rock quartzite. Footwall quartzite, Carletonville Member.

Rockmass Classification and General Comments

Fair to good quality rockmass from 2,00 m to 10,00 m.

Engineering Geological Log of Recovered Borehole Cores

Borehole number: R85
Page 2 of 3

Logged by: AMF Hundley
Date: 14th August 1989

Progress (m)	Core Recovery: Material recovery (%)	Core Recovery: Whole core recovery (%)	Core Recovery: RQD (%)	No. of sets	Inclination (degrees)	Type	Spacing	Roughness	Fill type	Fill thickness (mm)	Fill consistency	No. of discontinuities per set	Fracture frequency (m^{-1})	Depth (m)
	98	95	89	2	5	d	c	mr	–	–	–	12	15	10,00
					15	b	w	sr	sericite	1	r2	3		
11,00				2	5	d	c	mr	–	–	–	14	15	11,65
					15	b	vw	sr	sericite	1	r2	1		11,73
	96	92	81	2	5	d	w	mr	–	–	–	3	4	
					25	b	vw	sr	sericite	1	r2	1		
				2	5	d	m	mr	–	–	–	–	6	
					25	b	vw	sr	sericite	1	r2	1		
				2	5	d	c	mr	–	–	–	10	11	
					25	b	vw	sr	sericite	1	r2	1		
15,00	99	95	95	2	5	d	m	mr	–	–	–	3	5	
					20	b	w	sr	sericite	1	r2	2		
				2	5	d	w	mr	–	–	–	1	3	
					25	b	w	mr	–	–	–	2		
				2	25	b	w	mr	–	–	–	2	2	
18,20	99	94	87	1	25	b	w	mr	–	–	–	2	2	
				1	5	d	m	mr	–	–	–	4	4	20,00

Geological section: Pebble bands (11,65–11,73)

Geological Description

WITWATERSRAND SUPERGROUP
Central Rand Group
Johannesburg subgroup
Randfontein Formation

Light yellowish grey unweathered closely bedded very hard rock quartzite.
Footwall quartzite, Carletonville Member.

RQD (%) 20 40 60 80

Rockmass Classification and General Comments

Fair to good quality rockmass from 10,00 m to 20,00 m.

Engineering Geological Log of Recovered Borehole Cores

Borehole number: R85
Page 3 of 3

Logged by: MF Handley
Date: 14th August 1984

Progress (m)	Material recovery (%)	Whole core recovery (%)	RQD (%)	No. of sets	Inclination (degrees)	Type	Spacing	Roughness	Fill type	Fill thickness (mm)	Fill consistency	No. of discontinuities per set	Fracture frequency (m^{-1})	Depth (m)
	99	94	87	2	5	d	m	mr	–	–	–	6	8	20,00
					20	b	w	sr	sericite	1	r2	2		
21,95				1	5	d	m	r	–	–	–	10	10	
	98	94	79	1	5	d	m	r	–	–	–	7	7	
24,30				1	5	d	m	r	–	–	–	6	6	
	58	97	97	1	10	d	m	r	–	–	–	3	3	24,71 / 24,88
				2	5	d	m	mr	–	–	–	3	5	25,30
26,10					20	b	w	sr	sericite	50	r2	2		26,10

Geological Description

WITWATERSRAND SUPERGROUP
Central Rand Group
Johannesburg Subgroup
Randfontein Formation

Light yellowish grey unweathered closely bedded very hard rock quartzite.
Footwall quartzite, Carletonville Member.

Light grey streaked yellow and black intensely laminated very hard rock siliceous quartzite. Footwall quartzite, Carletonville Member.

As above, with loosely packed angular chert pebbles. North Leader, Carletonville Member.

5 cm sericite band

WITWATERSRAND SUPERGROUP
Mes. Rand Group
Jeppestown Formation

end of hole

Greenish grey streaked yellow medium to closely bedded medium grained very hard rock quartzite with sericite bands. Square Pebble Member.

Rockmass Classification and General Comments

Fair to good quality *rockmass from* 20,00 m to 26,10 m

Accelerometer cluster installed at 25,00 m to monitor microseismic activity generated *by the South West* Dyke, the Elf Fault, *and the 100/38 Long*wall.

APPENDIX B

Detailed results of laboratory tests

Specimen Ref N° 3

Diameter : 30,0 mm

Length : 59,8 mm

Mass : 116,5 g

RB1 : 30,49m

Load in kN	Stress in MPa	Total strain x 10^{-3}	
		Axial	Radial
0	0,00	0,000	0,000
5	7,07	0,075	-0,014
10	14,15	0,155	-0,028
15	21,22	0,247	-0,047
20	28,29	0,340	-0,061
25	35,37	0,422	-0,079
30	42,44	0,501	-0,098
35	49,51	0,580	-0,113
40	56,59	0,656	-0,132
45	63,66	0,729	-0,148
50	70,74	0,810	-0,167
60	84,88	0,883	-0,184
70	99,03	0,965	-0,206
80	113,18	1,127	-0,246
90	127,32	1,252	-0,289
100	141,47	1,395	-0,333
120	169,77	1,562	-0,390
140	198,06	1,898	-0,539

Load at failure : 146 kN

Uniaxial compressive strength : 206,56 MPa

Remark : Specimen contained cemented joint

Specimen Ref N° 4

Diameter : 30,0 mm
Length : 59,2 mm
Mass : 114,9 g

Bh RB1 30,89 m

Load in kN	Stress in MPa	Total strain x 10^{-3}	
		Axial	Radial
0	0,00	0,000	0,000
5	7,07	0,083	-0,016
10	14,15	0,164	-0,029
20	28,29	0,328	-0,059
30	42,44	0,516	-0,095
40	56,59	0,691	-0,128
50	70,74	0,842	-0,158
60	84,88	1,016	-0,195
70	99,03	1,192	-0,232
80	113,18	1,365	-0,271
90	127,32	1,539	-0,309
100	141,47	1,724	-0,356
110	155,62	1,914	-0,404
120	169,77	2,058	-0,473

Load at failure : 125,0 kN
Uniaxial compressive strength : 176,84 MPa
Remark : None

Specimen Ref N° 6

Diameter : 30,0 mm
Length : 60,0 mm
Mass : 116,4 g

BH RB2 21,31 m

Load in kN	Stress in MPa	Total strain x 10^{-3}	
		Axial	Radial
0	0,00	0,000	0,000
5	7,07	0,082	-0,010
10	14,15	0,166	-0,025
15	21,22	0,266	-0,043
20	28,29	0,343	-0,058
25	35,37	0,424	-0,075
30	42,44	0,493	-0,090
35	49,51	0,558	-0,106
40	56,69	0,636	-0,122
45	63,66	0,716	-0,141
50	70,74	0,777	-0,156
60	84,88	0,932	-0,196
70	99,03	1,073	-0,233
80	113,18	1,212	-0,269
90	127,32	1,376	-0,319
100	141,47	1,488	-0,351
120	169,77	1,796	-0,456
140	198,06	2,106	-0,604

Load at failure : 150 kN
Uniaxial compressive strength : 212,21 MPa
Remark : *Specimen contained cemented joint*

Specimen Ref N° 7

Diameter : 30,0 mm
Length : 60,0 mm
Mass : 116,9 g
RB2 : 21,82 m

Load in kN	Stress in MPa	Total strain x 10^{-3}	
		Axial	Radial
0	0,00	0,000	0,000
5	7,07	0,091	-0,013
10	14,15	0,189	-0,029
15	21,22	0,285	-0,042
20	28,29	0,381	-0,059
25	35,37	0,477	-0,075
30	42,44	0,578	-0,093
35	49,51	0,671	-0,110
40	56,59	0,779	-0,134

Load at failure : 44,2 kN
Uniaxial compressive strength : 62,53 MPa
Remark : Specimen contained cemented joint

Specimen Ref Nº 8

Diameter : 30,0 mm
Length : 60,7 mm
Mass : 118,0 g
RBI : 31,27m

Load in kN	Stress in MPa	Total strain x 10^{-3}	
		Axial	Radial
0	0,00	0,000	0,000
5	7,07	0,081	-0,015
10	14,15	0,168	-0,027
20	28,29	0,359	-0,059
30	42,44	0,533	-0,089
40	56,59	0,701	-0,114
50	70,74	0,886	-0,147
60	84,68	1,043	-0,174
70	99,03	1,221	-0,207
80	113,18	1,391	-0,239
90	127,32	1,554	-0,270
100	141,47	1,735	-0,309
110	155,62	1,935	-0,353
120	169,77	2,120	-0,399
130	183,91	2,323	-0,457
140	198,06	2,535	-0,533
150	212,21	2,757	-0,631
160	226,35	3,014	-0,792

Load at failure : 167,6 kN
Uniaxial compressive strength : 237,11 MPa
Remark : None.

Specimen Ref N° 9

Diameter : 30,0 mm
Length : 59,9 mm
Mass : 126,8 g
RB2 : 22,39 m

Load in kN	Stress in MPa	Total strain x 10^{-3}	
		Axial	Radial
0	0,00	0,000	0,000
5	7,07	0,064	-0,013
10	14,15	0,132	-0,025
15	21,22	0,210	-0,044
20	28,29	0,276	-0,058
25	35,37	0,351	-0,078
30	42,44	0,419	-0,094
35	49,51	0,495	-0,115
40	56,59	0,570	-0,136
45	63,66	0,637	-0,155
50	70,74	0,714	-0,178
60	84,88	0,869	-0,226
70	99,03	1,009	-0,272
80	113,18	1,156	-0,322
90	127,32	1,296	-0,375
100	141,47	1,456	-0,441

Load at failure : 117,6 kN
Uniaxial compressive strength : 166,37 MPa
Remark : Specimen contained cemented joint

Specimen Ref N° 10

Diameter : 30,0 mm

Length : 60,6 mm

Mass : 116,8 g

RBI : 31,58m

Load in kN	Stress in MPa	Total strain x 10⁻³	
		Axial	Radial
0	0,00	0,000	0,000
5	7,07	0,079	-0,013
10	14,15	0,163	-0,024
20	28,29	0,344	-0,053
30	42,44	0,520	-0,080
40	56,59	0,679	-0,106
50	70,74	0,835	-0,131
60	84,88	1,011	-0,160
70	99,03	1,163	-0,187
80	113,18	1,324	-0,216
90	127,32	1,499	-0,250
100	141,47	1,663	-0,279
110	155,62	1,838	-0,315
120	169,77	2,013	-0,357
130	183,91	2,193	-0,401
140	198,06	2,369	-0,451
150	212,21	2,548	-0,512
160	226,35	2,746	-0,594
170	240,50	2,951	-0,716
180	254,65	3,212	-1,120

NOTE: This result not included in Table 3.5 because strain relief reading made at 31,54 m was rejected (see Table 3.2).

Load at failure : 180,0 kN

Uniaxial compressive strength : 254,65 MPa

Remark : None

Specimen Ref N° 11

Diameter : ͵0,0 mm

Length : 59,0 mm

Mass : 113,5 g

RB2 : 22,85m

Load in kN	Stress in MPa	Total strain x 10^{-3}	
		Axial	Radial
0	0,00	0,000	0,000
5	7,07	0,082	-0,011
10	14,15	0,185	-0,028
20	28,29	0,353	-0,056
30	42,44	0,533	-0,087
40	56,59	0,712	-0,119
50	70,74	0,885	-0,150
60	84,88	1,047	-0,179
70	99,03	1,227	-0,214
80	113,18	1,399	-0,249
90	127,32	1,578	-0,286
100	141,47	1,778	-0,333
110	155,62	1,976	-0,381
120	169,77	2,172	-0,438
130	183,91	2,384	-0,511
140	198,06	2,637	-0,663

Load at failure : 144,8 kN

Uniaxial compressive strength :204,85 MPa

Remark : None

Specimen Ref N° 12

Diameter : 30,0 mm
Length : 59,8 mm
Mass : 116,4 g
RBI : 32,59m

Load in kN	Stress in MPa	Total strain x 10^{-3}	
		Axial	Radial
0	0,00	0,000	0,000
5	7,07	0,078	-0,013
10	14,15	0,171	-0,029
15	21,22	0,257	-0,044
20	28,29	0,342	-0,059
25	35,37	0,427	-0,075
30	42,44	0,515	-0,088
35	49,51	0,602	-0,104
40	56,59	0,690	-0,121
45	63,66	0,763	-0,133
50	70,74	0,853	-0,152
60	84,88	1,025	-0,184
70	99,03	1,182	-0,214
80	113,18	1,367	-0,253
90	127,32	1,557	-0,293
100	141,47	1,730	-0,332
120	169,77	1,911	-0,371

Load at failure : 127,4 kN
Uniaxial compressive strength : 180,23 MPa
Remark :

Specimen Ref N° 13

Diameter : 30,0 mm
Length : 60,4 mm
Mass : 116,2 g
RB3 : 10,19 m

Load in kN	Stress in MPa	Total strain x 10^{-3}	
		Axial	Radial
0	0,00	0,000	0,000
5	7,07	0,135	-0,011
10	14,15	0,240	-0,027
20	28,29	0,445	-0,061
30	42,44	0,629	-0,099
40	56,59	0,811	-0,138
50	70,74	1,029	-0,185
60	84,88	1,216	-0,229
70	99,03	1,421	-0,278
80	113,18	1,619	-0,331
90	127,32	1,831	-0,390
100	141,47	2,056	-0,460
110	155,62	2,279	-0,538

Load at failure : 116,2 kN
Uniaxial compressive strength : 164,39 MPa
Remark : Specimen end chipped.

Specimen Ref N° 14

Diameter : 30,0 mm
Length : 60,7 mm
Mass : 116,0 g
RB4 : 9,15 m

Load in kN	Stress in MPa	Total strain x 10^{-3}	
		Axial	Radial
0	0,00	0,000	0,000
5	7,07	0,087	-0,011
10	14,15	0,171	-0,023
20	28,29	0,369	-0,051
30	42,44	0,544	-0,078
40	56,59	0,721	-0,107
50	70,74	0,887	-0,133
60	84,88	1,070	-0,166
70	99,03	1,253	-0,199
80	113,18	1,424	-0,231
90	127,32	1,612	-0,270
100	141,47	1,799	-0,312
110	155,62	1,990	-0,364
120	16[illegible],77	2,200	-0,428
130	183,91	2,398	-0,502
140	198,06	2,598	-0,599
150	212,21	2,808	-0,738

Load at failure : 158,8 kN
Uniaxial compressive strength : 224,66 MPa
Remark : None

Specimen Ref N° 15

Diameter : 30,0 mm
Length : 60,8 mm
Mass : 116,5 g
RB3 : 10,48m

Load in kN	Stress in MPa	Total strain x 10^{-3}	
		Axial	Radial
0	0,00	0,000	0,000
5	7,07	0,080	-0,012
10	14,15	0,165	-0,026
20	28,29	0,3[illegible]	-0,059
30	42,44	0,535	-0,090
40	56,59	0,727	-0,123
50	70,74	0,916	-0,157
60	84,88	1,083	-0,191
70	99,03	1,283	-0,230
80	113,18	1,465	-0,267
90	127,32	1,660	-0,309
100	141,47	1,872	-0,360
110	155,62	2,053	-0,402
120	169,77	2,262	-0,459
130	183,91	2,473	-0,519
140	198,06	2,698	-0,590
150	212,21	2,930	-0,673
160	226,35	3,169	-0,772
170	240,50	3,421	-0,899

Load at failure : 171,2 kN
Uniaxial compressive strength : 242,20 MPa
Remark :None.

Specimen Ref N° 16

Diameter : 30,2 mm
Length : 60,5 mm
Mass : 116,1 g
RB4 : 9,31 m

Load in kN	Stress in MPa	Total strain x 10^{-3}	
		Axial	Radial
0	0,00	0,000	0,000
5	6,98	0,082	-0,014
10	13,96	0,180	-0,031
20	27,92	0,351	-0,062
30	41,88	0,531	-0,097
40	55,84	0,714	-0,131
50	69,80	0,899	-0,167
60	83,76	1,108	-0,206
70	97,72	1,291	-0,247
80	111,68	1,446	-0,284
90	125,64	1,650	-0,331
100	139,60	1,841	-0,382
110	153,56	2,055	-0,441
120	167,52	2,264	-0,504
130	181,48	2,494	-0,594
140	195,44	2,730	-0,707
150	209,41	3,024	-0,917

[illegible] failure : 156,2 kN
[illegible] compressive strength : 218,06 MPa
Remark : None

Specimen Ref N° 17

Diameter : 30,2 mm
Length : 60,5 mm
Mass : 115,7 g
RB3 : 10,75m

Load in kN	Stress in MPa	Total strain x 10^{-3}	
		Axial	Radial
0	0,00	0,000	0,000
5	6,98	0,087	-0,013
10	13,96	0,176	-0,027
20	27,92	0,361	-0,058
30	41,88	0,536	-0,091
40	55,64	0,721	-0,126
50	69,80	0,893	-0,159
60	83,76	1,070	-0,194
70	97,72	1,267	-0,235
80	111,68	1,444	-0,273
90	125,64	1,636	-0,315

Load at failure : 95,4 kN
Uniaxial compressive strength : 133,18 MPa
Remark : None

Specimen Ref N° 18

Diameter : 30,2 mm
Length : 60,5 mm
Mass : 115,7 g
RB4 : 9,58m

Load in kN	Stress in MPa	Total strain x 10^{-3}	
		Axial	Radial
0	0,00	0,000	0,000
5	6,98	0,106	-0,011
10	13,96	0,202	-0,026
20	27,92	0,394	-0,056
30	41,88	0,574	-0,086
40	55,84	0,766	-0,120
50	69,80	0,947	-0,153
60	83,76	1,132	-0,189
70	97,72	1,325	-0,225
80	111,68	1,513	-0,266
90	125,64	1,710	-0,310
100	139,60	1,942	-0,368
110	153,56	2,138	-0,419
120	167,52	2,379	-0,493
130	181,48	2,637	-0,594

Load at failure : 136,2 kN
Uniaxial compressive strength : 190,14 MPa
Remark : None

APPENDIX C

Calculation of the in situ stress tensor

Assume that σ_1 is vertical, σ_2 horizontal and parallel to the average directions of boreholes RB1 and RB4, while σ_3 lies parallel to boreholes RB2 and RB3. Re-arranging equations 2.1:

$$\sigma_1 = \frac{1}{a}(\sigma_1' - b\sigma_2 - c\sigma_3) \qquad \ldots\ldots (1)$$

$$\sigma_2 = \frac{1}{a}(\sigma_2' - b\sigma_1 - c\sigma_3) \qquad \ldots\ldots (2)$$

$$\sigma_3 = \frac{1}{a}(\sigma_3' - b\sigma_1 - c\sigma_2) \qquad \ldots\ldots (3)$$

Using the values calculated by Coates and Yu (1970), listed in Table 3.6:

$$\sigma_1 = \frac{1}{1,39}(\sigma_1' + 0,75\sigma_3) \qquad \ldots\ldots (4)$$

$$\sigma_2 = \frac{1}{1,39}(\sigma_2' + 0,75\sigma_3) \qquad \ldots\ldots (5)$$

$$\sigma_3 = \frac{1}{1,39}(\sigma_3' + 0,75\sigma_2) \qquad \ldots\ldots (6)$$

where

$$\sigma_1' = \frac{E}{1\ \nu^2}(\varepsilon_1' + \nu\varepsilon_2') \qquad \ldots\ldots (7)$$

and E, ν, ε_1' and ε_2' are the Young's modulus, Poisson's ratio, maximum principal strain relief and minor principal strain relief. A further two equations similar to (7) exist for σ_2' and σ_3'. Substituting the relevant values obtained from Borehole RB1 into equation (7):

$\sigma_1' = 108,69$ MPa and $\sigma_3' = 37,39$ MPa.

Applying the same procedure for the values obtained from RB2:

$\sigma_1' = 120,52$ MPa and $\sigma_2' = 64,56$ MPa

Substituting these values into equations (4), (5) and (6), the following result:-

$$\left.\begin{array}{l}\sigma_1 = 78,19 + 0,54\ \sigma_2\ \text{MPa} \\ \sigma_3 = 26,90 + 0,54\ \sigma_2\ \text{MPa}\end{array}\right\}\ \text{Borehole RB1}$$

$$\left.\begin{array}{l}\sigma_1 = 86,71 + 0,54\ \sigma_3\ \text{MPa} \\ \sigma_2 = 46,45 + 0,54\ \sigma_3\ \text{MPa}\end{array}\right\}\ \text{Borehole RB2}$$

Note that σ_1 can be determined for the values from both RB1 and RB2 while σ_2 and σ_3 are determined from RB2 and RB1 respectively, hence the four relationships between the principal stresses. Since there are four equations and three unknowns, four different combinations of three equations each exist for the solution of each principal stress, which means that four values for each principal stress can be found.

Therefore

σ_1 = 128,29; 126,34; 122,72; 124,67 MPa,

σ_2 = 92,78; 86,08; 82,46; 86,08 MPa,

and σ_3 = 77,00; 73,38; 66,68; 73,38 MPa.

These may be averaged and the 95% confidence interval found and expressed as follows:-

σ_1 = 125,51 ± 4,65 MPa

σ_2 = 86,85 ± 8,44 MPa

σ_3 = 72,61 ± 8,44 MPa

These results represent the stresses to the west of the Elf Fault.

To the east of the fault, the results for Boreholes RB3 and RB4 are considered. In the same way as described above, using the stress concentration factors calculated by Coates and Yu (1970):

σ_1 = 103,76 ± 11,95 MPa

σ_2 = 66,77 ± 21,67 MPa

σ_3 = 64,32 ± 21,67 MPa

The principal stresses both to the east and west of the *Elf Fault* were re-calculated using the stress concentration factors given by Hocking (1976). The results are listed together with the above results in Table 3.6.

APPENDIX D

Detailed results from the vibrating wire stressmeters

TABLE D.1 VIBRATING WIRE PERIOD READINGS

APPENDIX D

Date	RB1 T (exp-6 sec) h	RB1 45	RB1 v	RB2 T (exp-6 sec) h	RB2 45	RB2 v	RB3 T (exp-6 sec) h	RB3 45	RB3 v	RB4 T (exp-6 sec) h	RB4 45	RB4 v	RB6 T (exp-6 sec) v	Control T (exp-6 sec)
Initial	222,2	204,9	229,4	203,2	193,4	210,3	204,7	224,7	219,3	221,3	201,1	197,7	227,2	216,7
20/12/84	-	-	-	-	-	-	205,1*	224,9*	219,4*	-	-	-	-	216,7
21/12/84	-	-	-	205,9*	194,8*	212,8*	205,1*	224,8*	219,3	-	201,2*	198,3*	-	216,7
11/01/85	-	-	-	203,8*	193,6*	210,6*	204,7	224,7	219,3	-	201,2*	197,7	-	216,8
04/02/85	-	-	-	203,2	193,4	210,3	204,5	225,0	219,7	-	201,2*	197,7	-	216,7
01/04/85	-	-	-	202,2	192,8	211,3	204,3	225,6	221,2	-	201,1	197,7	227,8*	216,8
02/04/85	225,5*	212,0*	230,2*	-	-	-	-	-	-	230,0*	218,5*	197,7	-	216,8
12/04/85	222,2	204,9	229,5	202,2	192,7	211,5	204,3	225,8	221,5	221,3	201,1	197,8	227,2	216,8
21/04/85	222,2	204,2	229,5	202,2	192,7	211,7	204,4	226,0	221,8	220,5	201,0	197,9	227,3	216,8
06/05/85	222,3	203,7	229,6	202,1	192,8	212,2	204,3	226,2	222,2	220,0	201,1	198,1	227,4	216,7
20/05/85	222,5	203,5	229,7	202,1	192,8	212,5	204,3	226,4	222,6	219,7	201,3	198,3	227,7	216,8
29/05/85	222,7	203,5	229,8	202,0	192,8	212,8	204,3	226,6	223,2	219,7	201,3	198,4	227,8	216,7
05/06/85	222,8	203,5	229,9	201,9	192,8	213,1	204,3	226,8	223,5	219,6	201,3	198,6	227,9	216,7
21/06/85	223,2	203,6	230,1	201,8	192,9	213,8	204,3	227,2	224,3	219,7	201,4	198,9	228,2	216,8
17/07/85	223,9	203,7	230,5	201,6	192,9	215,1	204,3	228,0	225,7	219,8	201,3	199,4	228,5	216,7
22/08/85	224,5	203,9	230,8	-	-	-	-	-	-	219,6	201,3	200,1	-	216,7
28/08/85	225,2	204,3	230,9	201,4	193,0	217,5	203,2	227,9	229,5	219,7	201,5	200,5	228,9	216,8
30/08/85	225,3	204,4	231,0	201,5	193,2	217,7	203,4	228,1	229,9	219,8	201,7	200,7	229,0	216,7
03/09/85	225,5	204,4	231,0	201,5	193,2	217,9	203,3	228,2	230,2	219,8	201,6	200,8	229,0	216,8
12/09/85	226,0	204,6	231,3	201,5	193,3	218,7	203,3	228,8	231,4	220,0	201,6	201,3	229,2	216,6
18/09/85	226,2	204,7	231,4	201,5	193,3	219,1	203,3	229,1	231,9	220,1	201,7	201,5	229,3	216,7
25/09/85	226,7	204,9	231,6	201,5	193,4	219,8	203,3	229,4	233,0	220,3	201,7	202,[illegible]	229,4	216,7
02/10/85	227,1	205,1	231,8	201,4	193,4	220,3	203,3	229,6	233,7	220,4	201,7	202,3	229,6	216,8
04/10/85	227,4	205,2	232,0	201,4	193,4	220,8	203,2	229,7	234,4	220,4	201,7	202,5	229,5	216,7
11/10/85	228,0	205,4	232,2	201,5	193,5	221,6	203,3	230,2	235,6	220,7	201,8	203,2	229,9	216,7
18/10/85	228,3	205,5	232,3	201,5	193,5	221,9	203,3	230,3	236,0	220,8	201,8	203,4	229,8	216,8
23/10/85	228,5	205,5	232,4	201,5	193,5	222,0	203,2	230,4	236,4	220,8	201,8	203,6	229,9	216,8
05/11/85	229,9	206,2	232,9	201,7	193,6	224,1	203,3	231,4	239,1	221,3	201,9	204,9	230,0	216,8
18/11/85	232,3	207,1	233,7	201,7	193,7	227,3	203,1	232,7	244,1	221,2	202,0	207,7	230,2	216,8
26/11/85	233,5	207,6	234,3	201,5	193,7	229,0	203,1	233,7	246,8	220,9	202,0	209,7	230,3	216,7
29/11/85	233,9	207,8	234,7	201,4	193,7	229,7	203,0	234,0	247,9	220,8	202,0	210,4	230,5	216,9
05/12/85	235,7	208,8	235,3	201,2	193,3	232,7	203,0	235,2	252,6	219,8	201,7	214,6	230,7	216,8
11/12/85	237,0	209,4	236,0	201,1	193,1	234,5	203,0	236,0	255,5	219,1	201,6	217,7	231,2	216,8
20/12/85	241,2	211,2	237,6	201,3	192,8	239,2	203,2	239,2	265,0	218,9	201,7	230,1	231,9	216,7
27/12/85	244,8	212,6	239,0	201,4	192,8	243,2	203,0	242,0	276,5	-	-	-	232,3	216,8
31/12/85	249,2	214,1	239,7	201,9	192,7	247,2	202,9	245,4	292,6	-	-	-	232,5	216,7
02/01/86	253,5	215,1	240,2	202,8	192,5	249,1	203,0	248,1	307,3	-	-	-	232,6	216,8
03/01/86	256,1	216,1	240,7	203,1	192,4	250,8	203,0	250,4	323,5	-	-	-	232,7	216,8
06/01/86	260,0	217,6	241,5	203,5	191,9	252,3	202,9	253,2	351,6	-	-	-	232,8	216,8
07/01/86	261,8	218,2	241,9	203,8	191,8	253,3	203,2	256,2	369,7	-	-	-	232,8	215,8
08/01/86	263,5	218,9	242,2	204,0	191,7	254,4	203,2	258,4	385,7	-	-	-	232,9	216,7
09/01/86	266,7	220,2	242,9	203,9	191,4	256,8	202,5	260,0	446,6	-	-	-	232,8	216,8
15/01/86	271,3	221,7	244,0	203,9	191,2	258,6	202,2	261,9	526,3*	-	-	-	232,9	216,7
17/01/86	273,5	222,6	245,1	203,9	191,1	260,6	202,0	262,5	582,2*	-	-	-	233,0	215,8
22/01/86	275,4	223,0	245,6	204,0	191,1	261,1	201,9	262,6	649,0*	-	-	-	233,0	216,7
27/01/86	276,5	223,4	246,1	204,0	191,0	261,7	201,9	262,9	719,2*	-	-	-	233,0	216,8
11/02/86	283,9	225,3	247,7	203,7	190,8	268,7	201,4	265,7	-	-	-	-	233,3	216,8
03/03/86	294,8	229,1	250,7	204,6	190,5	278,4	201,1	266,1	409,6*	-	-	-	233,4	216,8
26/03/86	304,2	232,6	254,3	205,5	190,5	288,0	201,0	269,5	323,2*	-	-	-	233,5	216,7
08/04/86	307,0	233,3	255,1	205,8	190,6	290,7	201,1	269,8	309,5*	-	-	-	233,6	216,8
28/04/86	311,6	233,5	255,5	205,9	190,6	293,7	201,1	270,5	302,6*	-	-	-	233,7	216,6
06/06/86	313,8	233,7	256,0	206,0	190,6	295,6	201,1	271,1	294,0*	-	-	-	233,9	216,6
18/06/86	314,6	233,9	256,3	206,0	190,6	296,3	-	-	-	-	-	-	234,0	216,7
25/07/86	319,5	234,7	257,7	206,0	190,7	301,6	201,0	273,4	280,1*	-	-	-	234,4	216,8
08/08/86	321,7	235,3	258,2	206,4	190,8	304,0	201,0	274,1	274,9*	-	-	-	234,5	216,6
19/08/86	323,9	235,9	258,8	206,6	190,9	306,5	201,0	274,8	-	-	-	-	234,7	216,7
08/09/86	326,8	236,6	259,6	206,8	191,0	310,0	201,0	275,6	266,3*	-	-	-	235,0	216,6

*readings probably unreliable

TABLE D.2 UNIAXIAL STRESS CHANGES

APPENDIX D

	RB1			RB2			RB3			RB4			RB6
	stress (MPa)			stress (MPa)			stress (MPa)			stress (MPa)			stress (MPa)
Date	h	45	v	h	45	v	h	45	v	h	45	v	v
Initial	0,0	0,0	0,0	0,0	0,0	0,0	0,0	0,0	0,0	0,0	0,0	0,0	0,0
20/12/84	–	–	–	–	–	–	+0,2*	+0,1*	0,0	–	–	–	–
21/12/84	–	–	–	+1,5*	+1,0*	+1,3*	+0,2*	0,0	0,0	–	+0,1*	+0,4*	–
11/01/85	–	–	–	+0,4*	+0,1*	+0,2*	0,0	0,0	0,0	–	+0,1*	0,0	–
04/02/85	–	–	–	0,0	0,0	0,0	-0,1	+0,1	+0,2	–	+0,1*	0,0	–
01/04/85	–	–	–	-0,6	-0,4	+0,5	-0,2	+0,4	+0,8	–	0,0	0,0	+0,3*
02/04/85	+1,5*	+3,9*	+0,3*	–	–	–	–	–	–	+3,4*	+8,6*	0,0	–
12/04/85	0,0	0,0	0,0	-0,6	-0,5	+0,6	-0,2	+0,4	+0,9	0,0	0,0	+0,1	0,0
21/04/85	0,0	-0,4	0,0	-0,6	-0,5	+0,8	-0,2	+0,5	+1,1	-0,3	-0,1	+0,1	0,0
06/05/85	+0,1	-0,7	+0,1	-0,7	-0,4	+1,0	-0,2	+0,6	+1,2	-0,6	0,0	+0,2	+0,1
20/05/85	+0,1	-0,8	+0,1	-0,7	-0,4	+1,2	-0,2	+0,7	+1,5	-0,7	+0,1	+0,4	+0,2
29/05/85	+0,2	-0,8	+0,2	-0,7	-0,4	+1,3	-0,2	+0,8	+1,6	-0,7	+0,1	+0,4	+0,3
05/06/85	+0,3	-0,8	+0,2	-0,8	-0,4	+1,5	-0,2	+0,8	+1,8	-0,7	+0,1	+0,5	+0,3
21/06/85	+0,5	-0,8	+0,3	-0,9	-0,4	+1,8	-0,2	+1,0	+2,1	-0,7	+0,2	+0,7	+0,4
17/07/85	+0,8	-0,7	+0,5	-1,0	-0,3	+2,5	-0,2	+1,3	+2,6	-0,6	+0,1	+1,0	+0,6
22/08/85	+1,0	-0,6	+0,6	–	–	–	–	–	–	-0,7	+0,1	+1,4	–
28/08/85	+1,3	-0,4	+0,6	-1,1	-0,3	+3,7	-0,8	+1,3	+4,1	-0,7	+0,2	+1,6	+0,7
30/08/85	+1,4	-0,3	+0,7	-1,0	-0,1	+3,8	-0,7	+1,3	+4,3	-0,6	+0,3	+1,7	+0,8
03/09/85	+1,5	-0,3	+0,7	-1,0	-0,1	+3,9	-0,8	+1,4	+4,4	-0,6	+0,3	+1,8	+0,8
12/09/85	+1,7	-0,2	+0,8	-1,0	-0,1	+4,3	-0,6	+1,6	+4,8	-0,6	+0,3	+2,1	+0,8
18/09/85	+1,8	-0,1	+0,8	-1,0	-0,1	+4,5	-0,8	+1,7	+5,0	-0,5	+0,3	+2,2	+0,9
25/09/85	+2,0	0,0	+0,9	-1,0	0,0	+4,8	-0,8	+1,8	+5,4	-0,4	+0,3	+2,5	+0,9
02/10/85	+2,2	+0,1	+1,0	-1,1	0,0	+5,0	-0,8	+1,9	+5,6	-0,4	+0,3	+2,6	+1,0
04/10/85	+2,3	+0,2	+1,1	-1,1	0,0	+5,3	-0,8	+1,9	+5,9	-0,4	+0,3	+2,7	+1,0
11/10/85	+2,6	+0,3	+1,1	-1,0	+0,1	+5,6	-0,8	+2,1	+6,3	-0,3	+0,4	+3,1	+1,1
18/10/85	+2,7	+0,4	+1,2	-1,0	+0,1	+5,8	-0,8	+2,2	+6,5	-0,2	+0,4	+3,2	+1,1
23/10/85	+2,8	+0,4	+1,2	-1,0	+0,1	+5,8	-0,8	+2,2	+6,6	-0,2	+0,4	+3,3	+1,1
05/11/85	+3,3	+0,8	+1,4	-0,9	+0,1	+6,8	-0,8	+2,6	+7,5	0,0	+0,4	+4,0	+1,2
18/11/85	+4,3	+1,3	+1,7	-0,9	+0,2	+8,2	-0,9	+3,0	+9,1	0,0	+0,5	+5,5	+1,3
26/11/85	+4,8	+1,5	+2,0	-1,0	+0,2	+8,9	-0,9	+3,4	+9,9	-0,2	+0,5	+6,5	+1,3
29/11/85	+5,0	+1,7	+2,1	-1,1	+0,2	+9,2	-0,9	+3,5	+10,3	-0,2	+0,5	+6,8	+1,4
05/12/85	+5,7	+2,2	+2,4	-1,2	-0,1	+10,4	-0,9	+3,9	+11,6	-0,6	+0,3	+8,8	+1,5
11/12/85	+6,2	+2,5	+2,6	-1,3	-0,2	+11,1	-0,9	+4,2	+12,5	-0,9	+0,3	+10,2	+1,[illegible]
20/12/85	+7,7	+3,5	+3,2	-1,2	-0,4	+12,9	-0,8	+5,3	+14,9	-1,0	+0,3	+15,2	+2,0
27/12/85	+8,9	+4,3	+3,8	-1,1	-0,4	+14,3	-0,9	+6,2	+17,5	–	–	–	+2,1
31/12/85	+10,4	+5,0	+4,0	-0,8	-0,5	+15,7	-1,0	+7,3	+20,7	–	–	–	+2,2
02/01/86	+11,8	+5,5	+4,2	-0,2	-0,6	+16,3	-0,9	+8,1	+23,2	–	–	–	+2,2
03/01/86	+12,6	+6,0	+4,4	-0,1	-0,7	+16,8	-0,9	+8,8	+25,5	–	–	–	+2,3
06/01/86	+13,7	+6,8	+4,7	+0,2	-1,1	+17,3	-1,0	+9,6	+28,9	–	–	–	+2,3
07/01/86	+14,2	+7,1	+4,8	+0,4	-1,1	+17,6	-0,8	+10,4	+30,6	–	–	–	+2,3
08/01/86	+14,7	+7,4	+4,9	+0,5	-1,2	+18,0	-0,8	+11,0	+32,0	–	–	–	+2,4
09/01/86	+15,5	+8,0	+5,2	+0,4	-1,4	+18,7	-1,2	+11,4	+35,9	–	–	–	+2,3
15/01/86	+16,7	+8,7	+5,5	+0,4	-1,6	+19,2	-1,4	+11,9	+39,1*	–	–	–	+2,4
17/01/86	+17,3	+9,1	+5,9	+0,4	-1,6	+19,8	-1,5	+12,0	+40,6*	–	–	–	+2,4
22/01/86	+17,7	+9,3	+6,1	+0,5	-1,6	+19,9	-1,5	+12,1	+41,9*	–	–	–	+2,4
27/01/86	+18,0	+9,5	+6,3	+0,5	-1,7	+20,1	-1,5	+12,1	+42,9*	–	–	–	+2,4
11/02/86	+19,7	+10,3	+6,8	+0,3	-1,8	+22,0	-1,8	+12,8	–	–	–	–	+2,5
03/03/86	+21,9	+12,0	+7,8	+0,8	-2,1	+24,3	-2,0	+12,9	+33,7*	–	–	–	+2,6
26/03/86	+23,7	+13,4	+8,9	+1,4	-2,1	+26,5	-2,0	+13,7	+25,5*	–	–	–	+2,6
08/04/86	+24,2	+13,7	+9,1	+1,5	-2,0	+27,0	-2,0	+13,8	+23,5*	–	–	–	+2,6
28/04/86	+25,0	+13,7	+9,2	+1,6	-2,0	+27,6	-2,0	+14,0	+22,5*	–	–	–	+2,7
06/06/86	+25,3	+13,8	+9,4	+1,6	-2,0	+28,0	-2,0	+14,1	+21,0*	–	–	–	+2,7
18/06/86	+25,5	+13,9	+9,5	+1,6	-2,0	+28,1	–	–	–	–	–	–	+2,8
25/07/86	+26,2	+14,2	+9,9	+1,6	-1,9	+29,1	-2,0	+14,6	+18,3*	–	–	–	+2,9
08/08/86	+26,6	+14,4	+10,0	+1,9	-1,8	+29,6	-2,0	+14,8	+17,2*	–	–	–	+3,0
19/08/86	+26,9	+14,7	+10,2	+2,0	-1,8	+30,0	-2,0	+14,9	–	–	–	–	+3,1
08/09/86	+27,3	+14,9	+10,5	+2,1	-1,7	+30,6	-2,0	+15,1	+15,2*	–	–	–	+3,2

*result probably unreliable

TABLE D.3 BIAXIAL STRESS CHANGES

APPENDIX D

Date	RB1 stress (MPa) x	RB1 y	RB1 xy	RB2 stress (MPa) x	RB2 y	RB2 xy	RB3 stress (MPa) x	RB3 y	RB3 xy	RB4 stress (MPa) x	RB4 y	RB4 xy
Initial	0,0	0,0	0,0	0,0	0,0	0,0	0,0	0,0	0,0	0,0	0,0	0,0
20/12/84	-	-	-	-	-	-	+0,1*	+0,3*	0,0	-	-	-
21/12/84	-	-	-	+2,1*	+2,3*	-0,4*	+0,1*	+0,2*	-0,1*	-	-	-
11/01/85	-	-	-	+0,3*	+0,5*	-0,1*	0,0	0,0	0,0	-	-	-
04/02/85	-	-	-	0,0	0,0	0,0	-0,1	+0,2	+0,1	-	-	-
01/04/85	-	-	-	-0,5	+0,4	-0,3	+0,1	+0,8	0,0	-	-	-
02/04/85	+0,9*	+1,8*	+2,3*	-	-	-	-	-	-	+1,3*	+3,9*	+5,2*
12/04/85	0,0	0,0	0,0	-0,4	+0,5	-0,4	+0,1	+1,0	0,0	0,0	+0,1	0,0
21/04/85	0,0	0,0	-0,3	-0,4	+0,6	-0,4	+0,2	+1,1	+0,1	-0,3	0,0	0,0
06/05/85	+0,1	+0,1	-0,6	-0,4	+0,9	-0,5	+0,2	+1,3	+0,1	-0,5	+0,1	+0,1
20/05/85	+0,2	+0,2	-0,7	-0,3	+1,1	-0,5	+0,3	+1,6	0,0	-0,6	+0,1	+0,2
29/05/85	+0,3	+0,3	-0,8	-0,3	+1,2	-0,5	+0,4	+1,8	0,0	-0,6	+0,2	+0,2
05/06/85	+0,3	+0,4	-0,8	-0,3	+1,4	-0,6	+0,4	+1,9	0,0	-0,6	+0,3	+0,2
21/06/85	+0,5	+0,6	-0,9	-0,3	+1,8	-0,6	+0,5	+2,3	0,0	-0,5	+0,5	+0,1
17/07/85	+0,9	+1,1	-1,0	-0,2	+2,4	-0,8	+0,7	+2,9	+0,1	-0,3	+0,9	-0,1
22/08/85	+1,1	+1,4	-0,7	-	-	-	-	-	-	-0,3	+1,3	-0,2
28/08/85	+1,2	+1,7	-1,0	+0,2	+3,7	-1,2	+0,6	+4,3	-0,3	-0,2	+1,6	-0,2
30/08/85	+1,3	+1,8	-1,0	+0,3	+3,9	-1,1	+0,8	+4,5	-0,3	-0,1	+1,7	-0,2
03/09/85	+1,3	+1,9	-1,0	+0,3	+4,0	-1,2	+2,5	+5,2	-0,9	-0,1	+1,8	-0,2
12/09/85	+1,5	+2,2	-1,1	+0,4	+4,4	-1,3	+2,7	+5,7	-0,9	+0,2	+2,1	-0,4
18/09/85	+1,6	+2,3	-1,1	+0,5	+4,6	-1,3	+2,7	+5,9	-0,9	+0,2	+2,3	-0,4
25/09/85	+1,8	+2,6	-1,1	+0,6	+5,0	-1,4	+2,9	+6,4	-0,9	+0,5	+2,6	-0,5
02/10/85	+1,9	+2,8	-1,1	+0,7	+5,3	-1,5	+3,0	+6,6	-1,0	+0,6	+2,8	-0,6
04/10/85	+2,1	+3,0	-1,1	+0,8	+5,5	-1,6	+1,3	+6,3	-0,5	+0,6	+2,9	-0,6
11/10/85	+2,2	+3,3	-1,2	+1,0	+5,9	-1,7	+1,5	+6,8	-0,5	+0,8	+3,4	-0,8
18/10/85	+2,3	+3,5	-1,2	+1,0	+6,1	-1,7	+1,6	+7,0	-0,5	+1,0	+3,5	-0,8
23/10/85	+2,4	+3,6	-1,2	+1,0	+6,2	-1,7	+1,6	+7,1	-0,5	+1,0	+3,7	-0,9
05/11/85	+2,8	+4,2	-1,2	+1,5	+7,3	-2,1	+1,9	+8,1	-0,6	+1,5	+4,5	-1,2
18/11/85	+3,6	+5,5	-1,3	+2,0	+8,8	-2,6	+2,5	+9,9	-0,8	+2,0	+6,1	-1,7
26/11/85	+4,0	+6,1	-1,4	+2,2	+9,6	-2,8	+2,8	+10,9	-0,9	+2,2	+7,2	-2,0
29/11/85	+4,3	+6,4	-1,4	+2,2	+9,9	-2,9	+2,8	+11,2	-0,9	+2,3	+7,6	-2,1
05/12/85	+4,8	+7,2	-1,4	+2,5	+11,2	-3,5	+3,3	+12,8	-1,1	+2,6	+9,7	-2,8
11/12/85	+5,3	+8,0	-1,4	+2,7	+12,0	-3,8	+3,7	+13,7	-1,2	+2,8	+11,1	-3,3
20/12/85	+6,5	+9,9	-1,5	+3,5	+14,1	-4,7	+4,7	+16,5	-1,3	+4,6	+16,7	-5,1
27/12/85	+7,6	+11,5	-1,6	+4,1	+15,7	-5,3	+5,6	+19,4	-1,6	-	-	-
31/12/85	+8,4	+13,2	-1,6	+5,0	+17,3	-6,0	+6,7	+22,9	-2,0	-	-	-
02/01/86	+9,1	+14,8	-1,8	+5,8	+18,2	-6,5	+7,7	+25,8	-2,3	-	-	-
03/01/86	+9,6	+15,8	-1,8	+6,2	+18,9	-6,8	+8,6	+28,4	-2,7	-	-	-
06/01/86	+10,4	+17,2	-1,8	+6,3	+19,4	-7,2	+9,7	+32,1	-3,3	-	-	-
07/01/86	+10,7	+17,8	-1,8	+7,0	+20,0	-7,6	+10,6	+34,2	-3,4	-	-	-
08/01/86	+11,0	+18,3	-1,8	+7,3	+20,4	-7,8	+11,1	+35,7	-3,4	-	-	-
09/01/86	+11,6	+19,4	-1,8	+7,5	+21,2	-8,2	+12,1	+39,9	-4,5	-	-	-
15/01/86	+12,5	+20,9	-1,8	+7,7	+21,8	-8,5	+13,1*	+43,4*	-5,2*	-	-	-
17/0[illegible]/86	+13,1	+21,6	-1,9	+7,9	+22,4	-8,8	+13,6*	+45,1*	-5,6*	-	-	-
22/[illegible]/86	+13,5	+22,2	-2,0	+8,0	+22,6	-8,9	+14,0*	+46,5*	-6,1*	-	-	-
27/0[illegible]/86	+13,8	+22,6	-2,0	+8,1	+22,8	-9,0	+14,4*	+47,7*	-6,4*	-	-	-
11/02/86	+15,0	+24,7	-2,2	+8,6	+24,9	-9,7	-	-	-	-	-	-
03/03/86	+16,9	+27,6	-2,2	+10,1	+27,7	-11,0	+10,4*	+37,2*	-2,2*	-	-	-
26/03/86	+18,9	+30,0	-2,2	+11,5	+30,3	-12,0	+7,3*	+27,9*	+1,5*	-	-	-
08/04/86	+19,3	+30,6	-2,2	+11,8	+31,0	-12,2	+6,6*	+25,7*	+2,3*	-	-	-
28/04/86	+19,7	+31,6	-2,5	+12,2	+31,7	-12,5	+6,2*	+24,6*	+2,8*	-	-	-
06/06/86	+20,1	+32,0	-2,7	+12,1	+31,6	-12,4	+5,7*	+22,9*	+3,4*	-	-	-
18/06/86	+20,2	+32,2	-2,7	+12,4	+32,3	-12,7	-	-	-	-	-	-
25/07/86	+21,0	+33,2	-2,9	+12,8	+33,5	-13,0	+4,6*	+19,8*	+4,8*	-	-	-
18/08/86	+21,3	+33,7	-2,9	+13,2	+34,0	-13,2	+4,2*	+18,6*	+5,4*	-	-	-
19/08/86	+21,6	+34,1	-2,9	+13,5	+34,5	-13,3	-	-	-	-	-	-
08/09/86	+22,1	+34,7	-3,0	+13,8	+35,2	-13,5	+3,4*	+16,4*	+6,4*	-	-	-

*result probably unreliable

TABLE D.3 BIAXIAL STRESS CHANGES

	RB1			RB2			RB3			RB4		
	stress (MPa)			stress (MPa)			stress (MPa)			stress (MPa)		
Date	x	y	xy	x	y	xy	x	y	xy	x	y	xy
Initial	0,0	0,0	0,0	0,0	0,0	0,0	0,0	0,0	0,0	0,0	0,0	0,0
20/12/84	-	-	-	-	-	-	+0,1*	+0,3*	0,0	-	-	-
21/12/84	-	-	-	+2,1*	+2,3*		+0,1*	+0,2*	-0,1*	-	-	-
11/01/85	-	-	-	+0,3*	+0,5*		0,0	0,0	0,0	-	-	-
04/02/85	-	-	-	0,0	0,0		-0,1	+0,2	+0,1	-	-	-
01/04/85	-	-	-	-0,5	+0,4	-0,[illegible]	+0,1	+0,8	0,0	-	-	-
02/04/85	+0,9*	+1,8*	+2,3*	-	-	-	-	-	-	+1,3*	+3,9*	+5,2*
12/04/85	0,0	0,0	0,0	-0,4	+0,5	-0,4	+0,1	+1,0	0,0	0,0	+0,1	0,0
21/04/85	0,0	0,0	-0,3	-0,4	+0,6	-0,4	+0,2	+1,1	+0,1	-0,3	0,0	0,0
06/05/85	+0,1	+0,1	-0,6	-0,4	+0,9	-0,5	+0,2	+1,3	+0,1	-0,5	+0,1	+0,1
20/05/85	+0,2	+0,2	-0,7	-0,3	+1,1	-0,5	+0,3	+1,6	0,0	-0,6	+0,1	+0,2
29/05/85	+0,3	+0,3	-0,8	-0,3	+1,2	-0,6	+0,4	+1,8	0,0	-0,6	+0,2	+0,2
05/06/85	+0,3	+0,4	-0,8	-0,3	+1,4	-0,6	+0,4	+1,9	0,0	-0,6	+0,3	+0,2
21/06/85	+0,5	+0,6	-0,9	-0,3	+1,8	-0,6	+0,5	+2,3	0,0	-0,5	+0,[illegible]	+0,1
17/07/85	+0,9	+1,1	-1,0	-0,2	+2,4	-0,8	+0,7	+2,9	+0,1	-0,3	+0,9	-0,1
22/08/85	+1,1	+1,4	-0,7	-	-	-	-	-	-	-0,3	+1,3	-0,2
28/08/85	+1,2	+1,7	-1,0	+0,2	+3,7	-1,2	+0,6	+4,3	-0,3	-0,2	+1,6	-0,2
30/08/85	+1,3	+1,8	-1,0	+0,3	+3,9	-1,1	+0,8	+4,5	-0,3	-0,1	+1,7	-0,2
13/09/85	+1,3	+1,9	-1,0	+0,3	+4,0	-1,2	+2,5	+5,2	-0,9	-0,1	+1,8	-0,2
12/09/85	+1,5	+2,2	-1,1	+0,4	+4,4	-1,3	+2,7	+5,7	-0,9	+0,2	+2,1	-0,4
18/09/85	+1,6	+2,3	-1,1	+0,5	+4,6	-1,3	+2,7	+5,9	-0,9	+0,2	+2,3	-0,4
25/09/85	+1,8	+2,6	-1,1	+0,6	+5,0	-1,4	+2,9	+6,4	-0,9	+0,5	+2,6	-0,5
02/10/85	+1,9	+2,8	-1,1	+0,7	+5,3	-1,5	+3,0	+6,6	-1,0	+0,6	+2,8	-0,6
04/10/85	+2,1	+3,0	-1,1	+0,8	+5,5	-1,6	+1,3	+6,3	-0,5	+0,6	+[illegible],9	-0,6
11/10/85	+2,2	+3,3	-1,2	+1,0	+5,9	-1,7	+1,5	+6,0	-0,5	+0,8	+[illegible],4	-0,8
18/10/85	+2,3	+3,5	-1,2	+1,0	+6,1	-1,7	+1,6	+7,0	-0,5	+1,0	+3,5	-0,8
23/10/85	+2,4	+3,6	-1,2	+1,0	+6,2	-1,7	+1,6	+7,1	-0,5	+1,0	+3,7	-0,9
05/11/85	+2,8	+4,2	-1,2	+1,5	+7,3	-2,1	+1,9	+8,1	-0,6	+1,5	+4,5	-1,2
18/11/85	+3,6	+5,5	-1,3	+2,0	+8,8	-2,6	+2,5	+9,9	-0,8	+2,0	+6,1	-1,7
26/11/85	+4,0	+6,1	-1,4	+2,2	+9,6	-2,8	+2,6	+10,9	-0,9	+2,2	+7,2	-2,0
29/11/85	+4,3	+6,4	-1,4	+2,2	+9,9	-2,9	+2,8	+11,2	-0,9	+2,3	+7,6	-2,1
05/12/85	+4,8	+7,2	-1,4	+2,5	+11,2	-3,5	+3,3	+12,8	-1,1	+2,6	+9,7	-2,8
11/12/85	+5,3	+8,0	-1,4	+2,7	+12,0	-3,8	+3,7	+13,7	-1,2	+2,8	+11,1	-3,3
[illegible]/12/85	+6,5	+9,9	-1,5	+3,5	+14,1	-4,7	+4,7	+16,5	-1,3	+4,6	+16,7	-5,1
2[illegible]/12/85	+7,6	+11,5	-1,6	+4,1	+15,7	-5,3	+5,6	+19,4	-1,6	-	-	-
31/12/85	+8,4	+13,2	-1,6	+5,0	+17,3	-6,0	+6,7	+22,9	-2,0	-	-	-
02/01/86	+9,1	+14,8	-1,8	+5,8	+18,2	-6,5	+7,7	+25,8	-2,3	-	-	-
03/01/86	+9,6	+15,8	-1,8	+6,2	+18,9	-6,8	+8,6	+28,4	-2,7	-	-	-
06/01/86	+10,4	+17,2	-1,8	+6,3	+19,4	-7,2	+9,7	+32,1	-3,3	-	-	-
07/01/86	+10,7	+17,8	-1,8	+7,0	+20,0	-7,6	+1[illegible]	+34,2	-3,4	-	-	-
08/01/86	+11,0	+18,3	-1,8	+7,3	+20,4	-7,8	+11,1	+35,7	-3,4	-	-	-
09/01/86	+11,6	+19,4	-1,8	+7,5	+21,2	-8,2	+12,1	+39,9	-4,5	-	-	-
15/01/86	+12,5	+20,9	-1,8	+7,7	+21,8	-8,5	+13,1*	+43,4*	-5,2*	-	-	-
17/01/86	+13,1	+21,6	-1,9	+7,9	+22,4	-8,8	+13,6*	+45,1*	-5,6*	-	-	-
22/01/86	+13,5	+22,2	-2,0	+8,0	+22,6	-8,9	+14,0*	+46,5*	-6,1*	-	-	-
27/01/86	+13,8	+22,6	-2,0	+8,1	+22,8	-9,0	+14,4*	+47,7*	-6,4*	-	-	-
11/02/86	+15,0	+24,7	-2,2	+8,6	+24,9	-9,7	-	-	-	-	-	-
03/03/86	+16,9	+27,6	-2,2	+10,1	+27,7	-11,0	+10,4*	+37,2*	-2,8*	-	-	-
26/03/86	+18,9	+30,0	-2,2	+11,5	+30,3	-12,0	+7,3*	+27,9*	+1,5*	-	-	-
08/04/86	+19,3	+30,6	-2,2	+11,8	+31,0	-12,2	+6,6*	+25,7*	+2,3*	-	-	-
28/04/86	+19,7	+31,6	-2,5	+12,2	+31,7	-12,5	+6,2*	+24,6*	+2,8*	-	-	-
06/06/86	+20,1	+32,0	-2,7	+12,1	+31,6	-12,4	+5,7*	+22,9*	+3,4*	-	-	-
18/06/86	+20,2	+32,2	-2,7	+12,4	+32,3	-12,7	-	-	-	-	-	-
25/07/86	+21,0	+33,2	-2,9	+12,8	+33,5	-13,0	+4,6*	+19,8*	+4,8*	-	-	-
08/08/86	+21,3	+33,7	-2,9	+13,2	+34,0	-13,2	+4,2*	+18,6*	+5,4*	-	-	-
19/08/86	+21,6	+34,1	-2,9	+13,5	+34,6	-13,3	-	-	-	-	-	-
08/09/86	+22,1	+34,7	-3,0	+13,8	+35,2	-13,5	+3,4*	+16,4*	+6,4*	-	-	-

*result probably unreliable

APPENDIX E

Determination of effective rock mass constants

Fossum (1985) derived a constitutive model for an elastic rock mass with random joints. The first assumption that must be made about the rock mass at the monitoring site is that it approximates a randomly jointed linearly elastic medium. The fracture frequencies observed in Boreholes RB3 and RB4 are almost equal, even though they were drilled in mutually perpendicular directions, which means that the jointing in the footwall quartzites to the east of the fault may be fairly random in character. The frequencies observed in Borehole RB1 and RB2 differ significantly from each other only because RB2 penetrated an intensely fractured part of the rock mass as it passed through the Elf Fault but elsewhere frequencies are similar to those in RB1. The overall rock mass jointing at the monitoring site appears to be sufficiently random in character to employ the results presented by Fossum (1985). This is especially so when considering the numerous bedding surfaces, natural joints, fractures associated with faulting and the fault itself.

The second assumption concerns the properties of all the parting surfaces themselves. In general, all joints observed in deep gold mines are closed, without any infill and unweathered. This means that a confined joint surface, remote from any void will have properties similar to intact rock.

Fossum (1985) presents two equations which can be used to calculate the effective bulk and shear moduli for jointed rock if the Young's modulus and Poisson's ratio for the intact rock material are known and the joint spacing and properties can be estimated. The equations relating these variables are listed below:-

$$\bar{K} = \frac{1}{9}E\left[\frac{3(1-\nu)sk_n + 2E}{(1+\nu)(1-2\nu)sk_n + (1-\nu)E}\right] \qquad \text{..... E.1}$$

$$\bar{G} = \frac{1}{30}\,\frac{E}{(1+\nu)}\left[\frac{(1+\nu)(1-2\nu)sk_n + (7-5\nu)E}{(1+\nu)(1-2\nu)sk_n + (1-\nu)E}\right] + \frac{2}{5}\left[\frac{Esk_s}{2(1-\nu)sk_s + E}\right] \qquad \text{..E.2}$$

where
$\bar{K}$ = effective bulk modulus
$\bar{G}$ = effective shear modulus
S = joint spacing
k_n = normal joint stiffness
k_s = shear stiffness of joint surface
E = Young's modulus
ν = Poisson's ratio

The effective Young's modulus and Poisson's ratio are then found by the two relations given below:-

$$\bar{E} = \frac{9\bar{K}\bar{G}}{3\bar{K} + \bar{G}} \qquad \text{..... E.3}$$

$$\bar{\nu} = \frac{3\bar{K} - 2\bar{G}}{2(3\bar{K} + \bar{G})} \qquad \text{..... E.4}$$

where $\bar{E}$ and $\bar{\nu}$ are the effective Young's modulus and Poisson's ratio respectively.

In calculating the effective elastic constants for the vibrating wire stressmeters, the joint spacing used is the reciprocal of the overall average of the average fracture frequencies listed for Boreholes RB1 to RB4 in Table 3.1. The normal and shear stiffnesses of the joint surfaces were taken as equal to the intact rock properties, obtained from Table 3.5. These values with the exception of that for RB2 at 21,82 m are averaged and presented in Table E.1 together with the other variables.

TABLE E.1: VALUES OF VARIABLES USED TO CALCULATE THE EFFECTIVE ELASTIC CONSTANTS

ROCK TYPE	k_n(GN/m)	k_s(GN/m)	JOINT SPACING (*m*)	AVERAGE E (GPa)	AVERAGE ν
Hangingwall quartzite	86,662	35,989	0,824	86,662	0,204
Footwall quartzite	75,586	31,617	0,824	75,586	0,195

Direct substitution of the above values into equations E.1 and E.2 for the hangingwall and footwall quartzites respectively produce the values for the effective bulk and shear moduli. These results are then substituted into equations E.3 and E.4 for effective elastic constants required for the stressmeters. The results rounded off to the nearest whole number are presented in Table 4.2 in the text.

In the case of the numerical analyses all the values listed above are the same excepting the joint spacing. This arises from Heunis (1976) who describes a major joint system trending approximately north-south with a 3 m spacing. Since this system is thought to exist throughout the rock mass as a whole, and the MINSIM-D analyses encompass a large volume of rock, this spacing was used. The effective modu for both the footwall and hangingwall quartzites were again calculated using equations E.1 to E.4. The results were averaged to obtain a Young's modulus and Poisson's ratio for the entire rock mass volume. Since the averaged results of 71 GPa and 0,20 respectively are so close to the widely accepted values of 70 GPa and 0,20, the latter were used for the analyses.

APPENDIX F

Typical Examples of MINSIM-D output

```
------------------------------------------------------------------------------------------------------------------------------------
* MINSIM-D III *     COARSE FILE: WDLAC        100/25 CROSSCUT SEPTEMBER 1986                                  *   PAGE  26   *
*              *       FINE FILE: WDLAF        100/25 CROSSCUT SEPTEMBER 1986                                  *              *
------------------------------------------------------------------------------------------------------------------------------------
CFF-REEF BENCHMARKS: BM21-BM RBT
  FINE REFERENCE WINDOW:    FINE                SHEET REQUEST IN M.C.S. WITH ORIGIN:  XM =   385.0  YM =  1088.0  ZM =  3028.0
  (STANDARD PRINT LIST: 1, RESULTS IN M.C.S.)           STRIKE AXIS: ANGLE =   0.0  NO. OF POINTS =   1  INTERVAL SIZE =    6.0
                                                           DIP AXIS: ANGLE =  90.0  NO. OF POINTS =   1  INTERVAL SIZE =    6.0

 BMARK  RELIA-                              GRID COORDINATES     DISPLACEMENTS          TOTAL PRINCIPAL STRESSES IN M.C.S.
NUMBER  BILITY   MINE COORDINATES          WRT REF. WINDOW        IN  M.C.S.
RCW COL  FLG      XM      YM      ZM       XG      YG      ZG      U     V     W    SIG1 (AL1;AZ1)    SIG2 (AL2;AZ2)    SIG3 (AL3;AZ3)
  1   1         385.0 1082.0 3028.0    17.7    44.4     1.6    -25    10    -3  -113.9 ( 84;262)   -48.9 (  2;156)   -35.1 (  6; 65)
```

* MINSIM-D III * COARSE FILE: HOLAC 100/25 CROSSCUT SEPTEMBER 1988 * PAGE 14 *
* * FINE FILE: HOLAF 100/25 CROSSCUT SEPTEMBER 1988 * *

CPF-REEF BENCHMARKS: ON 9-ELF FAULT
FINE REFERENCE WINDOW: FINE   SHEET REQUEST IN M.C.S: WITH ORIGIN: XM = 390.0 YM = 995.0 ZM = 2730.0
(STANDARD PRINT LIST: 2, RESULTS IN S.C.S.)   STRIKE AXIS: ANGLE = -41.0 NO. OF POINTS = 1 INTERVAL SIZE = 6.0
DIP AXIS: ANGLE = 75.0 NO. OF POINTS = 49 INTERVAL SIZE = 12.5

MARK NUMBER ROW	COL	RELIA-BILITY FLG	FINE COORDINATES XN	YN	ZN	GRID COORDINATES WRT REF. WINDOW XG	YG	ZG	DISPLACEMENTS IN S.C.S. U	V	W	TOTAL STRESSES IN S.C.S. TXX	TYY	TZZ	TYZ	TZX	TXY	RESULTANT SHEAR/DIRN. TAU (ANG)	EXCESS SHEAR @30DEG TAUY	@45DEG TAUZ
1	1		390.0	995.0	2730.0	18.5	12.1	-39.2	2	20	6	-31.0	-65.2	-35.0	-12.9	-1.3	1.6	12.8(264)	-7.4	-22.4
2	1		392.1	997.4	2742.1	18.9	13.2	-37.5	2	20	7	-31.2	-65.7	-35.1	-12.7	-1.3	1.5	12.8(263)	-7.5	-22.3
3	1		394.2	999.9	2754.1	19.2	14.3	-35.7	1	20	7	-31.5	-66.1	-35.2	-12.9	-1.4	1.4	13.0(263)	-7.3	-22.2
4	1		396.4	1002.3	2766.2	19.6	15.4	-34.0	1	20	7	-31.5	-66.3	-35.5	-13.1	-1.4	1.6	13.2(263)	-7.4	-22.4
5	1		398.5	1004.8	2778.3	19.9	16.5	-32.3	1	21	8	-31.3	-66.4	-36.0	-13.3	-1.5	2.1	13.4(263)	-7.4	-22.7
6	1		400.6	1007.2	2790.4	20.3	17.6	-30.5	1	21	8	-31.8	-66.6	-36.2	-13.6	-1.5	1.8	13.6(253)	-7.2	-22.3
7	1		402.7	1009.6	2802.4	20.6	18.7	-28.0	0	21	8	-32.0	-66.9	-36.4	-13.8	-1.5	1.8	13.8(263)	-7.9	-22.5
8	1		404.9	1012.1	2814.5	21.0	19.8	-27.1	0	21	9	-32.2	-67.1	-36.6	-14.0	-1.6	2.1	14.1(263)	-7.1	-22.5
9	1		407.0	1014.5	2826.6	21.3	20.9	-25.3	-1	21	9	-32.5	-67.3	-36.8	-14.3	-1.6	2.0	14.4(263)	-6.8	-22.4
10	1		409.1	1017.0	2838.7	21.7	22.0	-23.6	-1	21	9	-32.8	-67.8	-37.0	-14.6	-1.7	1.8	14.7(263)	-6.6	-22.3
11	1		411.2	1019.4	2850.7	22.0	23.1	-21.9	-2	21	10	-33.1	-68.1	-37.1	-14.9	-1.6	1.8	14.9(263)	-6.5	-22.2
12	1		413.3	1021.9	2862.8	22.4	24.2	-20.1	-3	21	10	-33.4	-68.2	-37.9	-15.3	-1.9	1.9	15.4(265)	-6.4	-22.5
13	1		415.5	1024.3	2874.9	22.7	25.3	-18.4	-4	21	10	-33.8	-68.8	-38.0	-15.8	-1.8	1.7	15.9(263)	-6.1	-22.1
14	1		417.6	1026.7	2887.0	23.1	26.4	-16.7	-3	21	11	-34.1	-69.4	-37.8	-16.9	-1.8	1.9	16.4(263)	-5.5	-21.5
15	1		419.7	1029.2	2899.0	23.5	27.5	-14.9	-4	24	13	-34.1	-68.0	-38.8	-17.4	-2.1	2.5	17.5(263)	-4.9	-21.3
16	1		421.8	1031.6	2911.1	23.8	28.6	-13.2	-5	27	15	-34.5	-68.3	-39.3	-18.8	-2.7	2.2	19.0(261)	-3.6	-20.2
17	1		424.0	1034.1	2923.2	24.2	29.7	-11.5	-6	27	16	-35.1	-69.0	-39.3	-19.8	-2.1	2.1	20.0(262)	-2.7	-19.4
18	1		426.1	1036.5	2935.3	24.5	30.8	-9.7	-8	27	18	-36.2	-72.6	-38.0	-20.5	-1.5	1.7	20.8(269)	-1.3	-17.4
19	1		428.2	1038.9	2947.3	24.9	31.9	-8.0	-10	27	19	-38.0	-71.9	-38.3	-21.8	-1.0	1.9	21.8(267)	-0.3	-16.5
20	1		430.3	1041.4	2959.4	25.2	33.0	-6.3	-12	26	22	-39.7	-76.7	-37.8	-24.6	1.1	0.8	24.6(272)	2.8	-13.2
21	1		432.5	1043.8	2971.5	25.6	34.1	-4.5	-14	26	25	-41.0	-82.9	-37.7	-30.2	3.2	-0.9	30.4(275)	8.7	-7.3
22	1		434.6	1046.3	2983.6	25.9	35.2	-2.8	-17	24	30	-44.9	-99.9	-39.5	-38.0	6.9	-3.6	38.8(280)	15.8	-0.9
23	1		436.7	1048.7	2995.6	26.3	36.3	-1.1	-22	15	38	-49.1	-118.2	-95.8	-32.6	11.0	-8.1	34.4(288)	21.0	-61.5
24	1		438.8	1051.2	3007.7	26.6	37.4	0.7	-27	-36	24	1.8	-92.3	-34.8	20.2	8.7	-7.4	22.0(66)	2.0	-12.6
25	1		440.9	1053.6	3019.8	27.0	38.5	2.4	-31	-43	-5	-30.2	-98.8	-2.3	18.3	11.4	-9.1	21.5(57)	20.3	-19.3
26	1		443.1	1056.0	3031.9	27.3	39.6	4.1	-31	-46	-21	-34.2	-89.5	-10.5	16.5	2.0	-4.3	16.3(82)	10.4	5.9
27	1		445.2	1058.5	3043.9	27.7	40.7	5.9	-27	-49	-27	-32.7	-73.6	-13.2	17.8	-0.8	-7.0	17.8(92)	18.0	4.4
28	1		447.3	1060.9	3056.0	28.1	41.8	7.6	-22	-51	-27	-32.2	-70.3	-17.6	14.1	-2.7	-3.4	14.3(100)	4.2	-3.2
29	1		449.4	1063.4	3068.1	28.4	42.9	9.3	-18	-49	-25	-33.3	-66.3	-23.6	9.7	-3.8	-5.6	10.3(110)	-3.3	-13.3
30	1		451.6	1065.8	3080.1	28.8	44.0	11.1	-14	-46	-22	-34.4	-62.2	-29.5	4.0	-5.3	-7.6	6.8(143)	-10.4	-22.8
31	1		453.7	1068.2	3092.2	29.1	45.1	12.8	-12	-44	-20	-35.0	-63.5	-33.5	1.4	-5.3	-8.5	5.5(165)	-13.9	-28.0
32	1		455.8	1070.7	3104.3	29.5	46.2	14.5	-10	-42	-18	-35.4	-63.6	-38.4	-2.0	-5.7	-9.0	6.0(199)	-15.0	-30.3
33	1		457.9	1073.1	3116.4	29.8	47.3	16.2	-8	-39	-17	-35.6	-64.7	-38.4	-5.8	-4.9	-8.5	8.1(215)	-16.1	-32.3
34	1		460.0	1075.6	3128.4	30.2	48.4	18.0	-7	-35	-14	-35.6	-66.8	-40.4	-7.0	-4.2	-8.2	8.2(238)	-15.1	-32.2
35	1		462.2	1078.0	3140.5	30.5	49.5	19.7	-6	-33	-14	-35.7	-68.6	-40.3	-7.0	-4.0	-7.7	8.1(240)	-15.1	-32.1
36	1		464.3	1080.5	3152.6	30.9	50.6	21.4	-5	-32	-14	-35.8	-70.1	-40.0	-8.9	-3.8	-6.9	7.9(241)	-15.2	-32.1
37	1		466.4	1082.9	3164.7	31.2	51.7	23.2	-4	-31	-12	-35.9	-71.5	-41.3	-9.0	-3.3	-6.9	9.0(249)	-14.2	-31.7
38	1		468.5	1085.3	3176.7	31.6	52.8	24.9	-4	-31	-13	-35.3	-71.8	-41.9	-9.6	-3.3	-6.9	10.2(250)	-14.0	-31.7
39	1		470.7	1087.8	3188.8	31.9	53.9	26.6	-3	-35	-14	-35.6	-71.9	-41.9	7.3	-3.5	-6.9	9.9(249)	-14.2	-31.9
40	1		472.8	1090.2	3200.9	32.3	55.0	28.4	-2	-34	-14	-35.8	-72.7	-41.7	-9.1	-3.4	-6.5	9.7(249)	-14.4	-32.0
41	1		474.9	1092.7	3213.0	32.7	56.1	30.1	-2	-30	-12	-36.0	-74.1	-42.2	-10.3	-2.5	-5.7	10.6(258)	-13.8	-31.6
42	1		477.0	1095.1	3225.0	33.0	57.2	31.8	-2	-29	-11	-36.2	-75.0	-42.6	-10.7	-2.2	-5.3	10.9(258)	-13.6	-31.5
43	1		479.1	1097.5	3237.1	33.4	58.3	33.6	-2	-28	-11	-36.3	-75.6	-42.5	-10.9	-2.0	-4.9	11.0(259)	-13.5	-31.4
44	1		481.3	1100.0	3249.2	33.7	59.4	35.3	-1	-28	-11	-36.5	-76.0	-42.6	-10.7	-2.0	-4.7	10.9(259)	-13.6	-31.5
45	1		483.4	1102.4	3261.3	34.1	60.5	37.0	-1	-28	-11	-36.8	-76.5	-42.6	-10.6	-2.0	-4.4	10.8(259)	-13.7	-31.6
46	1		485.5	1104.9	3273.3	34.4	61.6	38.8	-1	-28	-11	-37.0	-76.9	-42.6	-10.5	-1.9	-4.2	10.7(259)	-13.8	-31.8
47			487.6	1107.3	3285.4	34.8	62.7	40.5	0	-27	-12	-37.1	-77.6	-42.4	-10.4	-1.9	-4.0	10.6(259)	-13.9	-31.8
48	1		489.8	1109.8	3297.5	35.1	63.6	42.2	0	-24	-9	-37.1	-78.7	-42.8	-11.5	-1.4	-3.6	11.6(261)	-13.1	-31.2
49	1		491.7	1112.2	3309.6	35.5	64.9	44.0	0	-23	-9	-37.2	-79.5	-42.9	-11.6	-1.3	-3.4	11.7(263)	-13.0	-31.2

APPENDIX G

Method of determining stress components in the plane of each borehole from the numerically derived results

A benchmark point was requested at each stressmeter cluster position in order to calculate stress and stress changes comparable with the underground measurements. The MINSIM-D stress analyses program originally used for the calculations could not calculate stresses in any plane but was limited to planes having any dip angle, but a strike angle parallel either to reef strike or reef dip. For this reason, manual calculations of the biaxial stress state in the plane of each borehole were necessary in order to convert the MINSIM-D results to a form directly comparable with the underground measurements.

The borehole direction as well as the principal stress directions are plotted on an equal angle stereonet as shown in Figure G.1. The borehole direction, in this case RB1, is obtained from Table G.1, page 214, while the principal stress directions are those calculated for RB1 for mining as at September 1986. The principal stress values appear in Appendix F. All the stress measurement boreholes were assumed to lie in a horizontal plane, which means that the vertical axis in the plane of each borehole is vertical, while the horizontal axis lies at 90° to the borehole direction in a horizontal plane. These axes are termed the y and x axes respectively according to the standard defined in Section 3.2.1 and shown in Figure G.1 The angle that each principal stress makes with each of the borehole axes on the stereoplot can be found, as shown in Figure G.1. The results are listed in Table G.2.

TABLE G.2: ANGLES AND DIRECTIONAL COSINES OF EACH PRINCIPAL STRESS AT BOREHOLE RB1 FOR SEPTEMBER 1986

PRINCIPAL STRESS		σ_1	σ_2	σ_3
Angle	wrt x-axis	94	-21	69
	wrt y-axis	6	88	84
Directional	wrt x-axis	-0,070	0,934	0,358
Cosine	wrt y-axis	0,995	0,035	0,105

The directional cosines are then substituted with the value of each corresponding principal stress into the elementary stress rotation equations given by Jaeger and Cook (1979) on page 26. The biaxial stress state thus calculated together with those for the other boreholes are listed in Table 5.2.

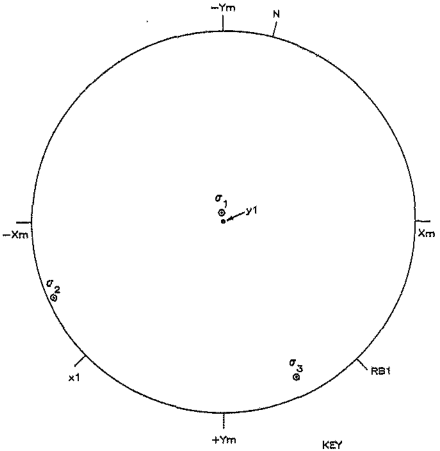

KEY

x1,y1: Borehole axes

Xm,Ym: MINSIM-D axes

Figure G.1

Stereoplot showing borehole axes and principal stress directions

TABLE G.1: SURVEYED POSITIONS OF THE STRESS MEASUREMENT BOREHOLES

BOREHOLE	COLLAR CO-ORDINATES (Mine Co-ordinate system) x (m)	y (m)	z (m)	CO-ORDINATES OF STRESSMETER CLUSTERS (Mine Co-ordinate System) x (m)	y (m)	z (m)	BOREHOLE DIRECTION (With respect to north) DIRECTION (degrees)	INCLINATION (degrees)	BOREHOLE DIRECTION (In MINSIM Co-ordinate System) DIRECTION (degrees)	INCLINATION (degrees)
RB1	28760,2	-37730,9	3028,2	28777,0	-37760,2	3027,0	119,8	+2,0	44,8	+2,0
RB2	28799,1	-37748,8	3028,0	28777,5	-37758,0	3027,5	23,1	+1,2	308,1	+1,2
RB3	28797,1	-37758,6	3028,3	28787,2	-3776[illegible],5	3027,6	30,8	+3,5	315,8	+3,5
RB4	28791,2	-37780,6	3028,3	28784,8	-37772,3	3028,0	307,6	+1,6	232,6	+1,6
RB6	28777,0	-37652,0	3028,2	28792,4	-37656,8	3027,5	162,7	+2,5	87,7	+2,5
RB7	28579,2	-37731,6	3028,2	-	-	-	120,0	+2,0	45,0	+2,0

REFERENCES

1. Amadei, B. (1985). Technical Note: Measurement of stress change in rock. Int J. Rock Mech. Min. Sci., 22, 177-182.

2. Barton, N., Lien, R. and Lunde, J. (1974). Engineering classifications of rock masses for the design of tunnel support. Rock Mechanics, 6, 189-236.

3. Briggs, D.J. (1982). Mechanical properties of quartzites and associated rock types. Chamber of Mines of South Africa Research Organization Research Report 13/83, October 1982.

4. Brown, E.T., (Ed.)(1981). Rock Characterization, Testing and Monitoring. ISRM Suggested methods, Pergamon Press pp 114-116.

5. Cahnbley, H. (1970). Grundlagenuntersuchungen über das entspannungsbohrverfahren während des praktishen einsatzes in grosser teufe. Dr.-Ing Dissertation, Technischen Universität Clausthal.

6. Chamber of Mines Research Organization, (1985). Minsim-D users' guide.

7. Chappel, B.A. (1979). Load distribution and redistribution in discontinua. Int. J. Rock Mech. Min. Sci., 16, 391-399

8. Coates, D.F. and YU, Y.S. (1970). A note on the stress concentrations at the end of a cylindrical hole. Int. J. Rock Mech. Min. Sci., 7, 583-588.

9. Cook, N.G.W. (1964). The application of seismic techniques to problems in rock mechanics. Int . J. Rock Mech. Min. Sci., 1, 169-179.

10. Cook, N.G.W., Hoek, E., Pretorius, J.P.G., Ortlepp, W.D. and Salamon, M.D.G. (1966). Rock mechanics applied to the study of rock bursts. J. S. Afr. Inst. Min. Metall., 66, 435-528.

11. Core Logging Committee of the South Africa Sectio f the Association of Engineering Geologists (1976). A guide to core logging for rock engineering. Proceedings of the Symposium on Exploration for Rock Engineering, Johannesburg, 1976, pp 71-86.

12. CSIR (1966). Instruction manual for the use of the CSIR strain gauge strain cell ("Doorstopper") equipment using the manually operated installing tool. CSIR Report MEG417, Pretoria, February, 1966.

13. Deacon, D.D. and Swan, R.H. (1965). Contribution to "The measurement of stress in rock" by E.R. Leeman. Symposium on Rock Mechanics and Strata Control in Mines, Johannesburg, April, 1963 - June, 1965, pp 366-374.

14. Deere, D.U. (1964). Technical description of rock cores for engineering purposes. Rock Mech. Engng. Geol., 1, 17-22.

15. Dieterich, J.H. (1972). Time-dependent friction in rocks. J. Geophys. Res., 77, 3690-3694.

16. Eccles, C.D. and Ryder J.A. (1984). Seismic location algorithms: a comparative evaluation. In: Rockbursts and Seismicity in Mines, Eds. N.C. Gay and E.H. Wainwright, Johannesburg, pp 89-92.

17. Fernandez, L.M., Graham, G., Hyres, M. and Ford, M. (1986). Seismological Bulletin, August 1986. Report 1986-0157, Geological Survey, Department of Mineral and Energy Affai , Republic of South Africa.

18. Fossum, A.F. (1985). Technical Note: Effective elastic properties of a randomly jointed rock mass. Int. J. Rock Mech. Min. Sci., 22, 467-470.

19. Gane, P.G., Hales, A.L. and Oliver, H.A. (1946). A seismic investigation of Witwatersrand earth tremors. Bulletin of Seismological Society of America, 36, 49-80.

20. Gay, N.C. (1972). Virgin rock stresses at Doornfontein Gold Mine, Carletonville, South Africa. Journal of Geology, 80, 61-80.

21. Gay, N.C. (1975). In situ stress measurements in Southern Africa. Tectonophysics, 29, 447-459.

22. Gay , N.C. (1979). The state of stress in a large dyke on E.R.P.M., Boksburg, South Africa. Int. J. Rock Mech. Min. Sci., 16, 179-185.

23. Gay, N.C., Spencer, D., van Wyk, J.J. and van der Heever, P.K. (1984). The control of geological and mining parameters on seismicity in the Klerksdorp Goldfield. In: Rockbursts and Seismicity in Mines. Eds. N.C Gay and E.H. Wainwright, Johannesburg, 1984.

24. Gray, W.M. and Toews, N.A. (1968). Analysis of accuracy in the determination of the ground-stress tensor by means of borehole devices. In: Status of Practical Rock Mechanics, Eds. N.E. Grosvenor and B.W. Paulding, Jr. The American Institute of Mining, Metallurgical and Petroleum Engineers, Inc., New York, 1968, pp 45-72.

25. Hagan, T.O. (1987). The stabilizing pillar design process at Western Deep Levels, Limited. The Changing Face of Mining, Third A.A.C. Group Mining Symposium, Johannesburg, September, 1987.

26. Hawkes, I. and Hooker V.E. (1974). The vibrating wire stressmeter. Proceedings 3rd Congress of the International Society of Rock Mechanics, Denver, 1974.

27. Heunis, R. (1976). Rock bursts and the search for an early warning system. Optima, 26, 1, pp 36-42.

28. High-Level Committee on Rockbursts and Rockfalls (1977). An industry guide to the amelioration of the hazards of rockbursts and rockfalls. Chamber of Mines of South Africa Research Organization, Johannesburg, 1977.

29. Hill, F.G. (1944). A system of longwall stoping in a deep level mine with special reference to its bearing on pressure bursts and ventilation problems. Papers and Discussions, Association of Mine Managers of the Transvaal, 1942-1945 pp 257-276.

30. Hocking, G. (1976). Three dimensional elastic stress distribution around the flat end of a cylindrical cavity. Int. J. Rock Mech. Min. Sci., 13, 331-337.

31. Jaeger, J.C. and Cook, N.G.W. (1979). Fundamentals of Rock Mechanics, 3rd ed. London: Chapman and Hall, 593p.

32. Lama, R.D. and Vutukuri, V.S. (1978). Handbook on Mechanical Properties of Rocks. West Germany: Trans Tech Publications, Vol 2, pp 60-62.

33. Leeman, E.R. (1965a): The measurement of stress in rock Part 1: The principles of rock stress measurements. Symposium on Rock Mechanics and Strata Control in Mines, Johannesburg, April, 1963 - June, 1965, pp 248-284.

34. Leeman, E.R. (1965b). The measurement of stress in rock Part 2: Borehole rock stress measuring instruments. Symposium on Rock Mechanics and Strata Control in Mines, Johannesburg, April, 1963 - June, 1965, pp 285-317.

35. Leeman, E.R. (1965c). The measurement of stress in rock Part 3: The results of some rock stress investigations. Symposium on Rock Mechanics and Strata Control in Mines, Johannesburg, April 1963 - June, 1965 pp 318 - 374.

36. Leeman, E.R. (1968). The determination of the complete state of stress in rock in a single borehole - laboratory and underground measurements. Int. J. Rock Mech. Min. Sci., 5, 31 - 56.

37. McGarr, A. (1984). Some applications of seismic source mechanism studies to assessing underground hazard. In: Rockbursts and Seismicity in Mines, Eds. N.C. Gay and E.H. Wainwright, Johannesburg, 1984.

38. Merrill, R.H.(1967). Three component borehole deformation gauge for determining the stress in rock. U.S. Bureau of Mines Report RI 7015.

39. Morris, D.M. and Vorster, F.A.L. (1984). A record of fail of ground accidents on gold mines, 1975 to 1981. In: Rockbursts and Seismicity in Mines, Eds. N.C. Gay and E.H. Wainwright, Johannesburg, 1984.

40. Obert, L. and Duvall, W.I. (1967). Rock Mechanics and the Design of Structures in Rock. New York: Wiley, pp 261-266.

41. Ortlepp, W.D. (1983). The mechanism and control of rock-bursts. In: Rock Mechanics In Mining Practice. Ed. S Budavari, Johannesburg, 1983, pp 257-281.

42. Ortlepp, W.D. (1984). Rockbursts in South African gold mines: A phenomenological view. In: Rockbursts and Seismicity in Mines, Eds. N.C. Gay and E.H. Wainwright, Johannesburg, 1984.

43. Ortlepp, W.D. and Nicoll, A. (1965). The elastic analysis of observed strata movement by means of an electrical analogue. Symposium on Rock Mechanics and Strata Control in Mines, Johannesburg, April, 1963 - June, 1965 pp 469-490.

44. Page, E.C., Orr, C.M. and Magni, E.R. (1976). A borehole log for engineering purposes. Proceedings of the Symposium on Exploration for Rock Engineering, Johannesburg, November, 1976.

45. Pallister, G.F. (1969). The Measurement of Virgin Rock Stress. MSc. Dissertation, University of the Witwatersrand, Johannesburg, 1969.

46. Pariseau, W.G. (1978). A note on monitoring stress changes in situ. Int. J. Rock Mech. Min. Sci., 15, 161-166.

47. Potgieter, G.J. and Roering, C. (1984). The influence of geology on the mechanics of mining-associated seismicity in the Klerksdorp Goldfield. In: Rockbursts and Seismicity in Mines, Eds. N.C. Gay and E.H. Wainwright, Johannesburg, 1984.

48. Rahn, W. (1984). Stress concentration factors for the interpretation of "Doorstopper" stress measurements in anisotropic rocks. In. J. Rock Mech. Min. Sci., 21, pp 313-326.

49. Richter, C.F. (1958). Elementary Seismology. San Francisco: Freeman.

50. Ryder, J.A. (1986). "Excess Shear Stress" assessment of geologically hazardous situations. Unpubl. Proceedings of the Colloquium on Mining in the Vicinity of Geological and Hazardous Structures, Randburg, Transvaal, June 1986.

51. Ryder, J.A., Ling, T. and Wagner, H. (1978). Slippage along a fault plane as a rockburst mechanism - static analysis. *Chamber of Mines* of South Africa Research Organization Research Report 31/78.

52. Ryder, J.A. and Napier, J.A.L. (1985). Error analysis and design of a large scale tabular mining stress analyser. Proceedings of the Fifth International Conference on Numerical Methods in Geomechanics, Nagoya, Japan, 1985.

53. Ryder, J.A. and Officer, N.C. (1965). An elastic analysis of strata movement observed in the vicinity of inclined excavations. Symposium on Rock Mechanics and Strata Control in Mines, Johannesburg, April, 1963 - June, 1965, pp 168 -193.

54. Salamon, M.D.G. (1965). Elastic analysis of displacements and stresses induced by the mining of seam or reef deposits. Symposium on Rock Mechanics and Strata Control in Mines, Johannesburg, April, 1963 - June, 1965, pp 71-167.

55. Salamon, M.D.G. (1983). Rockburst hazard and the fight for its alleviation in South African gold mines. Unpublished Proceedings of the Symposium on Rockbursts: Prediction and Control, Institute of Mining and Metallurgy, London, pp 11-36.

56. Salamon, M.D.G., Ryder, J.A. and Ortlepp, W.D. (1965). An analogue solution for determining the elastic response of strata surrounding tabular mining excavations. Symposium on Rock Mechanics and Strata Control in Mines, Johannesburg, April, 1963 -June, 1965 pp 375-402.

57. Sellers, J.B. (1977). The measurement of stress changes in rock using the vibrating wire stressmeter. International Symposium on Field Measurements in Rock Mechanics, Zurich, April, 1977, pp 275-288.

58. Spottiswoode, S.M. (1984). Source mechanisms of mine tremors at Blyvooruitzicht Gold Mine. In: Rockbursts and Seismicity in Mines, Eds. N.C. Gay and E.H. Wainwright, Johannesburg, 1984.

59. Voight, B. (1966). Bezeihung zwischen grossen horizontalen spannungen im gebirge und der tektonik und der abtragung. Proceedings of the First Congress of the International Society of Rock Mechanics, Lisbon, 1966, pp 51-56.

60. Worotnicki, G. and Walton, R.J. (1976). Triaxial hollow inclusion gauges for the determination of rock stress in situ. Proceedings of the International Society of Rock Mechanics Symposium on Investigation of Stress in Rock and Advances in Stress Measurement Supplement, Sydney, 1976, pp 1-8.